PE&RS
February 2024
Volume 90, Number 2
PHOTOGRAMMETRIC ENGINEERING & REMOTE SENSING
The official journal for imaging and geospatial information science and technology

GEO WEEK

geo-week.com

asprs THE IMAGING & GEOSPATIAL INFORMATION SOCIETY

ONE CONFERENCE PASS.

A world of geospatial education.

FEBRUARY 11-13, 2024 | DENVER, CO

In 2024, Geo Week and ASPRS are coming together more than ever to produce a single, comprehensive conference program. New this year, all conference attendees at the event will have access to both Geo Week and ASPRS sessions with a single conference pass.

Scan to View the Conference Program

ASPRS content includes **20+** TECHNICAL PROGRAM SESSIONS, ADD-ON WORKSHOPS and ACADEMIC HUB PRESENTATIONS.

REGISTER TODAY GEO-WEEK.COM

ASPRS MEMEBERS RECEIVE A DISCOUNT!
For questions regarding membership status or how to receive your discount please contact office@asprs.org.

The intersection of geospatial the built world

INDUSTRIES SERVED

Architecture, Engineering & Construction
Asset & Facility Management
Disaster & Emergency Response
Earth Observation & Satellite Applications
Energy & Utilities
Infrastructure & Manufacturing
Land & Natural Resource Management
Mining & Aggregates
Surveying & Mapping
Urban Planning & Smart Cities

EVENT PARTNERS

asprs THE IMAGING & GEOSPATIAL INFORMATION SOCIETY
isprs information from imagery
MAPPS
USIBD U.S. Institute of BUILDING DOCUMENTATION
WGIC World Geospatial Industry Council

ANNOUNCEMENTS

NV5 Geospatial, www.nv5.com, announced ahead of the 103rd Transportation Research Board (TRB) Annual Meeting that NV5 Geospatial's thermal infrared (TIR) Solutions for transportation infrastructure challenges are being implemented in transportation projects analyzing concrete bridges in the Midwest. This remote sensing technology offering enables local, regional and governmental transportation agencies to identify structural problems well before they reach the surface of concrete bridge decks.

This groundbreaking work comes at a time when 42% of U.S. bridges are over 50 years old and more than 46,000 of them are considered "structurally deficient" according to the American Society of Civil Engineers (ASCE) "2021 Report Card on Infrastructure." The ASCE report also found that "178 million trips are taken across these structurally deficient bridges every day," potentially endangering countless lives. The U.S. was ranked by the World Economic Forum 13th globally when it comes to the overall quality of infrastructure.

Concrete bridge decks are critical components of the structure that require periodic inspections for continuous maintenance, rehabilitation, and replacement work. TIR is integral to non-destructive inspection (NDI) techniques for analyzing concrete bridge decks and identifying potential delamination made quicker and more efficiently by aerial collection.

"For decades NV5 Geospatial has been trusted to provide on-target geospatial solutions for roadways, airports and all modes of rail infrastructure. Our clients trust us because we've proven time and time again that we can find a better way to ensure the right solutions for their specific needs," said Bob Vandermeer, vice president, State & Regional Lead, NV5. "We believe that our new bridge inspection approach enabled by our TIR Solutions is defining a new path for cost effective, highly accurate analysis that is sure to reap considerable benefits for departments of transportation and more importantly, support safer roads across America."

NV5 Geospatial recently conducted two separate pilot projects with two Midwestern states' Departments of Transportation utilizing aerial data collection to identify thermal anomalies of potential delamination for 200 bridge concrete surfaces. Both projects were completed by flying a fixed-wing aircraft at a low elevation with the thermal sensor mounted to its floor and without having to use ground based support.

Nearmap, www.nearmap.com, has signed an agreement to acquire Betterview, a leading property intelligence and risk management platform in the insurance industry.

Founded in Australia in 2007, Nearmap expanded operations into the U.S. in 2014 to help companies better visualize the truth on the ground to make more informed business decisions. Today's announcement marks a significant milestone in the advancement of the Nearmap global growth strategy. This will reinforce the company's position as a leading source of imagery intelligence, data and solutions, and expand and complement its expertise and capabilities for insurance customers and partners.

"The Nearmap acquisition of Betterview is transformative for the industry," said Andy Watt, CEO of Nearmap. "Integrating the Betterview platform and AI solutions into the Nearmap technology stack will enable better visualization of the truth on the ground with a richer, more powerful set of AI capabilities that combine the best of both companies. This is a significant milestone in our ongoing efforts to innovate solutions for insurance carriers, and expand our presence within the property and casualty space."

Betterview is an established and trusted source of property intelligence and risk management for the insurance industry, applying artificial intelligence and computer vision to help identify and mitigate property risk, improve and automate underwriting and inspection workflows, and provide a more productive, seamless customer experience.

"Combining the offerings of two best-in-class providers will deliver greater impact for insurers," said Betterview Co-Founder and CEO David Lyman. "The acquisition of Betterview by Nearmap will increase access to premium imagery and cutting-edge, scalable property intelligence solutions for the insurance industry."

"We are optimistic about the outcomes this acquisition will bring to our customers, the potential for developing even greater products together, and the impact it will have on the future of the insurance industry," said Betterview Co-Founder and COO Dave Tobias.

Nearmap and Betterview will harness the power of the leading image intelligence and property risk-management technology solutions — including a historical archive for change analysis, comprehensive post-catastrophe imagery, and AI attributes — to provide customers and partners with greater certainty and clarity, through:

- More efficient development of insurance solutions and capabilities
- Faster and more accurate underwriting, property condition identification, and overall mitigation of risk
- Enhanced visualization and interpretation of over 100 AI-powered property attributes
- Deeper analytics, with more recency, and regularity through insights easily accessible within a browser, via

API or business intelligence tools, or seamlessly integrated with existing underwriting or claims core systems

From imagery to insights to answers, this acquisition aligns with the Nearmap long-term global vision to be the source of truth that shapes our livable world.

Completion of the acquisition is subject to customary closing conditions. The financial terms of the deal have not been disclosed. Jefferies served as exclusive financial advisor to Betterview.

The Microsoft Flight Simulator team is excited to feature this storied part of the globe with sweeping improvements in this latest release. World Update XV covers Denmark, Finland, Iceland, Norway, Sweden, and also includes the Faroe Islands and Greenland (both self-governing countries within the Kingdom of Denmark). Developed in conjunction with Microsoft partners Bing Maps, **Vexcel** (https://vexceldata.com/), Maxar, Gaya Simulations, Orbx, and Kjetil Garpestad, this update promises to thrill the Microsoft Flight Simulator audience with its range of enhancements:

- 90 hand-made points of interest.
- 10 TIN (triangulated irregular network) cities.
- 5 hand-crafted airports.
- Broad-based, high-resolution geographic updates using significantly enhanced DEMs (digital elevation models) in Iceland, Norway, and Sweden.
- Fresh aerial imagery and satellite data across the entire region.

Some of the Points of Interest (POIs) include Denmark's Farø Bridges, Gråsten Palace, and Ribe Cathedral; Finland's Bengtskär Lighthouse, Kökar church, and Tähtiniemi Bridge; Greenland's Arctic Station, EastGRIP, and Summit Station; Iceland's Knarrarós Lighthouse, Laugardalsvöllur Stadium, and Ólafsvíkurkirkja Church; Norway's Andenes Lighthouse, Gjemnessund Bridge, and Svalbard Global Seed Vault; and Sweden's Älvsborg Bridge, Arctic Space Centre, and Aurora Sky Station.

The TIN cities in World Update XV include five in Denmark: Aarhus, Copenhagen, Frederikssund, Odense, and Roskilde; four in Sweden: Gothenburg, Linkoping, Malmö, and Visby; and Norway's Oslo. In addition, Gaya simulations created a splendid array of airports: Iceland's Akureyri Airport (BIAR), Norway's Mo i Rana Airport (ENRA), Sweden's Kiruna Airport (ESNQ), and Finland's Ivalo Airport (EFIV). Kjetil Garpestad created a stunningly realistic rendition of Leknes Airport (ENLK).

World Update XV: Nordics & Greenland also brings simmers ten exciting activities that will inspire and challenge, including:

- Four discovery flights: Bergen (Norway), Gothenburg (Sweden), the Faroe Islands (Denmark), and Reykjavík (Iceland).
- Three landing challenges: Akureyri Airport (BIAR), a famous challenge in northern Iceland; Ekeby Airport (ESSC), an epic sailplane challenge in Sweden; and a bold challenge at Norway's Mo i Rana Airport (ENRA).
- Three bush trips: the Baltic Coast of Denmark and Sweden which traverses some of Europe's most exquisite coastal landscapes; the adventurous Greenland Exploration; and Spitsbergen, which begins with an exploration of Norway's Spitsbergen, then crosses open water to visit northern mainland Norway.

World Update XV: Nordics & Greenland is available FREE to all owners of Microsoft Flight Simulator. Ensure that your simulator is updated to version 1.34.16.0 and download World Update XV. The sky is calling!

CALENDAR

- 11-13 February, **Geo Week**, Denver, Colorado; www.geo-week.com.
- 2-4 May, **GISTAM 2024**, Angers, France; https://gistam.scitevents.org.
- 13-16 May, **Geospatial World Forum**, Rotterdam, The Netherlands; https://geospatialworldforum.org.
- 11-14 June, **ISPRS Technical Commission II Symposium — The Role of Photogrammetry for a Sustainable World**, Las Vegas, Nevada; www.isprs.org/tc2-symposium2024.
- 15-19 July, **Esri User Conference**, San Diego, California; www.esri.com/en-us/about/events/uc/overview.

ASPRS WORKSHOP SERIES

It's not too late to earn Professional Development Hours

Miss an ASPRS Workshop or GeoByte? Don't worry! Many ASPRS events are available through our online learning catalog.

https://asprs.prolearn.io/catalog

PE&RS

PHOTOGRAMMETRIC ENGINEERING & REMOTE SENSING

The official journal for imaging and geospatial information science and technology

February 2024 Volume 90 Number 2

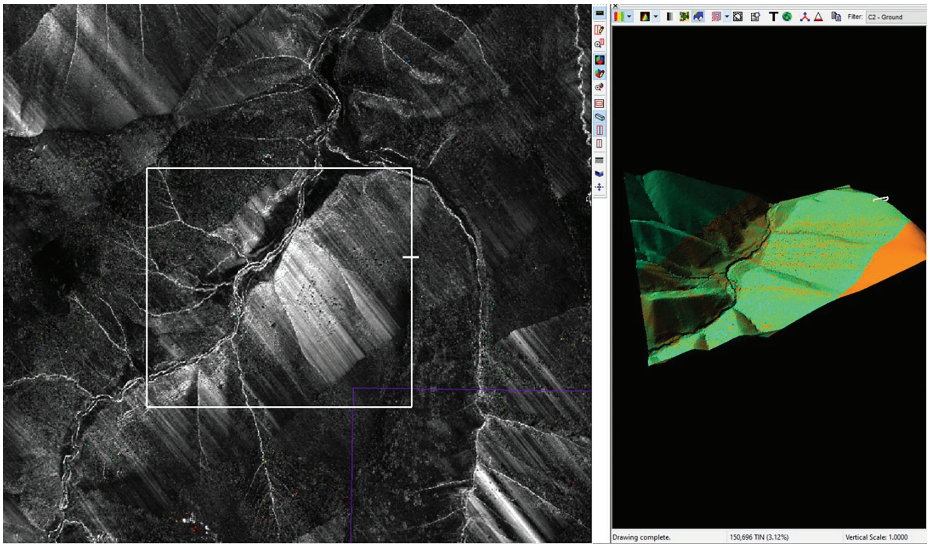

69 **Lidar Point Cloud Quality Control: Automating Accuracy and Precision Testing**
By Martin Flood, Nicolas Seube, and Darrick Wagg

COLUMNS

75 GIS Tips & Tricks — Some Old Habits Die Hard

79 SectorInsight.org — The Value of Membership in the American Society for Photogrammetry and Remote Sensing

81 Book Review — *Introduction to Pointcloudmetry*

ANNOUNCEMENTS

82 ASPRS Certifications

83 In Memoriam — Lyman J. Ladner

84 Headquarters News

84 New ASPRS Members
Join us in welcoming our newest members to ASPRS.

126 Call for *PE&RS* Special Issue Submissions — Ushering a New Era of Hyperspectral Remote Sensing to Advance Remote Sensing Science in the Twenty- first Century

DEPARTMENTS

65 Industry News

66 Calendar

98 Who's Who in ASPRS

120 ASPRS Sustaining Members

85 Remote Sensing Application in Water Quality of Lake Burdur, Türkiye
Aylin Tuzcu Kokal, Meltem Kacikoc, Nebiye Musaoglu, and *Aysegul Tanik*

The advancements in space technology have facilitated water quality (WQ) monitoring of lake conditions at a spatial resolution of 10 m by freely accessible Sentinel-2 images. The main aim of this article was to elucidate the necessity of spatiotemporal WQ monitoring of the shrinking Lake Burdur in Türkiye by examining the relation between field and satellite data with a state-of-the-art machine learning-based regression algorithm.

89 The Sight-Aesthetic Value of the Underwater Landscapes of Lakes in the Context of Exploration Tourism
Piotr Dynowski, Anna Źróbek-Sokolnik, Marta Czaplicka, and *Adam Senetra*

The aim of the study is to identify factors affecting the sight-aesthetic value of the underwater landscapes of lakes for the purposes of exploration tourism. The reason for undertaking this topic is the lack of such studies for inland water bodies. The results will contribute to expanding and supplementing the knowledge on the assessment of the sight-aesthetic attractiveness of landscapes and fill gaps in knowledge about the underwater landscapes of lakes.

99 Crop Monitoring System Using MODIS Time-Series Data for Within-Season Prediction of Yield and Production of US Corn and Soybeans
Toshihiro Sakamoto

In terms of contribution to global food security, this study aimed to build a crop monitoring system for within-season yield prediction of US corn and soybeans by using the Moderate Resolution Imaging Spectroradiometer (time-series data, which consists of three essential core algorithms [crop phenology detection, early crop classification, and crop yield prediction methods]).

121 A Few-Shot Semi-Supervised Learning Method for Remote Sensing Image Scene Classification
Yuxuan Zhu, Erzhu Li, Zhigang Su, Wei Liu, Alim Samat, and *Yu Liu*

Few-shot scene classification methods aim to obtain classification discriminative ability from few labeled samples and has recently seen substantial advancements. However, the current few-shot learning approaches still suffer from overfitting due to the scarcity of labeled samples. To this end, a few-shot semi-supervised method is proposed to address this issue.

See the Cover Description on Page 68

facebook.com/ASPRS.org
https://www.linkedin.com/company/asprs/about/
twitter.com/ASPRSorg
youtube.com/user/ASPRS

COVER DESCRIPTION

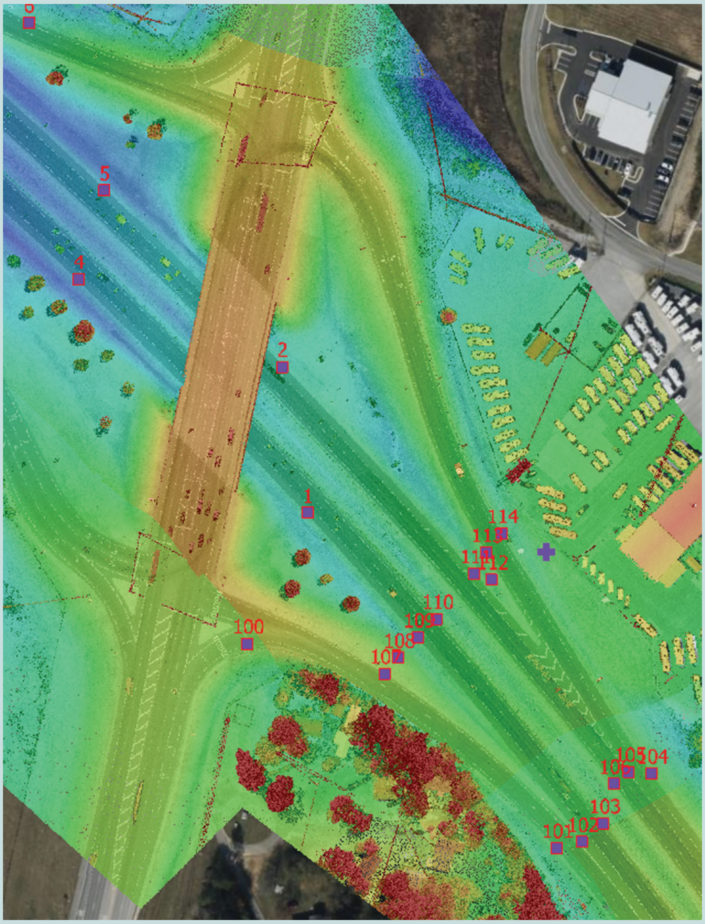

The cover image shows GeoCue TrueView 680 drone lidar data collected over a highway intersection. The TrueView 680 uses a Riegl VUX-1LR lidar integrated with an Applanix APX20 INS system. Flight altitude was 80 m AGL using a Freefly Alta X drone. All data was post-processed and adjusted to survey control using an Accuracy Star 3D ground target. Independent accuracy was assessed using 21 control panels. All data collection and data processing performed by Kevin Cowart (GeoCue Group) using the LP360 Drone software suite. Data courtesy of GeoCue Group, Earl Dudley, LLC and Gonzales Strength & Associates.

GeoCue TrueView 680 drone lidar payload mounted on a Freefly Alta X.

asprs

THE IMAGING & GEOSPATIAL INFORMATION SOCIETY

PHOTOGRAMMETRIC ENGINEERING & REMOTE SENSING

Journal Staff

Publisher ASPRS
Editor-In-Chief Alper Yilmaz
Director of Publications Rae Kelley
Electronic Publications Manager/Graphic Artist
Matthew Austin

Photogrammetric Engineering & Remote Sensing is the official journal of the American Society for Photogrammetry and Remote Sensing. It is devoted to the exchange of ideas and information about the applications of photogrammetry, remote sensing, and geographic information systems. The technical activities of the Society are conducted through the following Technical Divisions: Geographic Information Systems, Photogrammetric Applications, Lidar, Primary Data Acquisition, Professional Practice, Remote Sensing Applications, and Unmanned Autonomous Systems. Additional information on the functioning of the Technical Divisions and the Society can be found in the Yearbook issue of *PE&RS*.

All written correspondence should be directed to the American Society for Photogrammetry and Remote Sensing, PO Box 14713, Baton Rouge, LA 70898, including general inquiries, memberships, subscriptions, business and editorial matters, changes in address, manuscripts for publication, advertising, back issues, and publications. The telephone number of the Society Headquarters is 225-408-4747; the fax number is 225-408-4422; web address is www.asprs.org.

PE&RS. *PE&RS* (ISSN0099-1112) is published monthly by the American Society for Photogrammetry and Remote Sensing, 8550 United Plaza Blvd, Suite 1001, Baton Rouge, Louisiana 70809 . Periodicals postage paid at Bethesda, Maryland and at additional mailing offices.

SUBSCRIPTION. *PE&RS* is available as an e-Subscription (single-site and multi-site licenses) and an e-Subscription with print add-on (single-site license only). PE&RS subscriptions are on a calendar-year, beginning in January and ending in December.

The rate for a single-site e-Subscription for the USA/Non-USA is $1040 USD, for Canadian* is $1092 USD.

The rate for a multi-site e-Subscription for the USA/Non-USA is $1040 USD plus $250 USD for each additional license, for Canadian* is $1092 USD plus $263 for each additional license.

The rate for e-Subscription with print add-on for the USA is $1546 USD, for Canadian* is $1637 USD, and for Non-USA is $1596 USD.

*Note: Subscription prices for Canada includes 5% of the total amount for Canada's Goods and Services Tax (GST #135123065). **PLEASE NOTE: All Subscription Agencies receive a 20.00 USD discount.**

POSTMASTER. Send address changes to PE&RS, ASPRS, PO Box 14713, Baton Rouge, LA 70898. CDN CPM #(40020812).

MEMBERSHIP. Membership is open to any person actively engaged in the practice of photogrammetry, photointerpretation, remote sensing and geographic information systems; or who by means of education or profession is interested in the application or development of these arts and sciences. Membership is for one year, with renewal based on the anniversary date of the month joined. Membership Dues include a 12-month electronic subscription to *PE&RS*. Annual Individual Membership dues are $175.00 USD and Student Membership dues are $50.00 USD. A tax of 5% for Canada's Goods and Service Tax (GST #135123065) is applied to all members residing in Canada.

COPYRIGHT 2024. Copyright by the American Society for Photogrammetry and Remote Sensing. Reproduction of this issue or any part thereof (except short quotations for use in preparing technical and scientific papers) may be made only after obtaining the specific approval from ASPRS. The Society is not responsible for any statements made or opinions expressed in technical papers, advertisements, or other portions of this publication. Printed in the United States of America.

PERMISSION TO PHOTOCOPY. The copyright owner's consent that copies of the article may be made for personal or internal use or for the personal or internal use of specific clients. This consent is given on the condition, however, that the copier pay the stated per copy fee through the Copyright Clearance Center, Inc., 222 Rosewood Drive, Danvers, Massachusetts 01923, for copying beyond that permitted by Sections 107 or 108 of the U.S. Copyright Law. This consent does not extend to other kinds of copying, such as copying for general distribution, for advertising or promotional purposes, for creating new collective works, or for resale.

LIDAR POINT CLOUD QUALITY CONTROL:

AUTOMATING ACCURACY AND PRECISION TESTING

Mr. Martin Flood, *VP – Special Projects, GeoCue Group*
Dr. Nicolas Seube, *Chief Scientist, mdGroup*
Mr. Darrick Wagg, *VP – Customer Success, GeoCue Group*

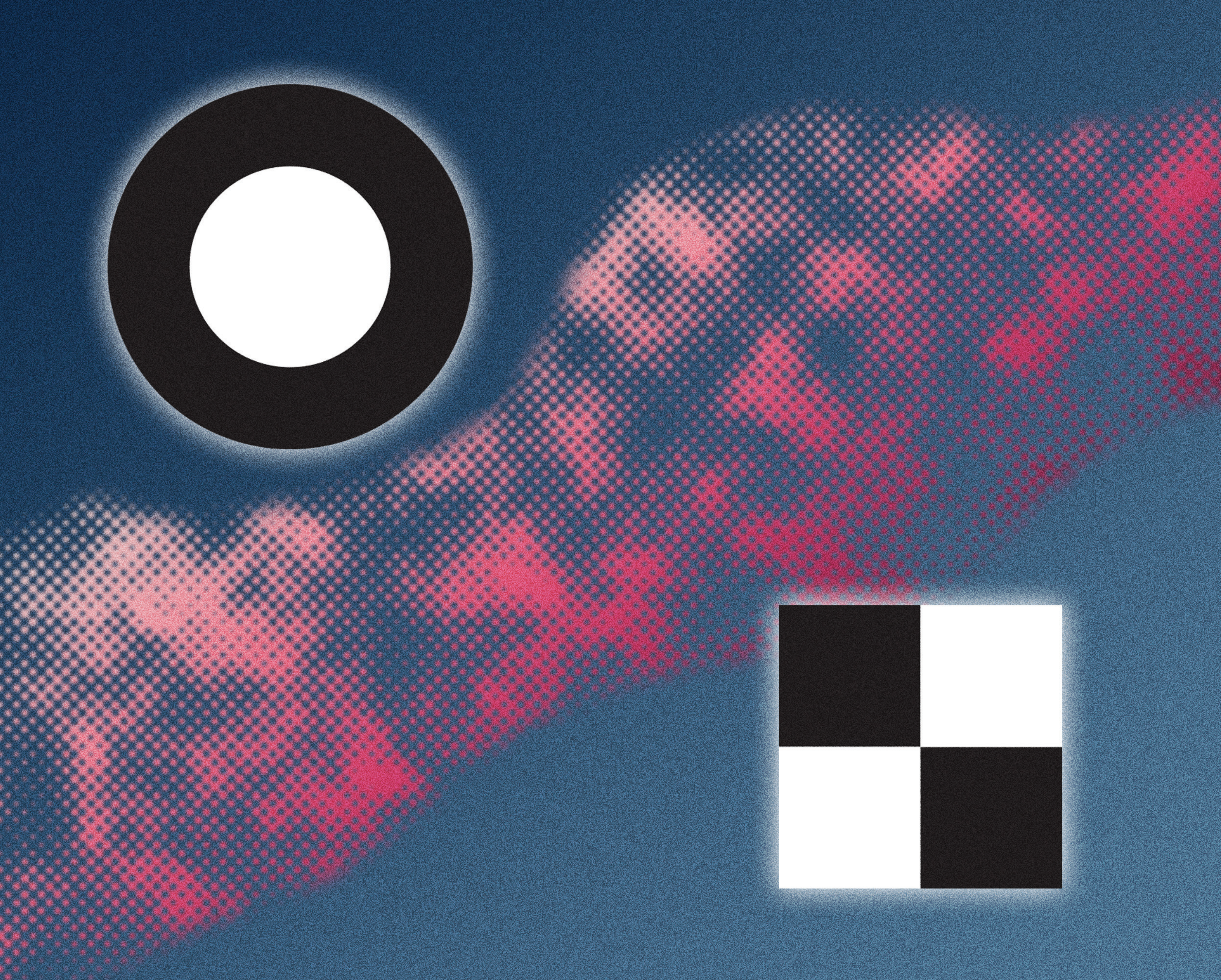

The creation of map products from lidar point clouds requires rigorous quality control procedures. Review processes include manual inspection ("eyes on") by a qualified technician in an interactive point cloud editing environment and increasingly automated quality checking tools to measure accuracy, precision, and other quality metrics. Increasing the efficiency of this review process is an important research area for lidar data producers and data users. Smaller lidar surveys, such as those collected by drones, require the same quality review and assessment tools for measuring accuracy and precision as larger scale surveys, so can benefit from more automation as well.

In this article we report on improved methods to automatically assess the accuracy and precision of lidar point clouds. We reference the *ASPRS Positional Accuracy Standards for Digital Geospatial Data* (*2nd Edition*) (the 'ASPRS Standard' or the 'Standard') throughout as the authoritative reference for lidar data quality assessment and reporting for map products. First, we will discuss the automatic detection of 3D lidar targets ("Accuracy Stars") in point cloud data to measure vertical and horizontal accuracy and derive translation/rotation corrections for the data. In the second part of the article, we discuss our use of computational geometry to measure and report precision over large project areas using Principal Component Analysis (PCA). Combined, these two techniques allow for more automated quality checking of lidar point cloud accuracy and precision, reducing the need for manual interaction and scaling efficiently over large (or small) project areas.

ACCURACY

Lidar accuracy assessment is typically done via classical methods inherited from photogrammetry. Vertical accuracy checking against the lidar surface at a known checkpoint (survey nail) is the most common approach in use today. Surface modelling of the lidar data is done using accepted Triangular Irregular Network (TIN) or Inverse Distance Weighted (IDW) methods. The orthogonal distance between the checkpoint and the lidar surface gives the vertical error. Using a collection of such checkpoints provides the statistical Root Mean Square Error (RMSE) in the vertical for the surface, assuming the checkpoints are well-distributed across the area. A minimum of 30 checkpoints are required by ASPRS for "Tested to Meet …" accuracy reporting. Many drone lidar projects will have less than 30 checkpoints and will be reported as "Produced to Meet …". Specific wording for each of these cases is outlined in the Standard, Section 7. 15.

The fit of a product (the lidar surface) to known checkpoints is the First Component of Positional Error. It is what has been traditionally reported as the "accuracy" of lidar data by vendors and data producers. With the increasing accuracy of lidar sensors, the ASPRS Standard now acknowledges the inherent error in the position of the checkpoints themselves is becoming significant and must also be considered when reporting the accuracy achieved. The uncertainty (error) in the checkpoint position, typically reported by the surveyor collecting the checkpoints, needs to be included in the final stated product accuracy. The statistical RMSE value of the checkpoint positions is referred to as the Second Component of Positional Error. Product accuracy is the Root Sum of Squares Error (RSSE) of the two components. See Section 7. 11 in the Standard for details. Practically, this means for lidar datasets the reported accuracy cannot be better than the checkpoint accuracy and typically will be slightly higher than the surface-to-checkpoint value measured by traditional point-to-TIN methods. Users should not assume this checkpoint error contribution is negligible when assessing a lidar system's achievable accuracy for a derived mapping product.

Horizontal positional accuracy is reported like vertical accuracy, with both First and Second component errors contributing to the final horizontal accuracy. Reporting is typically done as the radial or planimetric (XY) accuracy achieved rather than as individual single-axis errors. Traditionally, lidar datasets have used identifiable visible targets in the point cloud for horizontal error measurement. These can be specific targets deployed during the survey flights, like photogrammetric panels, or targets of opportunity that have been surveyed, such as building corners, manhole covers, road markings etc. The planimetric (XY) position of such targets in the point cloud is collected manually in post-processing, but this is labor-intensive and prone to interpretation error in the manual capture. Automating both the vertical and horizontal accuracy checking using detection algorithms to identify and locate the targets reduces the labor required, is less prone to user error, eliminates errors of interpretation in target location, and allows for a more rigorous calculation of offsets and corrections to be applied to the point cloud.

Our algorithmic approach to target detection relies on using monumented Ground Control Targets (GCTs) that can be "seen" within the point cloud. Such targets can be 2-dimensional (XY) such as checkerboard or concentric targets on the ground or they can be 3-dimensional (XYZ) objects such as spheres or discs configured in a well-defined pattern and mounted above the ground. Color contrast, such as alternating black and white segments, or high-reflectivity paint is used to enhance the detectability in the point cloud.

One 3D target we have tested extensively is an Accuracy Star (AS) (see Figure 1). This target consists of six high-reflectivity discs placed on rigid arms defining a hexagon. The discs are co-planar and leveled to the base. The algorithm determines the centerpoint of the hexagon formed by the discs in the point cloud and compares this to the known centerpoint measured independently (or provided by a co-mounted GNSS receiver) to accurately determine the XYZ offsets for the point cloud. This provides the first component (point cloud to checkpoint) accuracy while the accuracy of the AS location itself provides the second component (checkpoint position). Quality metrics on the fit of the algorithm are also provided. Transla-

Photogrammetric Engineering & Remote Sensing
Vol. 90, No. 2, February 2024, pp. 69–74.
0099-1112/22/69–74
© 2024 American Society for Photogrammetry and Remote Sensing
doi: 10. 14358/PERS.90.2.69

Figure 1. Accuracy Star Field Set-Up.

Figure 2. Checkerboard and Circular Panels Used for Automated Accuracy Assessment.

tions to correct the point cloud can be automatically computed from a single 3Dtarget, but when three or more 3D targets are deployed the algorithm can solve for a full 6-degree translation and rotation correction of the point cloud while quantifying both vertical (Z) and radial (XY) accuracy. The corrections can be saved for reference or automatically applied to the point cloud depending on the workflow.

A recent field test was performed with our partners at Earl Dudley, LLC to assess the accuracy of a TrueView 680 (Riegl VUX-based design) drone lidar survey of a highway intersection. A single Accuracy Star (AS) was set up over a known survey point. Two passes of the TrueView 680 were flown and the data post-processed in LP360 to a georeferenced and strip-matched point cloud. The target detection algorithm identified the AS in the point cloud with a high degree of confidence due to the point density and open sky above the target. The XYZ offsets measured using the AS were used to automatically apply a correction to the point cloud. The adjusted point cloud was then compared to 21 photogrammetric panel points surveyed by total station and digital level. The resulting RMSE(z) was 0. 33 cm (0. 011 feet). The surveyed positional accuracy RMSE(z) (First Component) of the AS was 0. 5 cm (0. 016 feet) (Second Component) for a final total RMSE(z) for the lidar surface of 0. 57 cm (0. 019 feet).

The use of 3D targets such as the Accuracy Star is not always required on a project. By extending the target detection algorithm to work with more traditional checkerboard targets and concentric circle targets, examples of which are shown in Figure 2, the same automated tools can be applied. This allows for XYZ offsets and corrections to be automatically extracted from the 2D targets, but not a full 6-degree solution with rotation. This is a practical intermediate use case for most surveyors; a more rigorous solution than traditional survey nails (Z assessment only) but requiring less set-up and hardware than a full set of 3D targets.

PRECISION

For lidar datasets, precision is commonly interpreted as the repeatability of the point data without regard to survey control or network accuracy. Practically it is a measure of the noise or "fuzziness" of the point cloud on a hard surface such as a road or roof. Many factors contribute to the precision of a given lidar sensor; laser shot noise, sensor stability, consistency of the position solution, rigidness of the calibration and boresight to name a few. The ASPRS Standard defines two measures of precision of interest to lidar data users; within-swath (intraswath or smooth surface precision) which applies to data from a single pass of the instrument, and swath-to-swath, (or interswath precision) which applies to data in the overlap area of two or more passes.

Historically, assessment of precision has been done by determining the noise level of the point cloud on test surfaces (e. g. , impervious hard surfaces). Recommended test methods include creating an elevation difference raster and computing a RMSE between min/max elevations (smooth surface) or between flight lines (interswath dZ) in each cell or performing a planar fit to the test surface and reporting the standard deviation of the fit. These values are then compared to the precision tolerances allowed for a given vertical accuracy class (see Table 7. 2 in the Standard). The general guideline is that the smooth surface precision (within swath) should be no greater than 0. 6x the vertical accuracy class required for the derived map product. Restrictions on the allowable swath-to-swath value for a given Quality Level (QL) level are also documented.

The test methods for smooth surface precision (within swath) are limited to spot-checking areas and often are labor-intensive, for example to identify suitable test plots for the analysis. They do not scale well to large projects. The Standard does not state a specific number of test points for precision assessment but does recommend testing precision "to the greatest extent possible" (see Section C. 10). A more automated, comprehensive test of the precision achieved over the entire project area is desirable. To develop such methods, we have been investigating applying computational geometry techniques based on a Principal Component Analysis (PCA) of the point cloud across the entire dataset. We want a rigorous, automated way to measure precision (noise) on smooth surfaces across both large and small data sets and present both qualitative and quantitative results back to the user. We want the measurements to be unbiased with respect to local slope and curvature of the terrain. We also assume no apriori information on the location of these smooth surfaces is available.

The approach we have been developing involves calculating the standard deviation along the surface normal (SDASN) for a given cell size across the entire project area. To accomplish this, we apply a Principal Component Analysis (PCA) to measure the local linearity, planarity, and sphericity of the neighborhood. While this analysis could be run for each individual point using a spherical neighborhood in 3D space, for computational efficiency we use a raster approach with a 2D grid and apply the PCA analysis to each cell in the grid. This gives us linearity, planarity, and sphericity, along with the standard deviation along the surface normal (SDASN) for each cell. This also gives us an estimate of local curvature for each cell by calculating the corresponding surface variation from the PCA parameters.

The measurement of smooth surface (intraswath) precision follows directly from the above analysis. The algorithm identifies cells with a high level of planarity, a low level of sphericity, and an absence of local curvature. Cells that meet these criteria are taken as planar (smooth) but are not necessarily horizontal. They have a SDASN that is an unbiased (by local slope and curvature) measure of precision of the point cloud in that cell. Unlike a basic dZ check that measures min/max elevation differences in a cell, SDASN quantifies the deviation of the points perpendicular to the planar fit to the local surface. We rasterize the entire grid to colorize the cells for qualitative analysis (like the popular "dZ" rasters used for overlap assessment) and extract the numerical values for a quantitative statistical analysis. The analysis can be restricted to only planar cells within a single flight line (intraswath) or planar cells with multiple flight lines (interswath), depending on the use case. The user is presented with a greyscale or colorized raster that highlights only those planar surfaces that exceed the specified value (for Pass/Fail testing) or based on a color ramp of user-defined bands. Quantitative measurements of the precision can also be extracted during the analysis. This approach allows for rapid assessment of lidar data precision in an automated and comprehensive method across the entire project area, automatically identifying those surfaces appropriate for precision testing.

Several examples of SDASN analysis are presented below from field tests conducted using a TrueView drone lidar system for small site testing and using publicly available 3DEP lidar data for broad area tests. All analysis was performed in the LP360 software suite using SDASN tools in development for future release.

The 3DEP project chosen for testing was from Utah; UT_StrawberryRiver_2019. This area is forested, with steep elevations and limited road access. The test data comprised 152 LAS files covering ~100 sq. mi. with 100 GB of QL1 data. The data was previously ground classified, allowing for the SDASN analysis to be performed against the ground surface. An example of the resulting raster product is shown in Figure 3. This is a 5 sq. mile area rasterized with 2 m pixels showing the relative SDASN (noise) values from Low (Black) to High (White) for the ground class. Terrain structure is revealed along with areas of high relative noise in the point cloud that indicate potential problem areas.

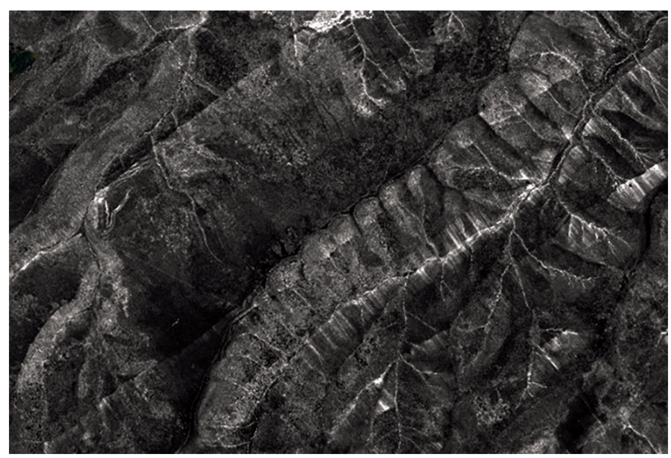

Figure 3. SDASN Raster Showing Low-to-High Precision (Noise).

The choice of cell size is an interesting one and we are continuing to investigate this parameter. For a rigorous PCA result, we want 10+ points per cell. The confidence level of the results drops off as we move to less dense data. Practically, we think this means we will need at least four points per sq. m to achieve minimum acceptable results. Our approach works well for QL1 or better data (or on dense drone lidar datasets) but will be less reliable for sparser QL2 data. We are investigating ways to increase the reliability with less dense data (beyond just increasing the cell size) to get more reliable results with QL2 data sets.

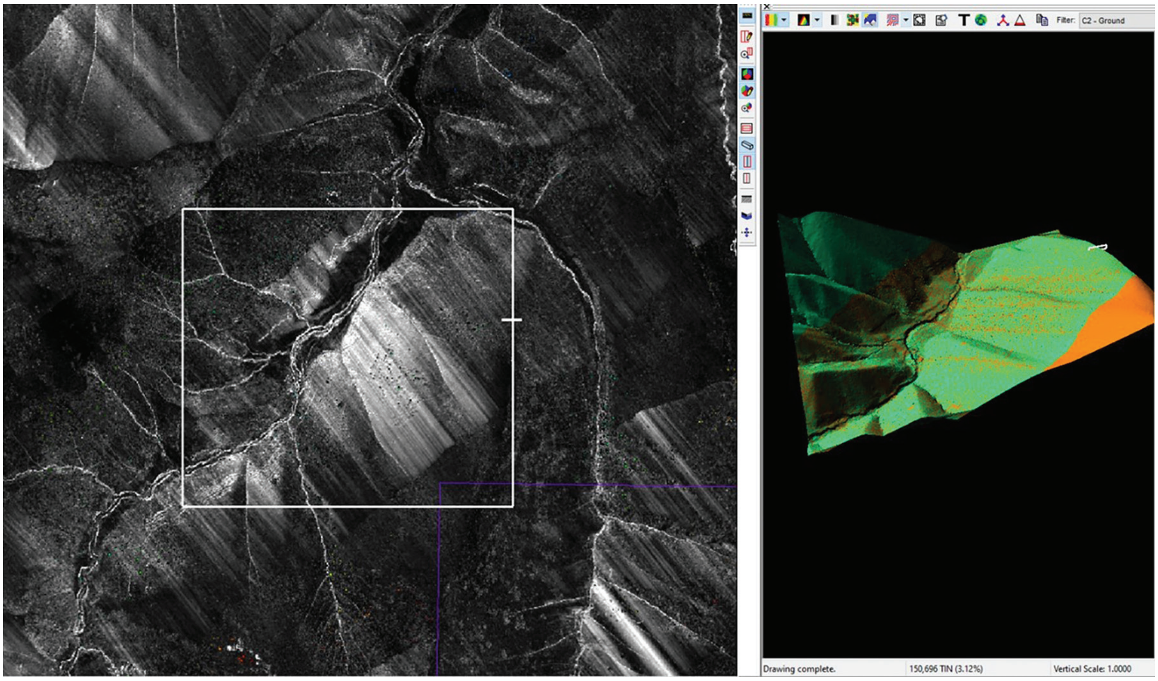

Figure 4. High SDASN Sections (White) Along Steep Slopes.

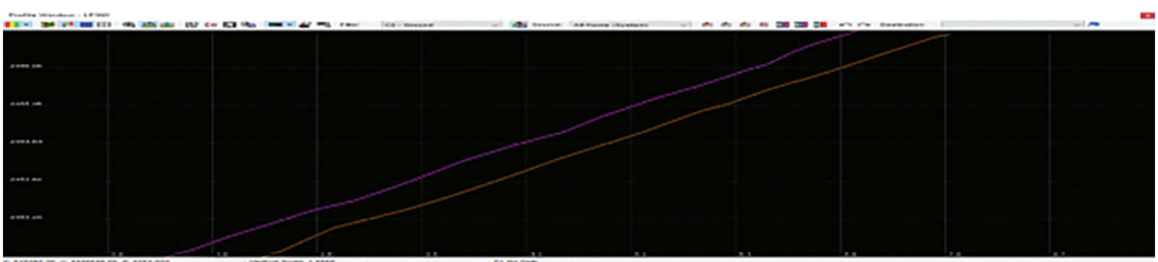

Figure 5. Dynamic Drift Between Flight Lines in High SDASN Areas.

Investigating the potential problem areas, Figure 4 and Figure 5 show a section of high noise on the side of a steep slope that, upon closer investigation, reveals a dynamic drift between flight lines that increases to a maximum of 45 cm before returning to within tolerance further along the flight line. Due to the remote location and lack of flat, open surfaces, such a dynamic error would not have been identified by the traditional sample plot testing for swath-to-swath precision.

Investigating small sites surveys, Figure 6. shows a SDASN raster for a drone lidar (TrueView 535) flight used to assess sensor calibration and boresight. In this use case the PCA analysis has been limited to only 0. 5 m planar cells. The colorization is from Low/Green (< 2 cm) to High/Red (> 8 cm) and shows the smooth surface precision (intraswath) on flat surfaces (the road, parking lots, and building roofs). The point data is unclassified. RMSE of the precision was 1. 2 cm.

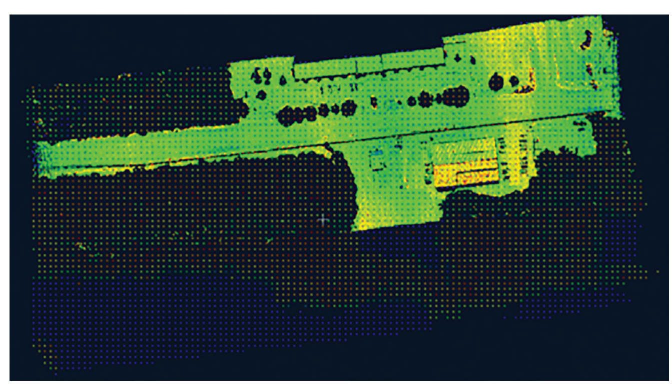

Figure 6. SDASN Raster of Planar Surfaces on Drone Lidar Calibration Site.

Continued on next page

Finally, as a secondary use for SDASN, we have been examining using the rasters to assist in the QC of the lidar ground surface. Misclassifications of the ground points often characterize as deviations from a smooth surface and an SDASN analysis can make these areas visually "pop" for the reviewer in the QC raster. We are investigating how to optimize this use case further and extend it to other features such as buildings. Figure 7. shows an example of a bust in the ground class easily identified in the SDASN QC raster.

In conclusion we have observed significant improvements in the efficiency and the reliability of quality checks performed on lidar point clouds by using automated 3D target detection for accuracy assessment and data correction and Standard Deviation Along Surface Normal (SDASN) analysis for precision assessment over an entire project area. These techniques apply equally well to both large and small project sites.

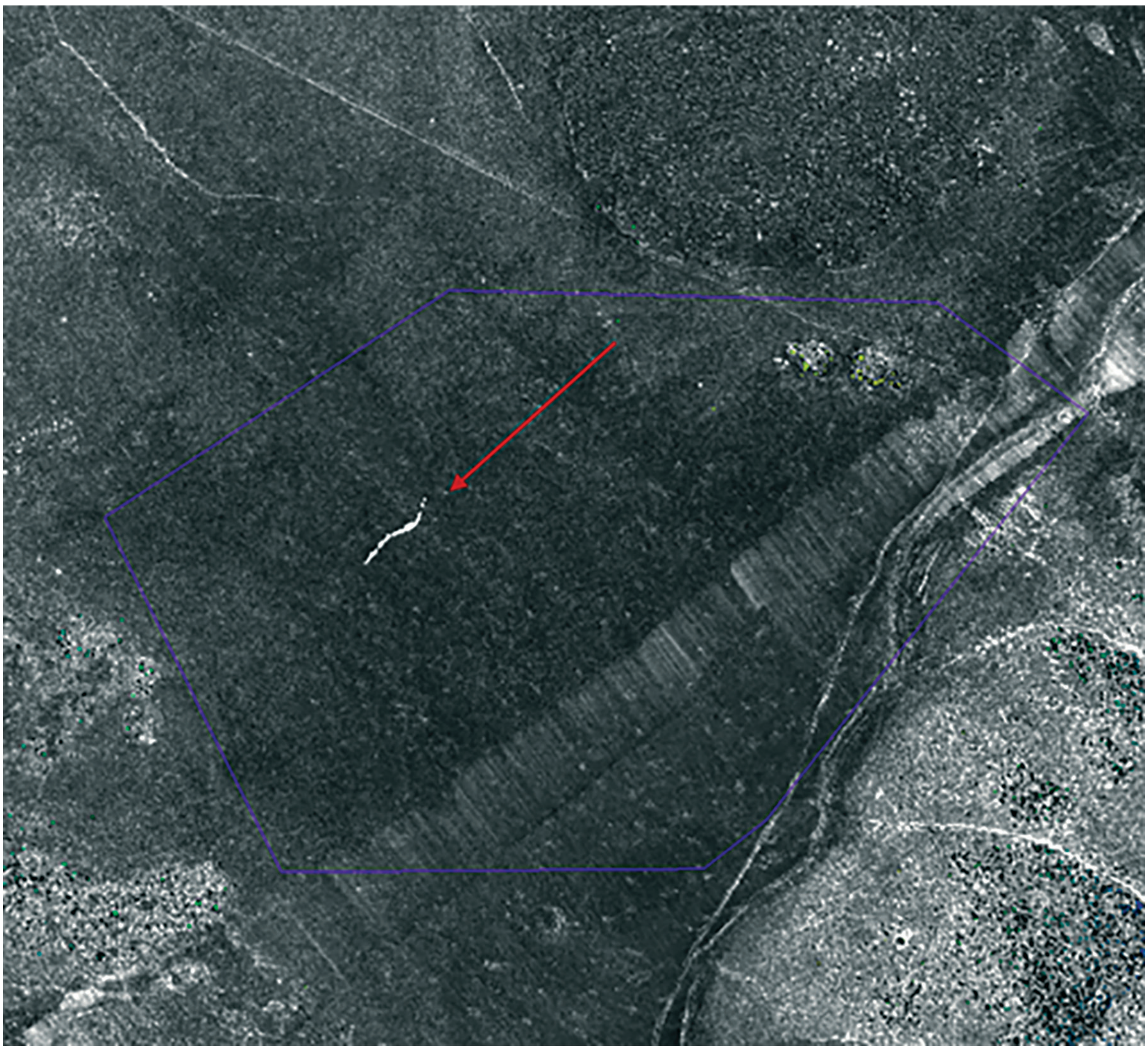

Figure 7. Poor Ground Classification Identified by High SDASN Values.

GIS
Tips & Tricks

By Al Karlin, Ph.D. CMS-L, GISP

Some Old Habits Die Hard

As with so many of my recent columns, this month's tips originated with questions from my GIS class. This semester (Fall 2023) at the University of Tampa, we updated the Esri software from ArcGIS Desktop and moved right into ArcGIS Pro 3.1. So, for some GIS students this was the first ArcGIS version that they experienced, while for others, not so. For those continuing students, some of the most perplexing issues (and there are many when switching from Desktop to Pro) are the bracketed red ellipses [...] that they found frequently in their map legends, as well as, how to select/unselect the items for the map legend. So, this month's Tips focus on changes between how the map legends are constructed in ArcGIS Desktop and ArcGIS Pro.

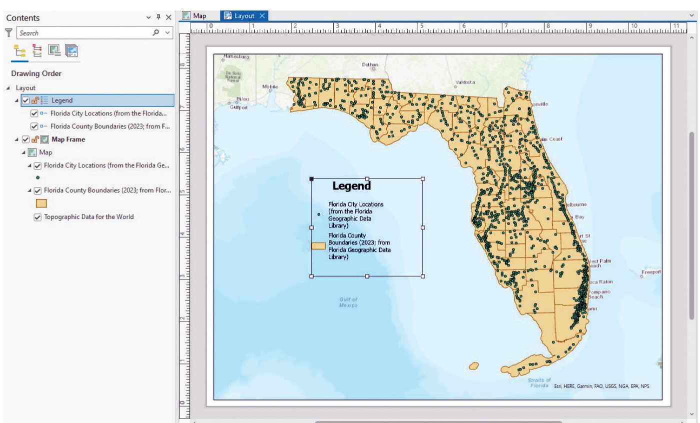

Figure 1. Default ArcGIS Pro map legend showing word wrapping for layers with multiple word titles.

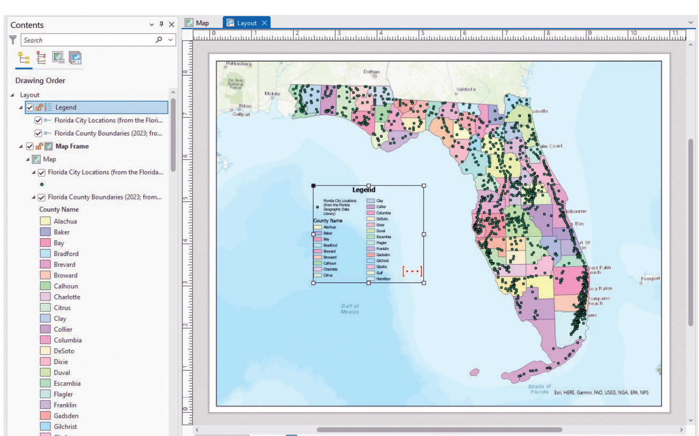

Figure 2. Red bracketed ellipses [...] appear when there are hidden elements in the map legend.

Tip #1 — The Red Bracketed Ellipses [...]

In ArcGIS Desktop, when the layer (feature class) titles in the legend contain numerous characters and there is insufficient space in the map legend, depending on your selection for the map legend format, ArcGIS Pro just word wraps to fill the available space as in Figure 1. Notice that I included the citation (from the Florida Geographic Data Library) in the title of each feature class and the word wrapped entries in the map "legend" (a pet peeve that I'll address later.)

When I change the symbology to include the name of each county, the dreaded red bracketed ellipses [...] appear as in Figure 2.

The red bracketed ellipses are indicating that there is hidden text (or features) that are not being displayed in the map legend. The fix is really pretty easy, in most cases, all you need to do is click and drag a corner of the map legend box, expanding it to accommodate the hidden text (or features) as in Figure 3.

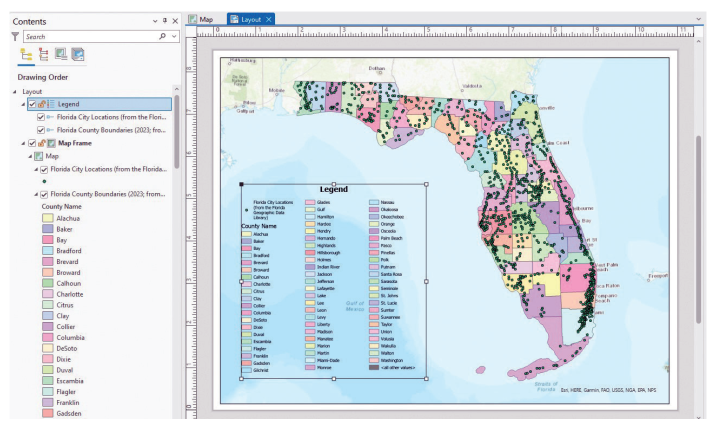

Figure 3. Expanding the map legend box to reveal the hidden text.

You may see multiple red bracketed ellipses (Figure 4) while you adjust the size of the map legend, so just keep adjusting the size of the map legend until the entire text (or features) are displayed in the map legend and the red bracketed ellipses are removed.

Photogrammetric Engineering & Remote Sensing
Vol. 90, No. 2, February 2024, pp. 75-77.
0099-1112/22/75-77
© 2024 American Society for Photogrammetry and Remote Sensing
doi: 10.14358/PERS.90.2.75

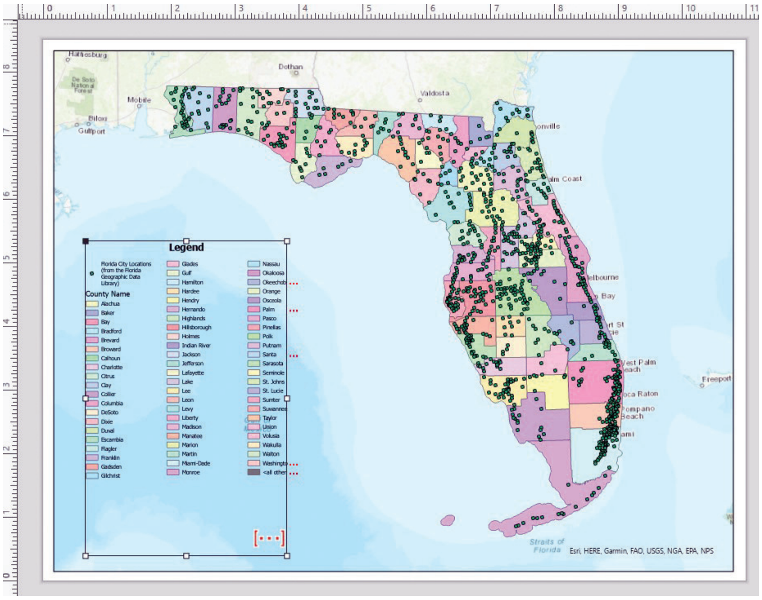

Figure 4. Multiple red bracketed ellipses [...] may appear while expanding the map legend box.

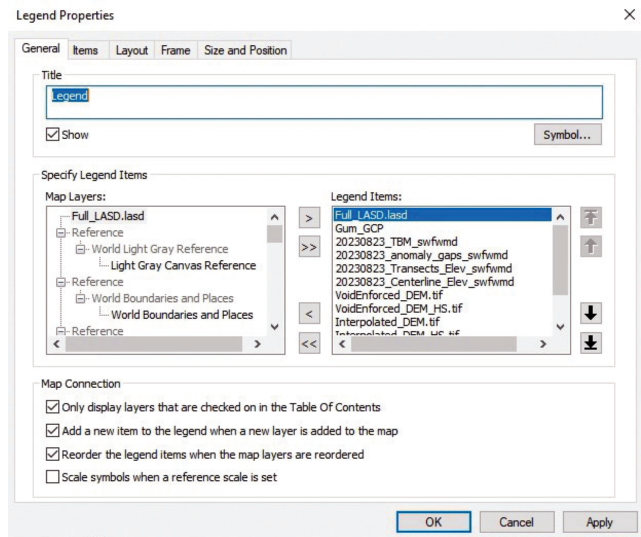

Figure 5. The ArcGIS Desktop Legend Properties window used to select items for the map legend.

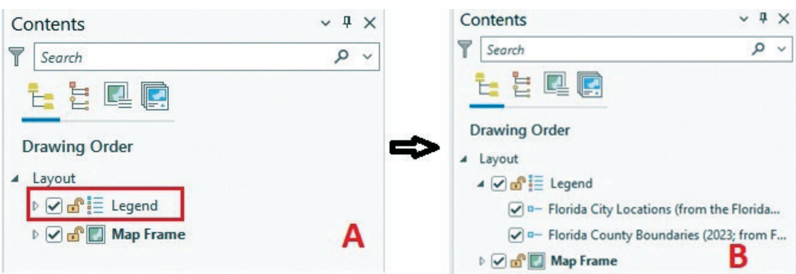

Figure 6. Clicking on the arrow next to the Legend object (6A) expands the legend to show the layers (6B) which can be turned off by clearing the checkbox.

Tip #2 — Removing Layer Names from the Map Legend

In the Esri software, the feature classes checked "on" in the Contents panel are displayed on the layout, but previous Esri software from ArcView (for those oldies) to ArcGIS Desktop used a selection panel in the Legend Properties (Figure 5) to select which feature classes would be displayed in the map legend.

In ArcGIS Pro, this functionality has been moved to the Contents panel on the Layout. When the Layout is constructed, the Legend object is collapsed (Figure 6a). Simply click on the arrow to the left of the Legend (Figure 6b) to expand this object and check on (or off) layers for display in the legend.

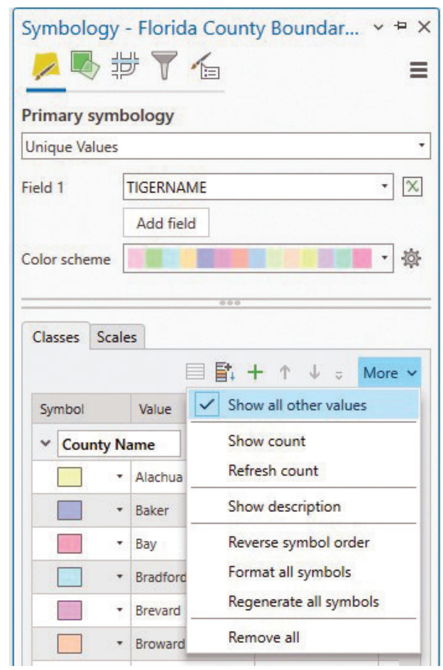

Figure 7. To remove the <all other values> text from the map legend, clear the check box from the More dropdown.

Tip #3 — Remove the <all other values> from the Map Legend

When you choose the Primary Symbology as Unique Values, ArcGIS Pro defaults to including the <all other values> item in the legend. Of course, in most cases, when you use the Unique Values symbology, you are showing all of the possible classes and the <all other values> should be turned off. To remove the <all other values> text from the legend, open the Symbology pane for the layer, and on either the Classes or Scales tab, expand the "More" button and uncheck the "Show all other values" item (Figure 7.)

Tip #4 — Remove "Legend" from the Map Legend

A personal pet peeve of mine is when a student (or any cartographer for that matter) leaves the default word "Legend" as the title for the map legend. For me, either simply remove it, i.e. no title, or replace the default with something meaningful. At first glance, it is a little confusing because on the Element | Legend pane, there appear to be two places where the word "Legend" appears; first in the Options | General space and again in the Legend | Title space. To customize the legend title, replace the Legend | Title with something meaningful (Figure 8) or uncheck the Title | Show box to produce a title-less legend.

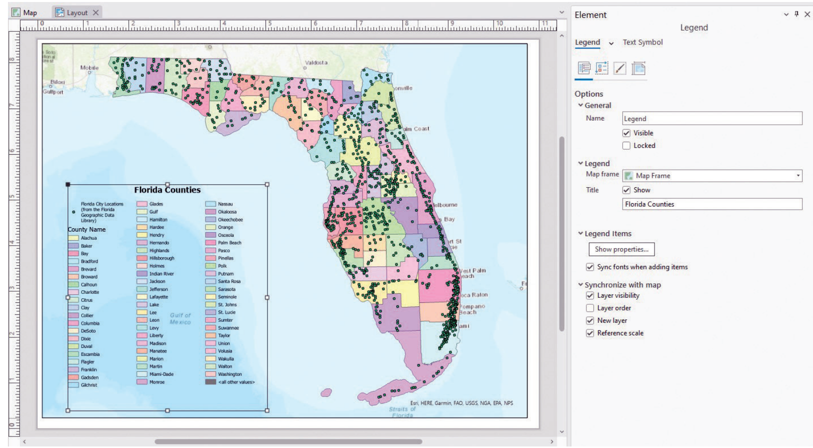

Figure 8. Use the Legend |Title, not the General | Name to customize the legend. You can also clear the Title | Show checkbox to remove the map legend title text.

Send your questions, comments, and tips to GISTT@ASPRS.org.

Al Karlin, Ph.D., CMS-L, GISP is a senior geospatial scientist with Dewberry's Geospatial and Technology Services group in Tampa, FL. Al works with all aspects of lidar, remote sensing, photogrammetry, and GIS-related projects. Al also teaches Mapmaking for the Social Sciences and Geographic Information Systems at the University of Tampa.

The layman's perspective on technical theory and practical applications of mapping and GIS

MAPPING MATTERS

YOUR QUESTIONS ANSWERED

by Qassim Abdullah, Ph.D., PLS, CP

Woolpert Vice President and Chief Scientist

- **Have you ever wondered about what can and can't be achieved with geospatial technologies and processes?**
- **Would you like to understand the geospatial industry in layman's terms?**
- **Have you been intimidated by formulas or equations in scientific journal articles and published reports?**
- **Do you have a challenging technical question that no one you know can answer?**

If you answered "YES" to any of these questions, then you need to read Dr. Qassim Abdullah's column, Mapping Matters. In it, he answers all geospatial questions—no matter how challenging—and offers accessible solutions.

Send your questions to Mapping_Matters@asprs.org

To browse previous articles of Mapping Matters, visit http://www.asprs.org/Mapping-Matters.html

"Your mapping matters publications have helped us a lot in refining our knowledge on the world of Photogrammetry. I always admire what you are doing to the science of Photogrammetry. Thank You Very much! the world wants more of enthusiast scientists like you."

"I read through your comments and calculations twice. It is very clear understandable. I am Honored there are experienced professionals like you, willing to help fellow members and promote knowledge in the Geo-Spatial Sciences."

asprs THE IMAGING & GEOSPATIAL INFORMATION SOCIETY

ASPRS MEMBERSHIP

WHERE DO YOU WANT TO GO? WHOM DO YOU WANT TO BECOME?

Joining ASPRS is a great way to boost your resume and learn valuable life lessons

WHY GET INVOLVED WITH ASPRS?

- Develop leadership skills
- Experience working on a team
- Gain valuable soft skills
- Network
- Learn about yourself
- Have fun!

Scholarships

The many ASPRS scholarships are only available to student members

Certification

The ASPRS certification program for mapping scientists, photogrammetrists and technologists is the only fully Accredited certification program in the geospatial sciences

Continuing Education

Earn professional development hours and CEUs by attending workshops at our conferences and on-line as well as our monthly on-line geobytes series

PE&RS

Our monthly journal, is packed with informative and timely articles designed to keep you abreast of current developments in your field. Now available in e-format.

Get Connected

facebook.com/ASPRS.org

linkedin.com/company/asprs/about/

twitter.com/ASPRSorg

youtube.com/user/ASPRS

Image and text courtesy the ASPRS Florida Region

asprs FLORIDA REGION THE IMAGING & GEOSPATIAL INFORMATION SOCIETY




Robert Ryerson, Brian Huberty,
Lauren McKinney-Wise, and Hamdy Elsayed

The Value of Membership in the American Society for Photogrammetry and Remote Sensing

Introduction

We have asked a number of members of the ASPRS to tell us what they see as the value proposition for ASPRS membership. Simply stated, our colleagues believe that ASPRS membership is a "vital resource" at every stage of one's career. As one contact told us, the ASPRS provides a "robust platform for networking that seamlessly spans academia, industry and government…fostering connections with like-minded individuals." The value in professional growth comes from these contacts, mentoring, and ready access to technical information, workshops, and conferences. That is not to say that social media are not useful but, in general, the ASPRS provides deeper, broader, and more personal interactions and hence more valuable contacts, information, and connections. But the true value is seen in the numerous outcomes that result from membership in the ASPRS. It is important to note that these outcomes tend to be additive – they build over time as one travels through the different and unique stepping stones of their geospatial careers.

Student

Like many, two of the authors of this column were interested in the use of remote sensing and mapping tools to gather information – in one case forestry and in the other agriculture. The ASPRS is a natural home for those students who have begun to explore the usefulness in their home fields of the technologies dealt with by the ASPRS. These "home fields" can include agriculturalists, foresters, geologists, planners, biologists, civil engineers and many others. It is from others who have followed this path in the past that useful lessons have been learned and applied anew as awareness grows of the usefulness of our technologies.

In many cases students found that the ASPRS served to introduce them to faculty members whose interests meshed with their own, helping them better focus on education that led to the best career path. Other benefits and useful outcomes included making a contact that directly led to employment and finding mentors who have jump-started careers. Another outcome from ASPRS membership found in all phases of a career is the development of lasting friendships, often developed while pursuing volunteer opportunities in the ASPRS.

The networking-related benefits noted above have been associated with regional and student chapters as well as conferences, workshops, and columns in the journal. And of course, beneficial outcomes also include lower cost access to key manuals and publications. Finally, we have seen older students become mentors for those who are younger and just starting out on their voyage of discovery. That sort of mentor activity pays dividends for both the mentor and mentee.

Early Professional

After college the ASPRS continues to provide value to the early professional. Again, many of the benefits are associated with connecting with others. One respondent told us that for "my first entry level job, I was hired by someone who I knew through ASPRS. Without that connection, I wouldn't be where I am today! ASPRS has been integral to my growth as an early professional."

The importance and value ascribed to supporting the needs of the early professional are seen in the ASPRS's Early Career Professionals Council. The continuing value for the early professional can include keeping up with how newer technology can be used in an operational setting to better meet the needs of one's employer. At the same time the ASPRS helps continuously expand one's community, linking the early professional to friends and future co-workers. These outcomes can be met through access to workshops, podcasts, the Journal, conferences, student chapters, regional meetings and other sources of information provided by the ASPRS. By the same token, early professionals can improve their career prospects through the information sources noted, as well as involvement in appropriate technical workshops. There is no better way to meet potential mentors and like-minded professionals than at ASPRS meetings and the more formal mentor programs that the ASPRS supports. And, as noted for students, early professionals can often serve in the role of mentor for those less experienced and by so doing build confidence and leadership skills.

Photogrammetric Engineering & Remote Sensing
Vol. 90, No. 2, February 2024, pp. 79-80.
0099-1112/22/79-80

© 2024 American Society for Photogrammetry
and Remote Sensing

doi: 10.14358/PERS.90.2.79

Mid-Career

The beneficial outcomes associated with ASPRS membership for mid-career professionals continue to expand over one's career. As one respondent noted "the society's firm commitment to professional growth has been a cornerstone of my career advancement. The access to conferences, workshops, and publications has not only kept me abreast of the latest trends and technologies in photogrammetry and remote sensing but has also provided a dynamic forum for engaging with industry experts and thought leaders from around the globe."

The opportunities to be involved through the ASPRS are numerous and interesting to the wide range of members the Society attracts. One respondent noted the opportunity developed under the auspices of the ASPRS to participate in collaborative research projects. Another noted the opportunity to be involved in the development of manuals and standards. An ASPRS member at the mid-career phase can often be involved as a volunteer committee member, workshop or pod-cast leader, on the Board or serving as a regional executive. One member noted that one of the most rewarding activities at mid-career and beyond has been mentoring.

With more experience and contact with others, those in the mid-career phase of their careers become candidates for one of the several professional certifications offered by the Society. Recognized in the US and around the world. ASPRS certifications and standards are "a testament to ASPRS's commitment to promoting excellence and professional standards within the geospatial field." These standards and certification activities lead to an important set of outcomes. These include building leadership skills, establishing a solid professional reputation, and learning from being a volunteer in the ASPRS' many technical activities. Lastly, there is the continuing nurturing of the friendships that the ASPRS is so well known for cultivating.

Senior Science Manager/Leader

The ASPRS plays a key role in the management and application of the science and technology with which the Society is engaged. Many members will become senior managers and leaders of organizations that develop and apply the science and technologies with which we work. At this stage of their careers, they may, for example, influence the transitioning of outdated approaches to those that bring improved efficiency and accuracy. In this case the beneficial outcome is for the organization – which in turn reflects on the organization's leader.

Long-time members who have become leaders have usually availed themselves of the many opportunities in the ASPRS to network and build a community of friends and colleagues upon which they can rely in their new roles. Indeed, several leaders responding for this column have attributed reaching this stage in their career to being active ASPRS members. Quite simply, the importance of developing a personal community earlier in a career pays off now.

At the same time, we know that many of those leading organizations that require our technologies to do the work with which they have been entrusted have come up through other fields and do not have the expertise in the spatial sciences that is often called for – and always needed. These leaders need the trusted voice and technical materials that the ASPRS members provide.

The senior science manager/leader is often found giving back to and through the ASPRS by hosting local meetings, providing student tours and serving as mentors. "That is what leaders do!"

Retirees

As a retiree the senior author has many reasons to remain an ASPRS member, as do many of those I first met almost fifty years ago. What is most important? We all still enjoy being part of a vibrant and exciting community. In that sense, we have come full circle from where we began in the student phase of our careers.

Authors

Robert "Bob" Ryerson is a Fellow of the ASPRS. He joined the ASPRS as a student member in 1968 and over the years has served on the ASPRS Board and several committees. He is a former Director General of the Canada Centre for Remote Sensing and is the retired President of Kim Geomatics Corporation. He held the designation CMS (RS115) until his retirement.

Brian Huberty (CMS 130RS) joined the ASPRS as a student member in 1982. Brian has served on the ASPRS Board, Primary Data Acquisition Division Director and Western Great Lakes Region President. He also co-chaired the 2011 ASPRS National Conference in Milwaukee. Brian is the past remote sensing leader for the U.S. Fish & Wildlife Service. He currently serves as the President of the Minnesota Forestry Association where he is mapping and monitoring our natural carbon storage factories - our forests.

Lauren McKinney-Wise is the former ASPRS Student Advisory Council Chair and has been active in her local student ASPRS chapter since 2016. She also helps to lead a local Women in GIS group. She was selected as one of the 23 GIS professionals to watch in 2023 by XYHeight magazine and recently completed her master's at Portland State University.

Hamdy Elsayed is an accomplished professional with over 17 years of global geospatial expertise, He obtained his Ph.D. in Geomatics Engineering from Toronto Metropolitan U, Canada. Presently, he is the Innovation Manager at Teledyne Geospatial, a co-editor of the ASPRS Sector Insight column, and serves on the board of directors for the Canadian Remote Sensing Society.

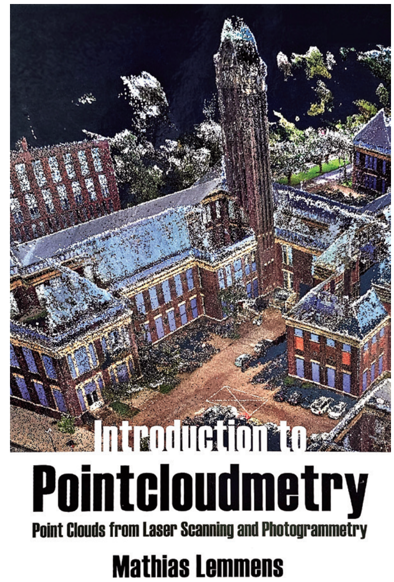

Introduction to Pointcloudmetry

Mathias Lemmens

Whittles Publishing Ltd.: Scotland, UK. 2023. ISBN 978-184995-479-2.

Reviewed by Toby M. Terpstra, Instructor, Society of Automotive Engineers (SAE) and Senior Visualization Analyst III, J.S. Held, Colorado.

Introduction to Pointcloudmetry, is as a geometrics reference book for point clouds derived from both lidar and multi-view photogrammetry. This book is structured as a textbook and covers electromagnetic energy, principles of light, photogrammetry, and lidar followed by the applications of point clouds to the geometrics discipline. Various software, interpolation, filtering, and visualization methods are then introduced and build upon the previously introduced concepts. The book title term "pointcloudmetry" is introduced as a "subbranch of geomatics" and the author asserts that this term "encompasses the technologies for obtaining accurate and detailed information about earth related objects, including bare earth surface, by acquiring and processing point clouds."

Chapters one through three deal with the electromagnetic spectrum, laser light, and the sources and characterizations of point clouds. The properties of lasers including divergence, reflectance, and refraction are covered, as are various contemporary uses for point clouds. These first three chapters are useful for establishing a basic understanding, and for those already familiar with these areas, these chapters serve as an excellent reference.

Chapters four through seven focus on the acquisition of point clouds. Chapter four focuses entirely on point clouds created through multi-view or photoscanning photogrammetry. It explains how software uses different types of image mapping to create three-dimensional coordinates from a series of photographs with varied camera coordinates. The author notes that "Usually, commercial software appears to be a black box, and reading the manual alone is not enough." The principles of photogrammetry are covered including feature-based image mapping, and least-squares image matching. Chapter five focuses on aerial lidar and covers various sensor types, multi-beam systems, georeferencing, point density, and how systematic errors can be accounted for and largely eliminated. Chapter six focuses on terrestrial laser scanning (TLS), or ground-based lidar, and mobile laser scanning (MLS). The difference between pulse based and phase shift scanners is discussed, targets for scan registration and simultaneous localization and mapping (SLAM). Automatic classification of points is also covered including a benefit comparison of point-based and segmentation-based classification methods. Chapter seven covers geodata acquisition, ground sample distance (GSD) for photoscanning photogrammetry with drones, and differences and potential pitfalls for lidar based point cloud density vs. sampling intervals. Validation and accuracy of digital elevation models (DEM) are also discussed.

Chapters eight through ten focus on DEMs, interpolation, and filtering. Chapter eight focus on the importance of DEMs and their uses, how they are derived from point clouds, taxonomy, triangular irregular networks (TINs), and sampling. Chapter nine deals with the importance of interpolation, and various methods of interpolation including, spatial, spline, TIN, bilinear, natural nearest, local polynomial, Gaussian, and interpolation weights. Chapter ten focuses on ground filtering, how filtering is used for point cloud classification, the complexity of non-ground classes, the reconstruction of a ground surfaces, and quality measures.

Chapters eleven through thirteen are focused on the three-dimensional mapping of point clouds as opposed to the 2.5D mapping in chapters eight through ten. Chapter eleven covers feature detection or automated detection of interest points in both imagery and point clouds. Concepts covered in this chapter are directly related to chapter four and include least-squares adjustment, edge detection, and operators that have been developed to aid in computer vision applications, and machine learning. Chapter twelve covers contemporary software used for processing point clouds including software for point clouds generated through lidar, photoscanning photogrammetry, feature extraction, and

Photogrammetric Engineering & Remote Sensing
Vol. 90, No. 2, February 2024, pp. 81-82.
0099-1112/22/81-82

© 2024 American Society for Photogrammetry and Remote Sensing

doi: 10.14358/PERS.90.2.81

various applications. Chapter thirteen covers pilot studies for various applications including road maintenance and inventorying, railway inspections and mapping, power line mapping, cultural heritage, mining, forestry, fire monitoring, and even gaming. It also covers the idea of integrating both lidar from TLS and UAS photogrammetry.

While this book focuses on point clouds as related to geomatics and delves into the specific benefits and uses in certain fields, other disciplines may also find inadvertent benefit. Professionals in industries that currently utilize point clouds such as aerospace, architecture, construction, crime investigation, forensics, and medicine may also see the application of various filtering, feature detection, and processing methods presented.

There is an ever-changing, driven, and competitive group of software and hardware manufactures, and developers that surround both point cloud generation and processing. The constant growth in this area can make up-to-date resources difficult to find. *Introduction to Pointcloudmetry*, Point Clouds from Laser Scanning and Photogrammetry, serves as a needed resource. Readers may look for future versions of this book to cover these technological advances with updated materials.

Introduction to Pointcloudmetry, is well-organized and covers point cloud data collection, processing, and application from beginning to end. This structure makes it well suited as a foundational resource for GIS students and professionals looking to better understand the power of point clouds, how they are derived, and to incorporate newer software, filtering, and processing methods.

STAND OUT FROM THE REST

EARN ASPRS CERTIFICATION

ASPRS congratulates these recently Certified and Re-certified individuals:

RECERTIFIED PHOTOGRAMMETRIST

Sean Kampe, Certification #R1644CP
Effective December 21, 2023, expires December 21, 2028

David H. Spradley, Certification #R1212CP
Effective October 11, 2023, expires October 11, 2028

Andrew M. Mitchell, Certification #R1647CP
Effective February 22, 2024, expires February 22, 2029

John A. Schmitt, Certification #R1389CP
Effective January 27, 2024, expires January 27, 2029

Clay D. Smith, Certification #R939CP
Effective January 11, 2024, expires January 11, 2029

William L. Johnson, Certification #R1643
Effective November 2, 2023, expires November 2, 2028

Scott Dodson, Certification #R1167CP
Effective November 29, 2023, expires November 29, 2028

David McKay, Certification #R1114CP
Effective January 2, 2024, expires January 2, 2029

Kevin Reid, Certification #R1557CP
Effective October 27, 2023, expires October 27, 2028

CERTIFIED PHOTOGRAMMETRIST

Cengiz Yagcioglu, Certification #CP1676
Effective December 23, 2023, expires December 23, 2028

RECERTIFIED MAPPING SCIENTIST UAS

Jason Rolfe, Certification #R015UAS
Effective November 3, 2022, expires November 3, 2027

RECERTIFIED MAPPING SCIENTIST LIDAR

Andrew M. Mitchell, Certification #R040L
Effective February 22, 2024, expires February 22, 2029

RECERTIFIED MAPPING SCIENTIST GIS/LIS

Michael Seidel, Certification #R298GS
Effective January 23, 2024, expires January 23, 2029

Brandon Tilley, Certification #R267GS
Effective January 10, 2024, expires January 10, 2029

CERTIFIED MAPPING SCIENTIST LIDAR

James Quirin, Certification #L085
Effective December 26, 2023, expires December 26, 2028

ASPRS Certification validates your professional practice and experience. It differentiates you from others in the profession. For more information on the ASPRS Certification program: contact **certification@asprs.org**, visit **https://www.asprs.org/general/asprs-certification-program.html.**

asprs THE IMAGING & GEOSPATIAL INFORMATION SOCIETY

Lyman J. Ladner

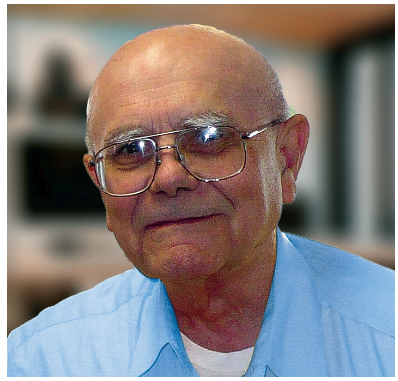

1934-2023

Lyman Ladner was born July 5, 1934 on a farm in Colorado. After high school graduation, wanting to "see the world," Lyman joined the US Marine Corps. The Corps, however, had other ideas for him. While stationed at Camp Pendleton in Southern California, the baseball coach noticed Lyman's athletic abilities. Lyman then spent his military career playing baseball at USMC camps throughout the US.

Following his discharge, Lyman worked for General Electric as an electronics assembler. He then took an assignment installing telecommunications equipment in Casper, Wyoming, where he met his future wife, Marguerite, who was also originally from Colorado. They moved and settled in Denver, Colorado, where they were married. Lyman then applied for a job with the US Geological Survey as a negative engraver. He later transferred to the USGS facility in Menlo Park, California, where he eventually become a photogrammetric compiler working on every analog stereoplotter used in the Western Mapping Center (WMC). He became very interested in photogrammetric science and took a leave of absence to study photogrammetry at ITC in The Netherlands. Following his return to Menlo Park, Lyman continued working as a compiler; however, he really wanted to apply the training he received at ITC and was eventually transferred to the aerotriangulation group. He also went to night school at San Jose State University where he received a BS degree in mathematics. Lyman later studied analytical photogrammetry at the University of California Berkley under Professor James M. Anderson.

Continuing his career, Lyman became the Chief of the Technology Office, where he and his team were responsible for developing the Digital Orthophoto (DOQ) production software. This development led to the WMC becoming the DOQ Center for the USGS.

Lyman, along with personnel from USGS headquarters and other federal agencies, developed the initial DOQ pilot project into a full production operation at WMC. The DOQ production effort eventually evolved into the National Digital Orthophoto Program at USGS. He was awarded the US Department of the Interior's Meritorious Service Award for his efforts. In 2020 he, along with his development team, were recognized nationally by the ASPRS with its Outstanding Technical Achievement Award. Eventually, Lyman advanced to become the Assistant Chief of the WMC Research and Development Office, the position he held until his retirement.

Throughout Lyman's career, he never lost sight of the objectives of the USGS and his role in it. As he moved up in the organization he was always mindful of his co-workers and colleagues and tried to be helpful to them in achieving their goals. He was particularly encouraging to new employees as they began their careers at USGS. Beyond work, he was also helpful to his friends and volunteered in numerous community activities. He continued his love of baseball by routinely attending baseball games at Stanford University until he departed the Bay Area.

Lyman eventually moved to Southern California so that Marguerite, who had by then developed dementia, could spend time with her family. His devotion to Marguerite was unquestionably his first priority. Lyman was a devoted husband, gentleman, scholar, professional, and a friend to all who met him. He will be sorely missed by his many friends and acquaintances.

Journal Staff

Editor-In-Chief
Alper Yilmaz, Ph.D., PERSeditor@asprs.org

Associate Editors
Ravishankar Dwivedi, Ph.D., rsdwivedi51@gmail.com
Valérie Gouet-Brunet, Ph.D., valerie.gouet@ign.fr
Petra Helmholz, Ph.D., Petra.Helmholz@curtin.edu.au
Dorota Iwaszczuk, Ph.D., dorota.iwaszczuk@tum.de
Desheng Liu, Ph.D., liu.738@osu.edu
Clement Mallet, Ph.D., clemallet@gmail.com
Sidike Paheding, Ph.D., spahedin@mtu.edu
Norbert Pfeifer, np@ipf.tuwien.ac.at
Rongjun Qin, Ph.D., qin.324@osu.edu
Ribana Roscher, Ph.D., ribana.roscher@uni-bonn.de
Zhenfeng Shao, Ph.D., shaozhenfeng@whu.edu.cn
Filiz Sunar, Ph.D., fsunar@itu.edu.tr
Prasad Thenkabail, Ph.D., pthenkabail@usgs.gov
Dongdong Wang, P.h.D., ddwang@umd.edu
Qunming Wang, Ph.D., wqm11111@126.com
Ruisheng Wang, Ph.D., ruiswang@ucalgary.ca
Jan Dirk Wegner, jan.wegner@geod.baug.ethz.ch
Bo Wu, Ph.D., bo.wu@polyu.edu.hk
Michael Yang, Ph.D., michael.yang@utwente.nl
Hongyan Zhang, zhanghongyan@whu.edu.cn

Contributing Editors

Highlight Editor
Jie Shan, Ph.D., jshan@ecn.purdue.edu

Feature Articles
Michael Joos, CP, GISP, featureeditor@asprs.org

Grids & Datums Column
Clifford J. Mugnier, C.P., C.M.S, cjmce@lsu.edu

Book Reviews
Sagar Deshpande, Ph.D., bookreview@asprs.org

Mapping Matters Column
Qassim Abdullah, Ph.D., Mapping_Matters@asprs.org

GIS Tips & Tricks
Alvan Karlin, Ph.D., CMS-L, GISP akarlin@Dewberry.com

SectorInsight
Youssef Kaddoura, Ph.D., kaddoura@ufl.edu
Bob Ryerson, Ph.D., FASPRS, bryerson@kimgeomatics.com
Hamdy Elsayed, Hamdy.Elsayed@teledyne.com

ASPRS Staff

Assistant Director — Publications
Rae Kelley, rkelley@asprs.org

Electronic Publications Manager/Graphic Artist
Matthew Austin, maustin@asprs.org

Advertising Sales Representative
Bill Spilman, bill@innovativemediasolutions.com

ASPRS ANNOUNCES THEIR 2024 NATIONAL ELECTION RESULTS

Join us at the Installation of Officers on Tuesday, February 13th at 8:00 AM (MT) at Geo Week 2024.

- **Vice President AL KARLIN**
- **GIS Assistant Director MICHAEL BARANOWSKI**
- **UAS Assistant Director REBECCA CAPPS**
- **PAD Assistant Director JAE SUNG KIM**
- **Lidar Assistant Director NORA MAY**
- **Committee Chairs Council DAVID DAY**
- **Early-Career Professionals Council GREG STAMNES**
- **Student Advisory Council OSCAR DURAN**
- **Sustaining Members Council PAUL BADR**

NEW ASPRS MEMBERS

ASPRS would like to welcome the following new members!

Ahmed Abdelmaged, GISP
Jacob Andresen
Daniel Bartlett
David Brandt
Laura Carson
M. Sean Chenoweth, Ph.D.
Steve Dickey
Joshua Ellis
Taryn Edward Girard
Marcus Glass
Hannah Victoria Herrero, Ph.D.
Alan Jamison
Steven Jones
K. K. Muyalde Kabasares, Ph.D.
Erin Lammott
Russ Henry Large
Angelos Leiloglou
Lily Lindros
Brody Manquen
Christopher Jacob Mulhollad
Philip Nalla
Alex John Nies
Victoria Oluwademilade Olajide
Olubusola Oluseun Oludele
Christian “Alex” Prichard
Damon S. Rushing
Maryn Sanders
Steven Sarich

FOR MORE INFORMATION ON ASPRS MEMBERSHIP, VISIT
HTTP://WWW.ASPRS.ORG/JOIN-NOW

Remote Sensing Application in Water Quality of Lake Burdur, Türkiye

Aylin Tuzcu Kokal, Meltem Kacikoc, Nebiye Musaoglu, and Aysegul Tanik

Abstract

The advancements in space technology have facilitated water quality (WQ) monitoring of lake conditions at a spatial resolution of 10 m by freely accessible Sentinel-2 images. The main aim of this article was to elucidate the necessity of spatiotemporal WQ monitoring of the shrinking Lake Burdur in Türkiye by examining the relation between field and satellite data with a state-of-the-art machine learning-based regression algorithm. This study focuses on detection of algal blooms and WQ parameters, which are chlorophyll-a (Chl-a) and suspended solids (SS). Furthermore, this study leverages the advantage of geographic position of Lake Burdur, located at the overlap of two Sentinel-2 frames, which enables the acquisition of satellite images at a temporal resolution of 2–3 days. The findings enrich the understanding of the lake's dynamic structure by rapidly monitoring the occurrence of algal blooms. High accuracies were achieved for Chl-a (R-squared: 0.93) and SS (R-squared: 0.94) detection.

Introduction

Water bodies are susceptible to a range of factors, including mainly anthropogenic activities and changes in water temperature, leading to water quality (WQ) deterioration that further harm the organisms living in water (Gholizadeh *et al.* 2016; Wu *et al.* 2023). One such case is possible in connection with the increasing sea surface temperature trend of the Sea of Marmara from 2015 to 2021, and the marine mucilage phenomenon experienced in 2021 (Tuzcu Kokal *et al.* 2022). Water pollution not only has adverse impacts on marine ecosystems, such as increasing phytoplankton biomass, changing the composition of phytoplankton species, deteriorating clarity and aesthetic appeal, taste and odor of water, the emergence of health problems, decreasing dissolved oxygen, and elevated risk of fish deaths, but it also affects terrestrial ecosystems by changing the structure of soil, plants, and animals (Smith *et al.* 1999). Given the severe impacts of the water pollution on both water and land, and considering the vital importance of WQ, it is essential to establish a robust monitoring system for the purpose of preserving their quality. While conventional methods are capable of measuring WQ with high accuracy, surveying wide regions frequently requires more time and cost. Monitoring WQ, such as algal blooms (Rodríguez-López *et al.* 2023), and marine mucilage (Tuzcu Kokal *et al.* 2022), necessitates high temporal resolution. Furthermore, the measurement of chlorophyll-a (Chl-a) can be subject to variability in objectivity, as it may be influenced by personal factors of the individual conducting the measurement. Through improvements in remote sensing technology, the detection of water pollution has been enhanced with various satellite platforms, including MODIS, Landsat, Sentinel, WorldView, and others (Gholizadeh *et al.* 2016). Therefore, satellite images (SI) have been used due to their ability to monitor wide and/or inaccessible regions in a comparatively more WQ researches (Gholizadeh *et al.* 2016; Blix *et al.* 2018; Peterson *et al.* 2019). The statistical regression models have been used to detect WQ parameters from spectral information (Gholizadeh *et al.* 2016). However, the parametric methods may not have sufficient capability to model complex relationships between SI and WQ parameters. To address this, the enhanced capabilities of non-parametric and machine learning (ML) algorithms, such as Gaussian process regression (GPR), in modeling complex relationships have already provided remarkable benefits (Peterson *et al.* 2019).

The choice of Lake Burdur for the current study was due to its brackish characteristic. Reduction in water flow from the rivers that supply freshwater, resulting from their utilization for agricultural purposes, has led to a decline in the water quantity of the lake (Benliay 2017).

Firatli *et al.* (2022) examined Lake Burdur from 1985 to 2020 by Landsat and precipitation data and concluded that the primary drivers of striking conditions were due to the effects of climate change and to over-utilization of water. There are still limited scientific studies on monitoring the WQ of Lake Burdur in a continuous and systematic manner by remote sensing (RS) data obtained via SI. In particular, the use of ML based regression algorithm coupled with SI to detect WQ has not been extensively researched to date. To address this literature gap, the current study aimed to detect concentration changes of Chl-a and suspended solids (SS), the two important WQ parameters that may be detected by RS technology of the shrinking Lake Burdur by establishing a linkage between WQ and RS data by a state-of-the-art ML algorithm. S2 images were selected due to its adequate spatial and high temporal resolution capability (SUHET 2013). As such, the study aims to assess these two parameters both spatially and temporarily with the key idea of deriving the variation in WQ over time.

Materials and Methods

Study Area and Data Used

Lake Burdur, a major lake in Türkiye, is located in the Burdur Closed Basin at an elevation of 805 m and a depth of 100 m (Firatli *et al.* 2022), which has experienced algal blooms (Figure 1).

A consistent decrease was observed in the lake's surface area over time (Firatli *et al.* 2022). Measurements were conducted at the same five stations in both of the cruises (Figure1). A set of satellite and field data were used. Samples were collected on 26 July 2019 and on 10 August 2022. Chl-a was extracted with 90% acetone and measured spectrophotometrically with a UV-visible spectrophotometer. Suspended solids were dried at 103–105°C and analyzed via the gravimetric method. The results of experimentation carried out in the laboratory of Environmental Engineering Department of Süleyman Demirel University (SDU) are tabulated in Table 1.

Aylin Tuzcu Kokal and Nebiye Musaoglu are with Istanbul Technical University (ITU), Faculty of Civil Engineering, Department of Geomatics Engineering, 34469 Maslak, Istanbul, Türkiye.

Meltem Kacikoc is with Süleyman Demirel University (SDU), Faculty of Engineering, Department of Environmental Engineering, 32260, Isparta, Türkiye.

Aysegul Tanik is with Istanbul Technical University (ITU), Faculty of Civil Engineering, Department of Environmental Engineering, 34469 Maslak, Istanbul, Türkiye.

Corresponding author: Aylin Tuzcu Kokal (tuzcuay@itu.edu.tr)

Contributed by Tolga Bakirman, June 10, 2023 (sent for review October 12, 2023; reviewed by Vagner Goncalves Ferreira, Osman Salih Yilmaz).

Photogrammetric Engineering & Remote Sensing
Vol. 90, No. 2, February 2024, pp. 85–87.
0099-1112/22/85–87

© 2024 American Society for Photogrammetry and Remote Sensing
doi: 10.14358/PERS.23-00040R2

PEER-REVIEWED CONTENT IS ONLY AVAILABLE TO ASPRS MEMBERS AND SUBSCRIBERS

FOR MORE INFORMATION VISIT MY.ASPRS.ORG

PEER-REVIEWED CONTENT IS ONLY AVAILABLE TO ASPRS MEMBERS AND SUBSCRIBERS

FOR MORE INFORMATION VISIT MY.ASPRS.ORG

Gain a professional advantage with

ASPRS CERTIFICATION

A growing number of scientific and technical disciplines depend on photogrammetry and the mapping sciences for reliable measurements and information.

It is in the interest of those who provide photogrammetric and mapping sciences services, as well as the user of these services, that such information and data be accurate and dependable.

The ASPRS Certification Program has as its purpose the establishment and maintenance of high standards of ethical conduct and professional practice among photogrammetrists, mapping scientists, technologists, and interns.

asprs THE IMAGING & GEOSPATIAL INFORMATION SOCIETY

ASPRS offers certification in the following areas

Photogrammetry

Remote Sensing

GIS/LIS

Lidar

UAS

Each area has 2 levels of certification

✓Mapping Scientist

✓Technologist

All exams offered via computer based testing through Prometric.com

asprs.org/certification

The Sight-Aesthetic Value of the Underwater Landscapes of Lakes in the Context of Exploration Tourism

Piotr Dynowski, Anna Źróbek-Sokolnik, Marta Czaplicka, and Adam Senetra

Abstract

The aim of the study is to identify factors affecting the sight-aesthetic value of the underwater landscapes of lakes for the purposes of exploration tourism. The reason for undertaking this topic is the lack of such studies for inland water bodies.The results will contribute to expanding and supplementing the knowledge on the assessment of the sight-aesthetic attractiveness of landscapes and fill gaps in knowledge about the underwater landscapes of lakes. The questionnaire survey implemented the direct comparison method described by Kendall (Kendall, M. G. 1970. Rank Correlation Methods*. Charles Griffin and Co: Glasgow, Scotland). According to respondents, animals and submerged anthropogenic elements are the most visually attractive in an aquatic environment The results obtained are the reason for conducting further research and developing the methodology for the assessment of the sight-aesthetic value of inland bodies of water based on the experience of terrestrial landscape researchers.*

Introduction

The landscape is the subject of research in a number of scientific disciplines that take different views on the concepts of a landscape and become a platform for research into its structure and evolution processes. The landscape is constantly being transformed by the forces of nature and human activities (Aretano *et al.* 2013; Vroom 2006). The definition of a landscape is constantly evolving. The first mention of a landscape appeared in the Book of Psalms. Psalm 48 describes the beauty of Jerusalem's landscape, referring to the awe-inspiring fortifications (Batista *et al.* 2012; P*ismo Święte Starego i Nowego Testamentu: Najnowszy Przekład z Języków Oryginalnych z Komentarzem* 2009). The term landscape (Landschaft) was already used over 1000 years ago in Old High German. Initially, it was a term for an area (from Latin regio) and then for its character (Zonneveld 1990). During the heyday of Flemish painting in the 16th and 17th centuries, a landscape was understood as a background characterizing the surroundings in which the action or story was set. In other words, a landscape is the physiognomy of a part of a geographical space, with a set of objects characteristic of it (Bobek and Schmithüsen 1949). From an ecological perspective, a landscape is understood as an area of the Earth's surface (land) covered with a mosaic of interacting ecosystems with a specific structure found in similar form at different locations (Forman and Godron 1986). Definitions derived from English- and French-speaking countries have laid the grounds for research into the perception of the value of landscape aesthetic qualities. This research is primarily conducted by landscape architects (Aretano *et al.* 2013; Böhm 2004; Poikane *et al.* 2015; Tsunetsugu *et al.* 2013).

Not only is the concept of a landscape used in a physical sense but also in a social, political, or cultural sense. A cultural landscape is defined as a transition between culture and nature. From another perspective, it is defined as an attempt to organize a space in a cognitive and symbolic manner. In an indirect meaning that links these two approaches, a cultural landscape is a "dwelling perspective" (Bedyński 2019; Frydryczak 2013). In social or political terms, a landscape may reflect events, facts, and determinants characterizing or creating certain phenomena (for example, a political landscape, a landscape after the battle [Medvedev 1997]). *The Report on the Developments in the Political Landscape* is a document of the European Parliament that describes the evolution of domestic political contexts in all European Union member states (European Parliament 2019).

The literature on landscapes includes studies on seascapes, addressing the importance of tropical seascapes, i.e., mosaics of interconnected mangroves, seagrasses, and corals. Seagrasses are of great importance in providing ecosystem services. They are an important element in the management of fishing grounds, as well as water quality and biological diversity (de la Torre-Castro *et al.* 2014). The concept of a seascape as a view of the sea or a view of the boundlessness of the sea has been extended to include a landscape of the coast and the adjacent water areas, including views from land towards the sea, from the sea towards land, and along the coastline (Hill *et al.* 2001; Pungetti 2012).

The character of a landscape can be assessed based on judgments concerning its form, which is subject to visual perception resulting from the level of development. The physical characteristics that determine the value of seascapes, including underwater ones, can be divided into physical (e.g., the scale, openness, landform and shape, landscape patterns and foci) and perceptual (e.g., how a particular seascape is experienced, context, sense of remoteness and naturalness) (Falconer *et al.* 2013).

Thanks to advances in technology, detailed seabed models are becoming increasingly accurate and widespread. Three-dimensional underwater bottom models derived from acoustic, laser, or optical mapping provide an opportunity to determine the relationship between benthic morphology (including topographic complexity) and the aquatic organisms and communities (Brock and Purkis 2009; Wedding *et al.* 2011).

The first references to an underwater seascape date back to the 19th century. The term was used by deep-sea divers as early as the years 1940 to 1950. Since the 1990s, it has been used by French researchers. The underwater landscape is increasingly appearing in public and social spaces through pictures, films, and photographs and also through three-dimensional mapping technologies. Underwater landscapes are not presented as a completely isotropic areas. They are a reflection of a mosaic of habitats and shapes and the associated elements of nature, anthropogenic objects with environmental, social, and economic issues, and those requiring management and protection. The application of the term landscape to the underwater world results in the development of numerous definitions. The possible variations

Department of Socio-Economic Geography, Institute of Spatial Management and Geography, Faculty of Geoengineering, Uniwersytet Warmińsko-Mazurski w Olsztynie, Poland, 15 Romana 7 Prawocheńskiego Street, 10-720 Olsztyn, Poland.

Corresponding author: Marta Czaplicka (marta.czaplicka@uwm.edu.pl)

Contributed by Tolga Bakirman, July 6, 2023 (sent for review November 7, 2023; reviewed by Darijus Veteikis, Tolga Bakirman).

Photogrammetric Engineering & Remote Sensing
Vol. 90, No. 2, February 2024, pp. 89–97.
0099-1112/22/89–97
© 2024 American Society for Photogrammetry
and Remote Sensing
doi: 10.14358/PERS.23-00054R2

PEER-REVIEWED CONTENT
IS ONLY AVAILABLE TO
ASPRS MEMBERS AND SUBSCRIBERS

FOR MORE INFORMATION VISIT
MY.ASPRS.ORG

PEER-REVIEWED CONTENT
IS ONLY AVAILABLE TO
ASPRS MEMBERS AND SUBSCRIBERS

FOR MORE INFORMATION VISIT
MY.ASPRS.ORG

PEER-REVIEWED CONTENT
IS ONLY AVAILABLE TO
ASPRS MEMBERS AND SUBSCRIBERS

FOR MORE INFORMATION VISIT
MY.ASPRS.ORG

PEER-REVIEWED CONTENT
IS ONLY AVAILABLE TO
ASPRS MEMBERS AND SUBSCRIBERS

FOR MORE INFORMATION VISIT
MY.ASPRS.ORG

**PEER-REVIEWED CONTENT
IS ONLY AVAILABLE TO
ASPRS MEMBERS AND SUBSCRIBERS**

**FOR MORE INFORMATION VISIT
MY.ASPRS.ORG**

**PEER-REVIEWED CONTENT
IS ONLY AVAILABLE TO
ASPRS MEMBERS AND SUBSCRIBERS**

**FOR MORE INFORMATION VISIT
MY.ASPRS.ORG**

PEER-REVIEWED CONTENT
IS ONLY AVAILABLE TO
ASPRS MEMBERS AND SUBSCRIBERS

FOR MORE INFORMATION VISIT
MY.ASPRS.ORG

PEER-REVIEWED CONTENT
IS ONLY AVAILABLE TO
ASPRS MEMBERS AND SUBSCRIBERS

FOR MORE INFORMATION VISIT
MY.ASPRS.ORG

WHO'S WHO IN ASPRS

Founded in 1934, the American Society for Photogrammetry and Remote Sensing (ASPRS) is a scientific association serving thousands of professional members around the world. Our mission is to advance knowledge and improve understanding of mapping sciences to promote the responsible applications of photogrammetry, remote sensing, geographic information systems (GIS) and supporting technologies.

BOARD OF DIRECTORS

BOARD OFFICERS

President
Bandana Kar
U. S. Department of Energy (DOE)

President-Elect
Amr Abd-Elrahman
University of Florida

Vice President
Alvan Karlin, PhD, CMS-L, GISP
Dewberry

Past President
Lorraine B. Amenda, PLS, CP
Towill, Inc

Treasurer
John McCombs
NOAA

Secretary
Harold Rempel
ESP Associates, Inc.

COUNCIL OFFICERS

ASPRS has six councils. To learn more, visit https://www.asprs.org/Councils.html.

Sustaining Members Council
Chair: Paul Badr
Deputy Chair: Melissa Martin

Technical Division Directors Council
Chair: Hope Morgan
Deputy Chair: Tao Liu

Early-Career Professionals Council
Chair: Greg Stamnes

Region Officers Council
Chair: Demetrio Zourarakis
Deputy Chair: Cody Condron

Committee Chairs Council
Chair: David Day

Student Advisory Council
Chair: Oscar Duran
Deputy Chair: Ali Alruzuq

TECHNICAL DIVISION OFFICERS

ASPRS has seven professional divisions. To learn more, visit https://www.asprs.org/Divisions.html.

Geographic Information Systems Division
Director: Denise Theunissen
Assistant Director: Michael Baranowski

Lidar Division
Director: Ajit Sampath
Assistant Director: Nora May

Photogrammetric Applications Division
Director: Ben Wilkinson
Assistant Director: Jae Sung Kim

Primary Data Acquisition Division
Director: Srini Dharmapuri
Assistant Director: Ravi Soneja

Professional Practice Division
Director: Hope Morgan
Assistant Director: Christian Stallings

Remote Sensing Applications Division
Director: Tao Liu
Assistant Director: Indu Jeyachandran

Unmanned Autonomous Systems (UAS)
Director: Jacob Lopez
Assistant Director: Rebecca Capps

REGION PRESIDENTS

ASPRS has 13 regions to serve the United States. To learn more, visit https://www.asprs.org/regions.html.

Alaska Region
Dave Parret

Cascadia Region
Jimmy Schulz

Eastern Great Lakes Region
Craig Fry

Florida Region
Matt LaLuzerne

Gulf South
Cody Condron

Heartland Region
Whit Lynn

Mid-South Region
David Hughes

North Atlantic Region
Kurt Lutz

Northeast Region
Trevis Gigliotti

Pacific Southwest Region
Omar Mora

Potomac Region
Jason Brown

Rocky Mountain Region
Trent Casi

Western Great Lakes Region
Adam Smith

Crop Monitoring System Using MODIS Time-Series Data for Within-Season Prediction of Yield and Production of US Corn and Soybeans

Toshihiro Sakamoto

Abstract

In terms of contribution to global food security, this study aimed to build a crop monitoring system for within-season yield prediction of US corn and soybeans by using the Moderate Resolution Imaging Spectroradiometer (time-series data, which consists of three essential core algorithms (crop phenology detection, early crop classification, and crop yield prediction methods)). Within-season predictions for 2018–2022 were then made to evaluate the performance of the proposed system by comparing it with the United States Department of Agriculture's (USDA's) monthly forecasts and the fixed statistical data. The absolute percentage errors of the proposed system for predicting national-level yield and production were less than 5% for all simulation years as of day of year (DOY) 279. The prediction accuracy as of DOY 247 and DOY 279 were comparable to the USDA's forecasts. The proposed system would enable us to make a comprehensive understanding about overview of US corn and soybean crop condition by visualizing detail spatial pattern of good- or poor harvest regions on a within-season basis.

Introduction

According to the United Nations (The United Nations 2022), the global population was projected to reach eight billion by November 2022, and is projected to further increase to 9.7 billion by 2050. Based on this population growth, global food production will need to increase by 21% to meet the food demand over the next 27 years. The equilibrium between the global food supply and demand is maintained through the international food trade, which depends on exported food from a limited number of countries (Puma et al. 2015). There are a variety of international growing risks destabilizing the global food supply–demand balance, including the 2022 Russia–Ukraine war and the related international energy and fertilizer price hikes and global extreme weather events. The continental United States (US) suffered severe drought damage in 2022 (National Drought Mitigation Center 2022). Record-breaking floods have damaged two million acres of crops and orchards in Pakistan (Devi 2022). Therefore, satellite remote sensing is a powerful tool for the timely visual assessment of crop conditions on a continental scale. Through international policy coordination, the Group on Earth Observations Global Agricultural Monitoring Initiative provides scientific data from satellite observations on crop conditions and agricultural weather data, which is used for early warnings for global food crises using the Crop Monitor for AMIS and EARLY WARNING (https://earthobservations.org/geoglam.php). Remote sensing-based crop monitoring systems can play an important role in helping agricultural policy makers around the world, and for building an international consensus overview of the current global food supply and demand. Against this background, this study aimed to build a crop monitoring system for the US, the world' largest food exporter of corn and soybeans, using high-frequency observation satellite data.

Previous studies have shown that high-frequency observation satellite images such as Moderate Resolution Imaging Spectroradiometer (MODIS)/Terra and Aqua are effective for predicting US corn and soybean yields. These studies used the existing crop classification maps (i.e., the Cropland Data Layers (CDL)) to preliminarily identify the pixels which represent planted corn or soybeans (Bolton and Friedl 2013; Johnson 2014; Sakamoto *et al.* 2013; Sun *et al.* 2019). However, the model performance in many previous studies have not been sufficiently validated in terms of within-season applications because the CDL for current growing target crops was published in early February of the following year after the crop harvest. Moreover, not all studies compared prediction accuracies of the remote-sensing-derived predictions and the United States Department of Agriculture (USDA)-National Agricultural Statistics Service (NASS) monthly forecasts. Therefore, this study integrated three essential core algorithms (crop phenology detection, early crop classification, and yield prediction methods) to build a crop monitoring system that can predict US corn and soybean yields at a within-season time scale. The study aim was to evaluate the performance of the proposed system regarding the generation of an alternative intelligence source that could contribute to global food security. A within-season simulation analysis was conducted for 2018–2022 to explore the potential advantages.

Previous Studies Using High-Frequency Observation Satellite Data for Crop-Yield Prediction

There are two approaches in the use of explanatory variables on remote sensing-based crop-yield prediction systems: (1) Vegetation Index (VI) as the main variable for explaining yield variation; and (2) weather-related data (such as land surface temperature and precipitation) along with the VI.

Prior studies based on the first approach include the following. Ferencz *et al.* (2004) proposed a new indicator, called the General Yield Unified Reference Index, to estimate county- and country-level yields of seven crops (corn, wheat, sunflower, barley, potato, sugar beet, and alfalfa) in Hungary. This was calculated using the time integration values of the difference between the near-infrared and red reflectance observed by the National Oceanic and Atmospheric Administration (NOAA) Advanced Very High Resolution Radiometer (AVHRR). Mkhabela *et al.* (2011) found that the power function regression model using the running average 10-day composite MODIS-Normalized Difference Vegetation Index (NDVI) at certain timings could forecast the yields of four crops (barley, canola, field peas, and spring wheat) in Canada. Liu *et al.* (2019) evaluated the possibility of using MODIS-Enhanced Vegetation Index 2 (EVI2) to estimate grain yields of three major crops (corn, soybean, and winter wheat) grown in Ontario, Canada from 2003 to 2016. They established a multiple

Institute for Agro-Environmental Sciences, NARO, Division of Soil Environment Management Research, Agro-Environmental Informatics Group, Tsukuba, Ibaraki, Japan 305-8604.

Corresponding author: Toshihiro Sakamoto (sakamt@affrc.go.jp)

Contributed by Ravi Dwivedi, June 23, 2023 (sent for review September 11, 2023; reviewed by Manik H. Kalubarme, Markand Oza).

Photogrammetric Engineering & Remote Sensing
Vol. 90, No. 2, February 2024, pp. 99–119.
0099-1112/22/99–119
© 2024 American Society for Photogrammetry and Remote Sensing
doi: 10.14358/PERS.23-00052R2

linear regression model that accounted for the long-term yield trends by adding the year as an additional variable. Meng *et al.* (2014) compared MODIS-derived various spectral indices with corn yield data in Northeast China and found that the Land Surface Water Index showed the strongest correlation with the county-level corn yield 55–60 days after green-up date. Zhang and Zhang (2016) analyzed the NOAA satellite long-term AVHRR data and MODIS/Terra observations to develop a stepwise regression model using amplitude and integration values of EVI2 time-series data for monitoring interannual variation in global cereal yield from 1982 to 2012. Various types of linear or multivariate regression models were proposed to estimate or predict the US crop yields using phenology-related VI metrics, such as peak VI value, slope, and specific crop growth stage VI values, which were highly correlated with statistical yields of corn, soybean, wheat, and cotton (Becker-Reshef *et al.* 2010; Bolton and Friedl 2013; Ji *et al.* 2021, Johnson 2014; Johnson *et al.* 2021; Sakamoto *et al.* 2013, 2014). This study also used MODIS-derived VIs as the main explanatory variable in the crop-yield prediction model. An additional explanatory variable, "number of year" (Liu *et al.* 2019), was investigated to improve prediction accuracy and consider the long-term trends in increasing yields assuming that improvements of crop variety and agricultural technology occurred over the years.

As for using the second approach (weather-related data coupled with VI values), Kogan (1997) devised vegetation health indices using the AVHRR/NOAA vegetation condition index (VCI), which was calculated using the NDVI, temperature condition index (TCI), and brightness temperature of the thermal infrared band, to detect global drought-related vegetation stress. It was shown that the regression models based on VCI and TCI could accurately forecast deviations from normal yields, months before the harvests for winter wheat, sorghum, and corn in Kansas, USA (Kogan *et al.* 2012), and for corn in Jinlin Province, China (Kogan *et al.* 2005). Stepanov *et al.* (2020) developed the multivariate regression model using the MODIS-NDVI time-series with reanalysis data (precipitation, soil temperature, humidity, and photosynthetically active radiation) to predict soybean yield at the regional scale in the Khabarovsk district, Russia. Franch *et al.* (2019) proposed a new crop-yield model based on the Difference Vegetation Index and land surface temperature of MODIS/Terra and Aqua to estimate the national and subnational winter wheat yield in the US and Ukraine from 2001–2017. Prasad *et al.* (2006) developed the piecewise linear regression model with the breakpoint Quasi-Newton method that uses monthly average rainfall data, surface temperature, soil moisture, and monthly composite AVHRR-NDVI data for estimating corn and soybean yields in Iowa during 1982–2001. In recent years, crop-yield prediction models coupling MODIS-VIs with additional variables were proposed using machine learning algorithms (Sakamoto 2020; Schwalbert *et al.* 2020; Sun *et al.* 2019). Khaki *et al.* (2021) proposed the simultaneous yield prediction algorithm using a deep transfer learning algorithm to predict corn and soybean yields directly from the MODIS surfaces spectral reflectance and land surface temperature, without pre-calculating vegetation indices in the US Midwest.

Materials and Methods

Study Area

The study area covers a total of 37 states for which USDA statistical records are available (Supplemental Table 1). Maps of the county-level irrigated and harvested corn and soybean areas are shown in Figure 1. The major irrigated areas for corn and soybean cultivation are distributed in the region between Nebraska (NE) and Texas (TX), where groundwater is available from the Ogallala Aquifer (Green *et al.* 2018), and Arkansas (AR) and Mississippi (MS) along the Mississippi River (Figure 1C). The US was the world's largest exporter of corn (33%) and second largest exporter of soybeans (33%) after Brazil (45%) for 2021–2022 (USDA-FAS 2022a, 2022b). The majority of US corn and soybean production comes from a limited number of states. About 80% of the national corn production was harvested in the following 10 states (total share ranged from 78.3 to 83.8% during 2010–2022); Iowa (IA), Illinois (IL), Nebraska (NE), Minnesota (MN), Indiana (IN), South Dakota (SD), Kansas (KS), Ohio (OH), Wisconsin (WI), and Missouri (MO) and more than 80% of the total soybean production was harvested in 11 states (total share ranged from 80.1 to 83.9% during 2010–2022): IA, IL, MN, NE, IN, OH, SD, North Dakota (ND), MO, AR, and KS. In this study, the states with higher production volumes are referred to as "major producing states" and the other states as "minor producing states." Specifically, the top five major corn and soybean producing states were IA, IL, IN, MN, and NE, which accounted for more than 50% of the nation's corn and soybean production. These states cover most of the Corn Belt in the midwestern US and are spread

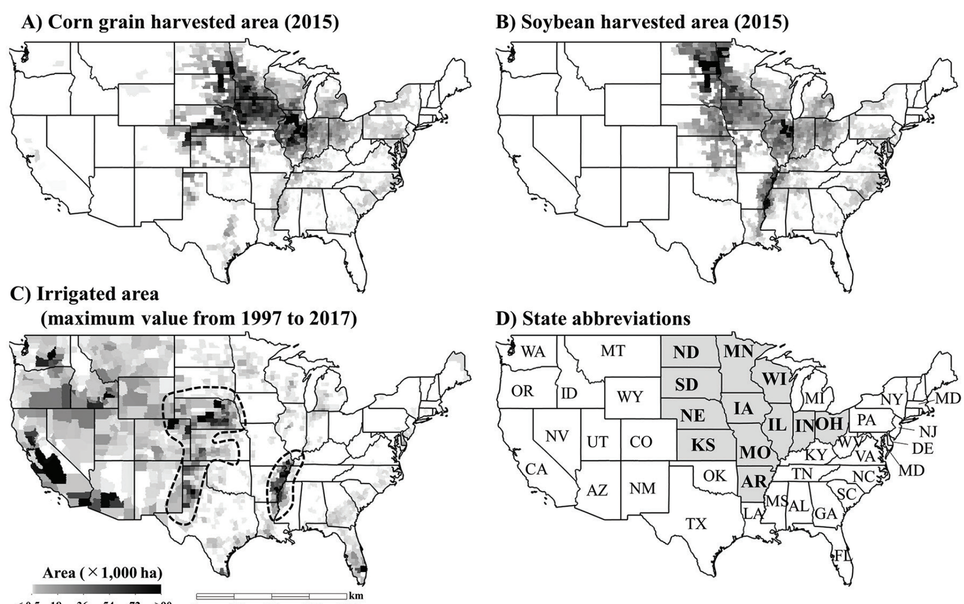

Figure 1. Maps of county-level harvested areas using the United States Department of Agriculture-National Agricultural Statistics Service (USDA-NASS) statistical data for 2015 for (A) corn grain; (B) soybeans; (C) county-level irrigated area ratio map derived from agricultural census data from 1997 to 2017, and (D) top 80% of corn grain- or soybean-producing states (filled in gray color), also showing the abbreviations for the US states. The major irrigated regions spreading over the Ogallala Aquifer and the downstream Mississippi River area are enclosed by dashed lines(C).

across non-irrigated areas (Figure 1C and 1D). This indicates that annual fluctuations in precipitation are directly related to yearly changes of US corn and soybean production.

USDA-NASS-Released Monthly Forecasts, Agricultural Statistical Data, and CDLs

The national- and state-level early forecasts of planted crop areas were published annually at approximately the end of June in the USDA-NASS Acreage Report (Supplemental Table 2). The state-level early forecasts of yield, production, and harvested areas were released monthly at mid-August, September, October, and November in the Crop Production Reports. These early forecasts were available only in 32 states for corn and 29 states for soybeans. The state- and national-level fixed statistical data were released in January of the following year in the Crop Production Annual Summary Report. The county-level fixed statistical data were uploaded on the online database "Quick Stats" in February of the following year (USDA-NASS 2023). As one of the explanatory variables for the Random Forest (RF)-based crop-yield prediction algorithm (Sakamoto 2020), the county-level irrigated ratios were calculated using USDA-NASS agricultural census records for 1997–2017 (Figure 1C). The multi-year maximum ratio between "agricultural harvested and irrigated cropland area" and "agricultural harvested area" was defined as the county-level irrigated ratio. The CDLs were also freely available through the USDA/NASS website (Johnson and Mueller 2010; USDA-NASS 2022). The CDL map projection was converted from Universal Transverse Mercator into Sinusoidal projection to overlap with the MODIS products. The fraction of corn, soybean, and other crops within each MODIS pixel of 231.7 m resolution was calculated from the CDL with a spatial resolution of 30 m. The threshold of the fraction was set to 80% to identify target corn and soybean pixels in accordance with the findings of the previous studies (Sakamoto 2018, 2021). The CDLs for 2008–2021 were used as training data of the RF-based regression algorithm using MODIS data for within-season early crop classification (Sakamoto 2021).

MODIS Surface Reflectance Products and Vegetation Index

In this study, the eight-day composite time-series data of the MODIS/Terra and Aqua Surface Reflectance products (MOD09A1, MOD09Q1, MYD09A1, and MYD09Q1, version: 6.1) from 2010 to 2022 were used, which are freely available from the National Aeronautics and Space Agency Administration Earthdata website (https://search.earthdata.nasa.gov/). The MODIS tile grids that cover the study area are as follows: h08v04, h08v05, h08v06, h09v04, h09v05, h09v06, h10v04, h10v05, h10v06, h11v04, h11v05, h12v04, h12v05, and h13v04. The surface reflectance layers of the red band (band 1, 620–670 nm) and near-infrared band ((NIR) band 2, 841–876 nm) of the MOD09Q1 and MYD09Q1 products were used for calculating the Wide Dynamic Range Vegetation Index (WDRVI) with a 231.7 m pixel resolution. The WDRVI (Gitelson 2004) was used because it had a stronger linear relationship with the green leaf area index (LAI) of corn and soybeans than the NDVI (Gitelson *et al.* 2007; Guindin-Garcia *et al.* 2012; Kira *et al.* 2017). The surface reflectance layers of the blue band (band 3, 459–479 nm) and the day of the year (DOY) for the pixels in the MOD09A1 and MYD09A1 products were resampled from a resolution of 463.3 to 231.7 m using the nearest neighbor method. These were then used for cloud cover detection and temporal weighting of data acquisition timing in the refined Shape Model Fitting method (rSMF) of crop phenology detection algorithm. The cloud covered pixels were defined by a blue reflectance value greater than 0.2. The WDRVI is calculated as follows (Equation 1):

$$\text{WDRVI} = (\alpha\rho_{\text{NIR}} - \rho_{\text{red}})/(\alpha\rho_{\text{NIR}} + \rho_{\text{red}}) \quad (1)$$

where ρ_{NIR}, and ρ_{red} are the NIR and red reflectance, and α is a weighting coefficient ($\alpha = 0.1$ was applied as per Sakamoto (2020)).

In this study, the time between the date of the MODIS product file name and the date when the prediction results would be available was assumed to be 14 days. This time lag included the waiting period for the MODIS data to become available on the website as well as the computing time for the calculation of the early crop classification and yield prediction. For example, the earliest prediction result, which was derived from the MODIS eight-day composite time-series data (DOY 65–201), was completed on 3 August (DOY 215), for a non-leap year (Supplemental Table 3).

Within-Season Prediction of Corn-Grain and Soybean Yields and Production

A flow chart of the data processing of within-season crop-yield prediction consists of three steps, as shown in Figure 2. First, an early crop classification map was created to identify the pixels which represent areas planted with corn or soybeans (Figure 2A). The early crop classification maps as of DOY 215 would be less accurate due to the uncertainty caused by the shorter MODIS observation period. The accuracy improves as the early prediction maps of emergence date and crop classification were sequentially updated in line with the MODIS observation period (Sakamoto 2021). Second, the county-level corn and soybean yields were predicted by the preliminarily trained algorithm

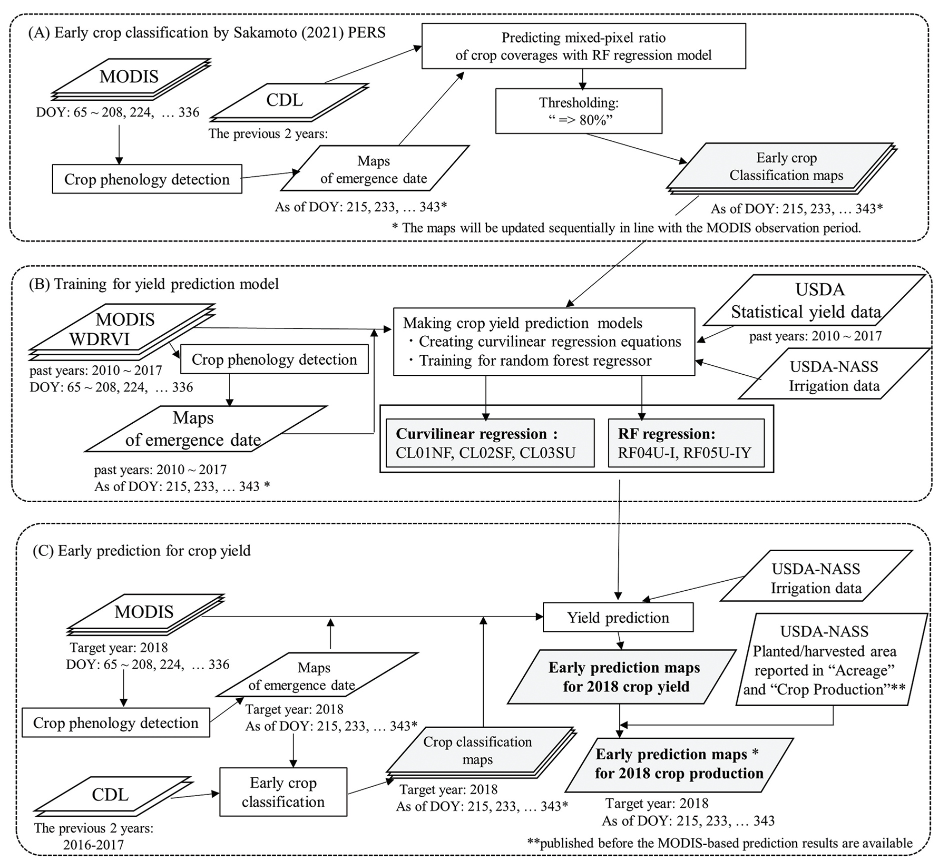

Figure 2. Flowchart of within-season crop prediction system for US corn and soybean production.

(Figure 2B). Third, the county-level predicted yields were aggregated to produce state-level yields using the early crop classification prediction maps (Figure 2C). The MODIS-based early crop classification algorithm was used to identify where to apply the MODIS-based yield prediction algorithm, and not to predict total planted area for corn or soybean. The total US corn or soybean production was also calculated on a within-season basis by multiplying with the preliminarily published state-level planted or harvested area data of the USDA-NASS monthly forecasts (Supplemental Figure 1). The normal yield was defined as the previous five-year average model-derived or statistical yields for each county separately and were used to create anomaly yield maps to visualize percentage variations from the normal yield.

Algorithm for Crop Phenology Detection: Refined-Shape Model Fitting Method

The rSMF method (Sakamoto 2018) had two functions for estimating crop emergence date and smoothing the time-series WDRVIs. The rSMF explored the optimal values of geometrically scaling parameters that fit the preliminarily defined shape model on the observed MODIS WDRVI data. The model then obtained the crop emergence date using the combination of the optimized values of the two parameters and the preliminarily calibrated phenological emergence parameter, using Equation 2:

$$\text{Xest} = \text{xscale} \times (\text{X0} + \text{tshift}) \tag{2}$$

where Xest is the estimated emergence date; xscale and tshift are the geometrically scaling parameter; and X0 is the phenological parameter of emergence (X0 = 147; for details, see Sakamoto (2018) and Sakamoto *et al.* (2010)).

Algorithm for Early Crop Classification

This study applied the RF-based crop classification algorithm (RF-CCA) using a random forest regression algorithm coded in the Python language (Sakamoto 2021). The RF-CCA performs machine learning based on a historical training data set, which uses the rSMF crop emergence date and the past two years of historical CDL data as explanatory variables to estimate the fraction of corn, soybean, and the other crops within each MODIS pixel. Then, MODIS pixels are classified into one of four classes: corn, soybean, the other crops, and mixture based on the fraction rate with a threshold of 80% (Sakamoto 2018, 2020). The MODIS pixels that showed predominantly corn or soybeans were identified every 16 days after 3 August on a within-season basis (Figure 2A). This RF-based mixed-pixel decomposition algorithm was trained on the state level. The amount of historical data increased with each year which provided additional input training data; therefore, the classification accuracy was expected to improve with each year.

Algorithms for Crop-Yield Prediction: Calibration for Curvilinear Regression Models and Training for RF-Based Regression Models

The yield prediction models were created or trained by curvilinear regression or RF regression using historical statistical data at the county level. In this study, five models were tested to compare the yield prediction performance. Three of these were curvilinear regression models (CL01NF; CL02SF, and CL03SU) and two were random forest regression models (RF04U-I and RF05U-IY); details of each model are described in Table 1. The CL01NF model used one common third-degree polynomial regression equation for the US, which was based on the relationship between county-averaged WDRVI and county-level statistical data (Sakamoto 2020) during the fixed calibration period (2010–2017). The timing of the highest correlation between them was preliminary investigated using historical statistical data (Sakamoto *et al.* 2014). This was set as the benchmark for existing simple prediction models (Johnson 2014; Meng *et al.* 2014; Sakamoto *et al.* 2013). The CL02SF model also used third-degree polynomial regression equations determined individually for each state. This was compared to the CL01NF model to investigate the effect of state-by-state fine tuning on prediction accuracy. The regression equations for CL02SF were calibrated only once using the fixed calibration period (2010–2017), as for CL01NF. The calibration approach of the CL03SU was the same as the CL02SF, except that annual recalibration was performed using annually updated and increased historical calibration data. For example, 2010 to 2017, 2010 to 2018, and so on, up to 2010 to 2021. The RF04U-I and RF05U-IY algorithms were based on RF regression models, commonly using county-averaged WDRVI, its squared value (WDRVI^2), and its cubic value (WDRVI^3) with an extra explanatory variable; the county-level irrigated ratio. Both algorithms also recalibrated the models annually for each state using annually updated training data. The use of county-level irrigated ratio in the RF-based regression models improved the yield prediction accuracy by correcting bias errors in irrigated regions (Sakamoto 2020; Sakamoto *et al.* 2013). The RF05U-IY algorithm considered the additional variable; "number of year" that was calculated by subtracting 2010 from the target year to correct model bias error assuming long-term increasing trends of potential crop yields. This was intended to evaluate the improved crop variety and agricultural technology, which could not be explained using only the annual variation of VIs. Except for CL01NF, the models could not predict the corn and soybean yield for the states where the historical county-level statistical data were not available, such as AR, Florida (FL), Oregon (OR), and Utah (UT). In the prediction model, although physiological stress during the reproductive stages can be assessed using weather and soil moisture data (Sakamoto 2020), it will require additional computational resources because of the increase in the volume of data with a high temporal resolution. Therefore, this study chose not to use weather and soil moisture data as explanatory variables to keep the computational scheme for the crop monitoring system as simple as possible for future operation on the Google Earth Engine.

Evaluation of Prediction Accuracy of Corn and Soybean Yields

The accuracy of the predicted crop yields was verified by comparing the USDA-NASS statistical data on county, state, and national levels with the following indices: root mean square error (RMSE); coefficient of variation (CV), absolute percentage error (APE); mean absolute percentage error (MAPE), and mean bias error (MBE), as per the following equations:

$$\text{RMSE}\ (t/ha) = \sqrt{\frac{1}{N}\sum_{i=1}^{N}\left(Y_i^{\text{MODIS}} - Y_i^{\text{NASS}}\right)^2} \tag{3}$$

$$\text{CV}(\%) = \left(\frac{\text{RMSE}}{\frac{1}{N}\sum_{i=1}^{N} Y_i^{\text{NASS}}}\right) \times 100 \tag{4}$$

$$\text{APE}(\%) = \left(\left|\frac{Y_i^{\text{MODIS}} - Y_i^{\text{NASS}}}{Y_i^{\text{NASS}}}\right|\right) \times 100 \tag{5}$$

Table 1. List of tested yield prediction models.

Model Name	Regression Method	Model Tuning Level	Training Data Period	Range of Statistical Data Used for Model Training	Number of Types of Explanatory Variables	
CL01NF	Curvilinear regression	National	Fix: 2010–17	Only counties with <10% irrigated ratio	1	WDRVI
CL02SF		State	Fix: 2010–17			
CL03SU			Updating: 2010–17, –18, ..., –21			
RF04U-I	Random Forest regression	State	Updating: 2010–17, -18, ..., –21	All	2	WDRVI, irrigated ratio
RF05U-IY			Updating: 2010–17, –18, ..., –21		3	WDRVI, irrigated ratio, number of year

$$\mathrm{MAPE}(\%) = \left(\frac{1}{N}\sum_{i=1}^{N}\left|\frac{Y_i^{\mathrm{MODIS}} - Y_i^{\mathrm{NASS}}}{Y_i^{\mathrm{NASS}}}\right|\right) \times 100 \quad (6)$$

$$\mathrm{MBE}\ (t / ha) = \frac{1}{N}\sum_{i=1}^{N}\left(Y_i^{\mathrm{MODIS}} - Y_i^{\mathrm{NASS}}\right) \quad (7)$$

where Y^{MODIS} is the model-derived prediction and Y^{NASS} is the USDA-NASS fixed statistical data.

Results and Discussion

Early Crop Classification Map

The temporal changes in crop classification accuracy were verified to reveal the spatial pattern of the kappa index at a county level for 2021 (Figure 3) and used to summarize various classification indicators at the national level for 2018–2021 (Supplemental Table 4). The central regions of the Corn Belt in the top five major crop producing states (IL, IN, IA, MN, and NE, Figure 1A and 1B) show higher kappa indices for the agreement levels, ranging from moderate (0.41–0.60) to substantial (0.61–0.80). The low production areas away from the Corn Belt (Figure 1) showed lower kappa indices of a poor to fair level (<0.41). Temporally, the kappa index for the classification accuracy gradually increased until DOY 279, after which no considerable changes were observed (Figure 3). Subsequent to DOY 215, the user's accuracy of corn and soybeans remained at a high level of 0.86 at the national level; however, the producer's accuracy gradually increased from 0.39–0.48 to 0.54–0.58 (Supplemental Table 4). The classification accuracy of the other crops was at the same level as that of corn and soybean (Supplemental Table 5). The main reason for the omission error was that pixels that should have been classified into the corn, soybean, or the other class were misclassified into the mixture class. This relationship was biased in time and space compared to the population of the entire corn and soybean fields (Sakamoto 2021). Therefore, the lower producer's accuracy from DOY 215 to DOY 247 may have had a negative effect on yield prediction accuracy. In recent years, many studies have focused on resolving the mixed-pixel effect on crop classification and achieving yield prediction results by integrating time-series lower-resolution MODIS and Visible Infrared Imaging Radiometer Suite (VIIRS) data and data from higher-resolution satellite images such as Sentinel-2. and Landsat data (Hilker *et al.* 2009; Jia *et al.* 2014; Li *et al.* 2015; Shen *et al.* 2022; Zhou *et al.* 2020). Although the data fusion approaches would improve the crop classification accuracy, these approaches still cause a trade-off issue that requires adequate computational resources to process the high quantity of higher-resolution time-series images, especially for continental-scale yield predictions.

Optimal Crop Growth Stage for WDRVI-Based Crop-Yield Prediction

The correlation between the county-averaged MODIS-WDRVI and the crop yields were temporally investigated to explore the optimal timings of the WDRVI used as explanatory variables in the third-degree polynomial regression models. For example, as of DOY 279, the CL01NF model showed optimal crop growth stages at which the county-averaged MODIS-WDRVI showed the highest correlation with corn and soybean yields, at 71 days (around R1: silking stage, $R^2 = 0.77$) and 76 days (around R5: beginning seed stage, $R^2 = 0.61$), respectively, after the rSMF emergence date. The time-series pattern of the determination coefficient showed a gentle bell-curve shape for corn and a steep bell-curve shape for soybean. The peak values for corn were higher than soybean and appeared a few days earlier than those of soybean (Supplemental Figure 2). This is consistent with the results of previous studies, which investigated the relationship between MODIS-NDVI and the statistical yields of corn and soybean in the central US (Bolton and Friedl 2013; Johnson 2014). The state-by-state optimal crop growth stages were also comprehensively explored on a within-season basis for the other prediction models (CL02SF, CL03SU, RF04U-I, and RF05U-IY). A summary of the national results for the five major states is shown in Supplemental Table 6.

Validation of Prediction Accuracy for County-Level Yields

The yield prediction accuracy of the tested models was compared using the following four categories: (A) all counties; (B) counties with an irrigated ratio of ≥10%; (C) counties in the major states with an irrigated ratio of <10%; and (D) counties in the minor states with an irrigated ratio of <10% (Figure 4). The reason for comparing the prediction results as of DOY 279 is that the accuracy of early crop classification accuracy is near its peak at that timing. The CL02SF model showed a lower accuracy than CL01NF in the counties with an irrigated ratio of ≥10% for both crops. The CL03SF model also had a lower prediction accuracy than CL01NF for soybeans in irrigated counties. The correlation between county-average vegetation index and crop yields was not always the same for irrigated and non-irrigated regions (Sakamoto 2020). Therefore, it was possible that a regression model calibrated especially for a state where both irrigated and non-irrigated regions are mixed would not be applicable to either irrigated or non-irrigated counties, and conversely. This implies that the state-by-state model calibration using curvilinear regression models may show different effects on the prediction accuracy, where it is lower in the irrigated regions and higher in the less irrigated regions. In non-irrigated regions, the CL02SF and CL03SU models showed a higher prediction accuracy than CL01NF (Figure 4C, 4D, 4G, and 4H). The higher prediction

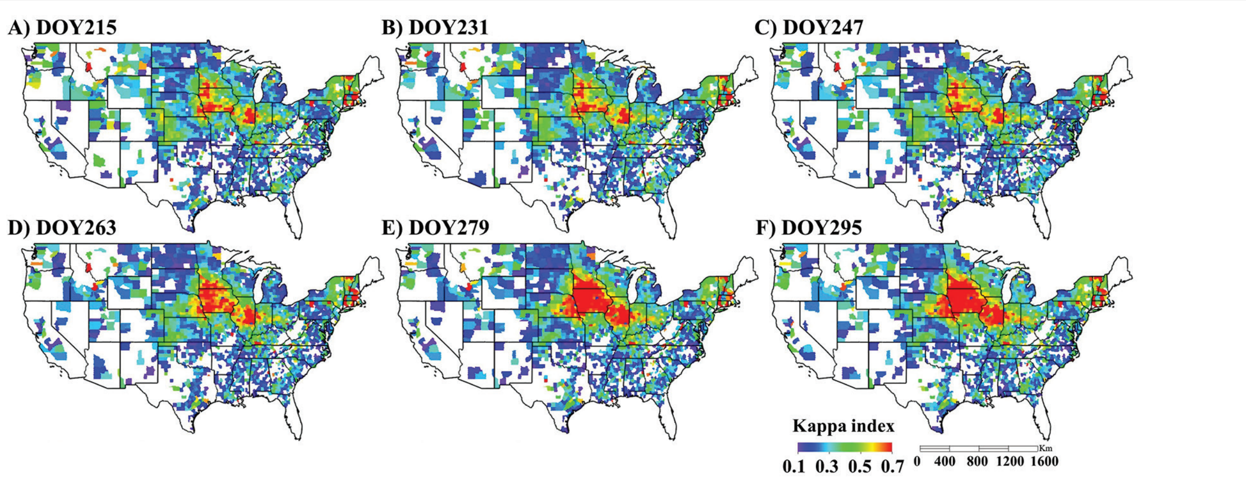

Figure 3. Accuracy assessment of crop classification maps, which were classified into four categories: corn, soybean, other crops, and a mixture. Resolution is at 250 m, from day of year (DOY) 215 (A) to DOY 295 (F) in 2021. The kappa index was calculated for each county and compared to the United States Department of Agriculture-National Agricultural Statistics Service (USDA-NASS) Cropland Data Layers data.

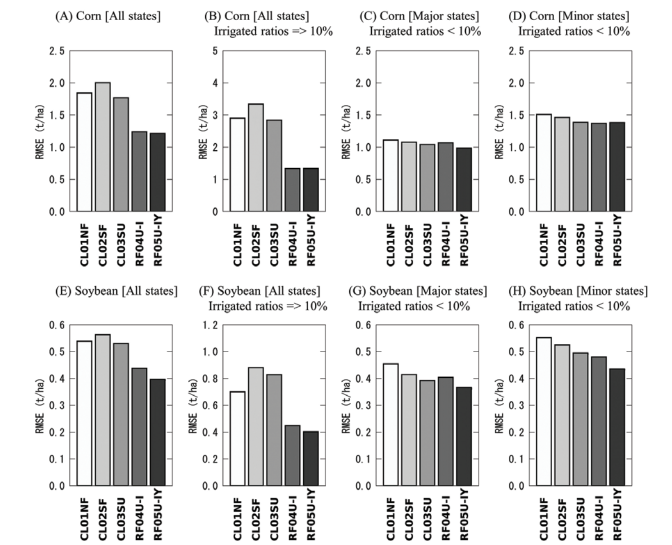

Figure 4. Model comparison of prediction accuracy as of day of year (DOY) 279 for county-level corn (A–D) and soybean (E–H) yields. The root-mean-square errors (RMSEs) were averaged over a five-year period (2018–2022) for each of the four categories, which were all counties (A and E), the counties with irrigated ratios of 10% or higher (B and F), the counties in the major corn or soybean producing states (C and G), and the counties in the other minor states (D and H).

accuracy of CL03SU than CL02SF suggests that the annual model re-calibration process of CL03SU resulted in a higher prediction accuracy (Tables 2 and 3). The performance of CL03SU was much lower than those of the RF04U-I and RF05U-IY, particularly in the irrigated regions. The RMSE values of the CL03SU were 1.5 (corn) and 0.38–0.43 t/ha (soybean) higher than the RF04U-I and RF05U-IY (Figure 4B and 4F). The RF-based models provided a slightly higher prediction accuracy than the CL03SU model in the counties of the minor corn producing states with <10% of county-level irrigated area (Figure 4D).

The performance of RF05U-IY was slightly better than the RF04U-I in all categories. According to the temporal changes in the model prediction accuracy for all counties (Table 2), the RMSE of RF05U-IY were 0.024 (corn) and 0.042 t/ha (soybeans) lower than the RF04U-I (at DOY 279). Figures 5 and 6 show the scatter plots for the predicted county-level yields and the fixed statistical data for each major producing state. The RMSE and CV showed no considerable difference in the prediction accuracy between the RF-based models (RF04U-I and RF05U-IY) and the curvilinear regression model (CL03SU). However, the RF05U-IY model always showed the smallest absolute value of the MBE, displaying the superiority of the model. In addition, a majority of the scatter plots derived from the RF05U-IY model were distributed within a 10% error margin (Figures 5 and 6), implying a lower model bias error than those of the other models. The comparisons of models based on the MBE (Table 3) show that the RF05U-IY was an order of magnitude smaller than those of the other models. The results showed that the prediction accuracy of the RF05U-IY was significantly different at the 1% level than those of the other models, except for the RMSE of corn. This is a result of the additional explanatory variable; "number of year" used in RF05U-IY. Consequently, the county-level verification results suggested that the RF05U-IY model showed the best performance of crop-yield prediction. The scatter plots for the predicted county-level yields, and the fixed statistical data for the other major producing states are shown in Supplemental Figures 5 and 6.

Validation of Prediction Accuracy for State-Level Yields

Table 4 summarizes the model performance of state-level yield prediction as of DOY279 on the major five producing states and group categories. The RF05U-IY model showed a higher accuracy, especially in the major corn and soybean producing states of IL, IN, and

Table 2. Comparison of county-level prediction accuracies (RMSE: t/ha) for the tested models for corn grain and soybean yield during 2018–2022 on a within-season basis. Model prediction accuracy assessed using multiple comparisons at the 1% significance level.

		Models				
Crop	DOY	CL01NF	CL02SF	CL03SU	RF04U-I	RF05U-IY
Corn	215	2.90	2.13	2.03	1.43	1.42
	231	1.87	1.90	1.80	1.31	1.32
	247	1.84	2.08	1.79	1.25	1.25
	263	1.80	1.95	1.83	1.23	1.23
	279	1.84	2.00	1.77	1.24	1.21
	295	1.84	1.72	1.69	1.21	1.21
	311	1.86	1.76	1.73	1.22	1.21
	327	1.87	1.80	1.70	1.23	1.22
	343	1.88	1.96	1.90	1.24	1.23
Multiple comparison*		a	ab	ac	d	d
Soybeans	215	0.69	0.59	0.57	0.50	0.51
	231	0.62	0.80	0.60	0.48	0.47
	247	0.58	0.56	0.52	0.46	0.43
	263	0.55	0.59	0.53	0.45	0.41
	279	0.54	0.56	0.53	0.44	0.40
	295	0.54	0.56	0.52	0.44	0.40
	311	0.54	0.55	0.52	0.44	0.40
	327	0.54	0.55	0.52	0.44	0.40
	343	0.55	0.55	0.52	0.44	0.40
Multiple comparison*		a	a	a	b	c

DOY = day of year.
*Letters are assigned based on the results of paired t-tests. When the letters between models differ, it indicates a significant difference in the root-mean-square error (RMSE) at the 1% significance level.

Table 3. Comparison of county-level mean bias error (MBE: t/ha) for the tested models for corn grain and soybean yield during 2018–2022 on a within-season basis. Model prediction accuracy assessed using multiple comparisons at the 1% significance level.

		Models				
Crop	DOY	CL01NF	CL02SF	CL03SU	RF04U-I	RF05U-IY
Corn	215	−9.6E-01	−8.6E-01	−7.6E-01	−4.2E-01	−5.3E-03
	231	−8.2E-01	−7.2E-01	−6.8E-01	−3.2E-01	8.3E-03
	247	−7.6E-01	−8.2E-01	−6.9E-01	−2.9E-01	1.3E-02
	263	−7.7E-01	−8.2E-01	−6.9E-01	−2.9E-01	−1.2E-02
	279	−8.6E-01	−8.6E-01	−7.2E-01	−3.5E-01	-2.1E-02
	295	−8.6E-01	−7.7E-01	−6.8E-01	−3.2E-01	−2.0E-02
	311	−8.8E-01	−7.7E-01	−6.8E-01	−3.1E-01	4.4E-04
	327	−9.0E-01	−8.1E-01	−6.9E-01	−3.2E-01	−1.5E-03
	343	−9.0E-01	−8.4E-01	−7.4E-01	−3.3E-01	6.6E-04
Multiple comparison*		a	a	b	c	d
Soybeans	215	−2.5E-01	−2.6E-01	−2.3E-01	−1.9E-01	−1.1E-02
	231	−2.5E-01	−3.0E-01	−2.5E-01	−2.1E-01	−8.2E-03
	247	−3.3E-01	−3.3E-01	−2.8E-01	−2.3E-01	−3.8E-02
	263	−3.1E-01	−3.4E-01	−2.8E-01	−2.3E-01	−3.3E-02
	279	−3.0E-01	−3.2E-01	−2.8E-01	−2.2E-01	−2.7E-02
	295	−2.9E-01	−3.1E-01	−2.7E-01	−2.1E-01	−1.8E-02
	311	−2.9E-01	−3.1E-01	−2.7E-01	−2.2E-01	−2.2E-02
	327	−3.0E-01	−3.2E-01	−2.7E-01	−2.2E-01	−2.2E-02
	343	−3.0E-01	−3.2E-01	−2.7E-01	−2.1E-01	−2.1E-02
Multiple comparison*		a	b	c	d	e

DOY = day of year.
*Letters are assigned based on the results of paired t-tests. When the letters between models differ, it indicates a significant difference in the root-mean-square error (RMSE) at the 1% significance level.

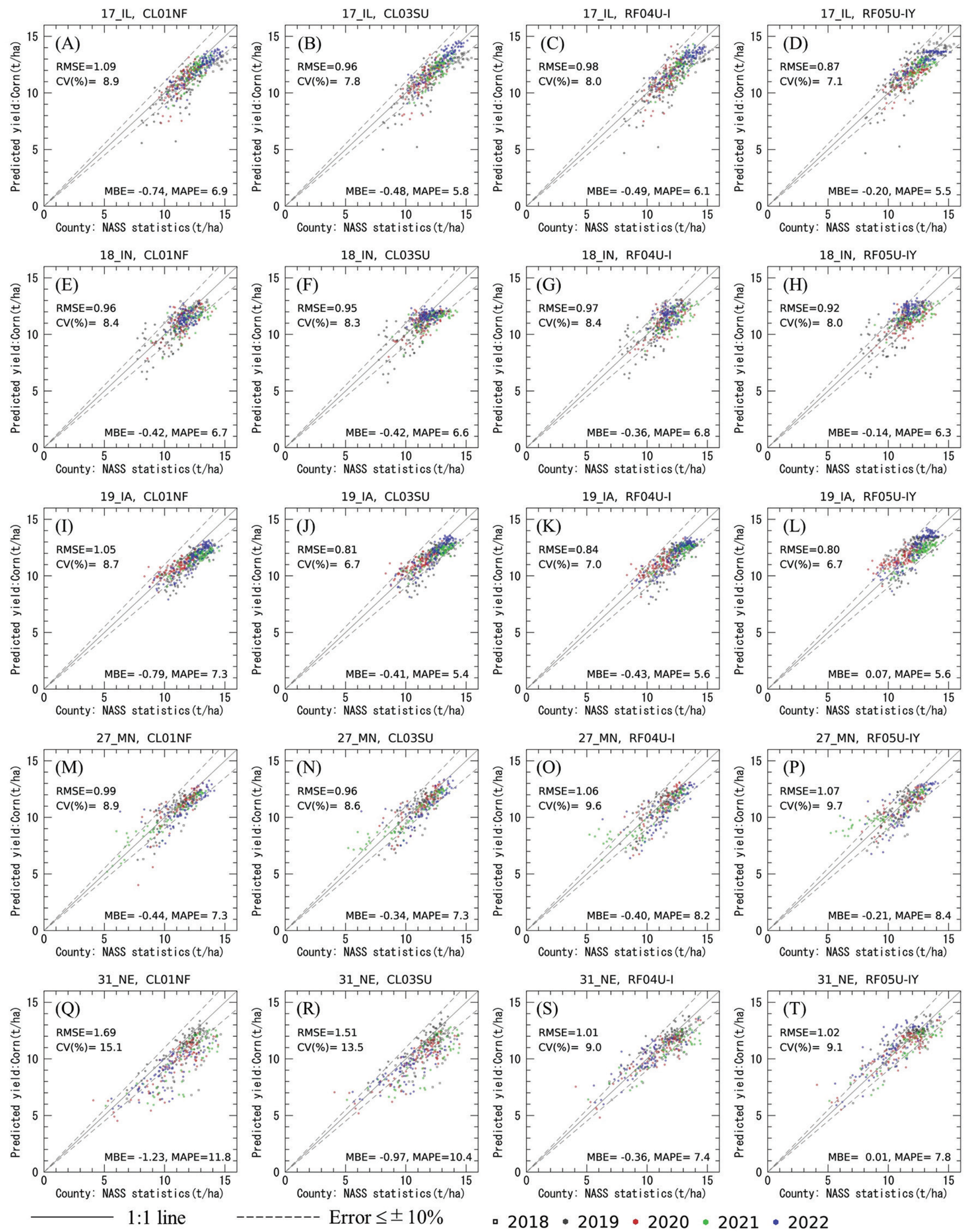

Figure 5. Comparison between the United States Department of Agriculture-National Agricultural Statistics Service (USDA-NASS)-derived fixed statistical data and the county-level corn grain yields predicted by the tested models (CL01NF, CL03SU, RF04U-I, and RF05U-IY) as of day of year (DOY) 279 in Illinois (A–D), Indiana (E–H), Iowa (I–L), Minnesota (M–P), and Nebraska (Q–T). CV: coefficient of variation (%), MAPE: mean absolute percentage error (%), ME: mean error (t/ha), RMSE: root mean square error (t/ha).

IA, owing to the model bias correction effect caused by the additional variable used in the model. Figure 7 shows the scatter plots for the USDA-NASS fixed statistical data and the state-level yield predictions of the RF05U-IY, as of DOY 215, 247, 279, and 311 for both crops from 2018 to 2022. The figure shows that the RMSE and CV values decreased between DOY 215 and DOY 279, and then increased slightly until DOY 311. At DOY 215, there were 128 points of 185 (69.2%) with an APE of <10% for corn, and 90 of 146 (61.6%) points for soybeans. By DOY 279, the numbers increased further to 146 (78.9%) for corn and 113 (77.4%) for soybeans, as well as showing an improved prediction accuracy of the RF05U-IY. When limited to the major crop producing states, the RMSE and CV values were 0.47 t/ha and 4.3% for corn, and 0.22 t/ha and 6.6% for soybeans, respectively, at DOY 279. The results suggest that in the major producing states, RF05U-IY had the ability to determine if a state was tending toward a good or poor harvest that crop yields. In contrast, it was also confirmed that the additional explanatory variable, "number of year," may result in poor prediction accuracy in some cases as in NE (Table 4).

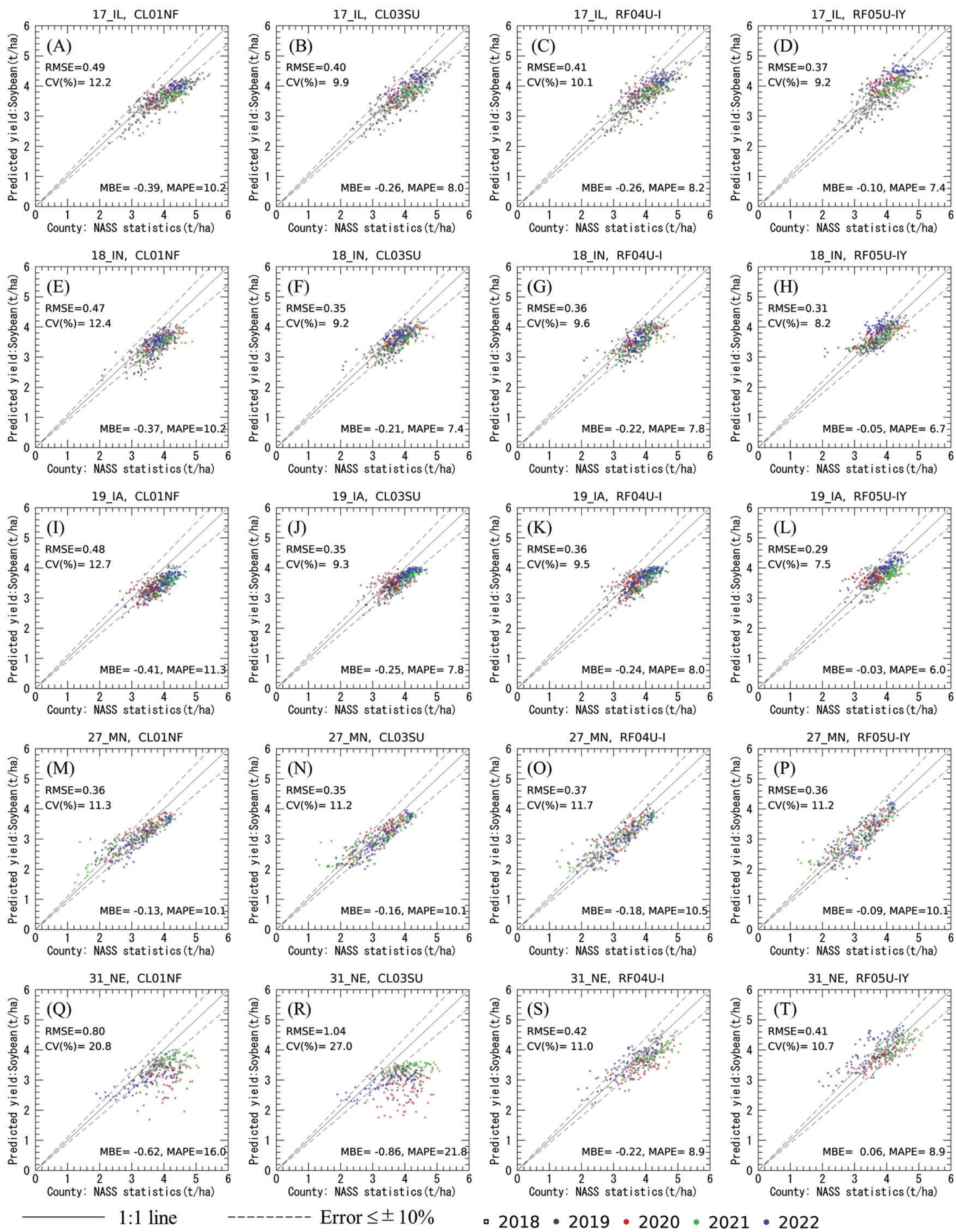

Figure 6. Comparison between the United States Department of Agriculture-National Agricultural Statistics Service (USDA–NASS)-derived fixed statistical data and the county-level soybean yields predicted by the tested models (CL01NF, CL03SU, RF04U-I, and RF05U-IY) as of day of year (DOY) 279 in Illinois (A–D), Indiana (E–H), Iowa (I–L), Minnesota (M–P), and Nebraska (Q–T). CV: coefficient of variation (%), MAPE: mean absolute percentage error (%), ME: mean error (t/ha), RMSE: root mean square error (t/ha).

Within-Season Visualization of US Crop Yields

Crop-yield maps were visualized using the RF05U-IY predictions and USDA-NASS statistical data, as shown in Figure 8 (corn) and Figure 9 (soybeans). The maps as of DOY 215 partially show extreme differences near state boundaries. Examples for corn are the IL-IN border in 2018, the IA-MN border in 2020, and the IA-IL border in 2021 (Figure 8); soybean examples include the ND-SD border from 2018 to 2022 and the IL-IN border in 2018 and 2020 (Figure 9). These gaps were owing to the shorter MODIS input data period as of DOY 215, which is insufficient to accurately classify crop types and emergence dates (Figure 3, Supplemental Table 6). Subsequent to DOY 215, the RF05U-IY showed similar spatial patterns to that of USDA–NASS-derived data with less extreme changes across state boundaries and could successfully predict high-yielding regions with irrigation (i.e., Arkansas and Georgia, in addition to the area where the Ogalla aquifer is distributed) (Figures 1C, 8, and 9).

There are two advantages of the RF05U-IY-predicted crop-yield maps over the reports of the USDA-NASS monthly forecasts. The first is that the RF05U-IY maps can provide a detailed understanding of crop-yield spatial patterns more than six months earlier than when the county-level statistical data are available online in February. The second is that the RF05U-IY maps presented fewer counties of missing predictions than the USDA-NASS maps. In recent years, the number of USDA-NASS county-level statistical data records has been declining. According to the search results of the Quick Stats for surveying corn grain and soybean yields (USDA-NASS 2023), the number of county-level statistical data records has decreased by 306–600 records for both crops over the past 20 years. A decrease in county-level statistical data can hinder a detailed visual understanding of the geospatial distribution of crop yields. In the Corn Belt, this was most noticeable in 2019 and 2021 (Figures 8 and 9).

Table 4. Comparison of state-level prediction accuracies (RMSE: t/ha) as of DOY 279 for the tested models for corn grain and soybean yield from 2018–2022 on a within-season basis.

Crop	States	CL01NF	CL02SF	CL03SU	RF04U-I	RF05U-IY
Corn	Illinois	0.66	0.47	0.43	0.43	0.22
	Indiana	0.54	0.62	0.54	0.52	0.41
	Iowa	0.83	0.54	0.47	0.46	0.38
	Minnesota	0.56	0.53	0.49	0.51	0.52
	Nebraska	1.07	0.94	0.89	0.44	0.55
	Major 10 states	0.77	0.72	0.67	0.54	0.47
	Minor 27 states	3.03	3.03	2.93	0.85	0.91
	All states	2.66	2.66	2.57	0.77	0.82
Soybeans	Illinois	0.41	0.32	0.28	0.28	0.23
	Indiana	0.41	0.29	0.24	0.23	0.13
	Iowa	0.45	0.34	0.29	0.29	0.19
	Minnesota	0.23	0.26	0.23	0.23	0.19
	Nebraska	0.54	0.93	0.80	0.26	0.29
	Major 11 states	0.41	0.46	0.43	0.27	0.22
	Minor 19 states	0.40	0.47	0.42	0.32	0.29
	All states	0.40	0.46	0.43	0.30	0.27

DOY = Day of Year; RMSE = root-mean-square error.

Visualizing the Spatial Pattern of Good or Poor Harvest Counties on a Within-Season Basis

Yield anomalies can reveal spatial characteristics of good (shades of blue: yields 10% above normal) and poor (shades of red: yields 10% below normal) harvest regions, which are greatly affected by annual weather conditions (Figures 10 and 11). According to the 2017 Census of Agriculture (USDA-NASS 2023), more than 80% of the US cropland is cultivated under non-irrigated conditions. Therefore, corn and soybean yields can be nearly 40% lower than normal in drought years, especially in inland regions with lower annual precipitation and poor crop concentration (Figure 1). Similar to the crop-yield prediction maps (Figures 8 and 9), the spatial distribution patterns of the yield anomalies were more similar to the USDA-NASS statistical data maps, especially after DOY 247. In 2021 and 2018, the highest and second-highest crop-yield years, the distribution of the good harvest regions had already been detected in the Corn Belt since DOY 247 (Figures 10 and 11), which was consistent with the fact the 2018 and 2021 corn and soybean yields in IA, IL, and IN were higher than normal (Supplemental Figures 3 and 4). 2019 shows the lowest crop-yield year, owing to the historical heavy precipitation that caused a delayed planting in the spring; the poor-harvest regions were noticeably larger in 2019 than in the other years at DOY 247. However, when analyzing the differences in spatial patterns of yield anomalies between RF05U-IY and the USDA-NASS statistical data, the RF05U-IY incorrectly predicted good and poor harvest regions in some places. For example, it predicted that eastern North Carolina would yield a good corn harvest by DOY 279 in 2021; however, in fact, these regions subsequently had poor harvests. It also predicted that western Minnesota would yield a poor corn harvest in DOY 279; however, in fact, these regions subsequently had good harvests.

The high-resolution yield anomaly prediction maps intuitively enable an understanding of the overall distribution trends of good and poor harvests. The cost of transportation of crops from the production area to the consumption area was affected by the geographic distribution of good and poor harvest regions, which varied from year to year. Therefore, it can be inferred that the geo-informative yield prediction

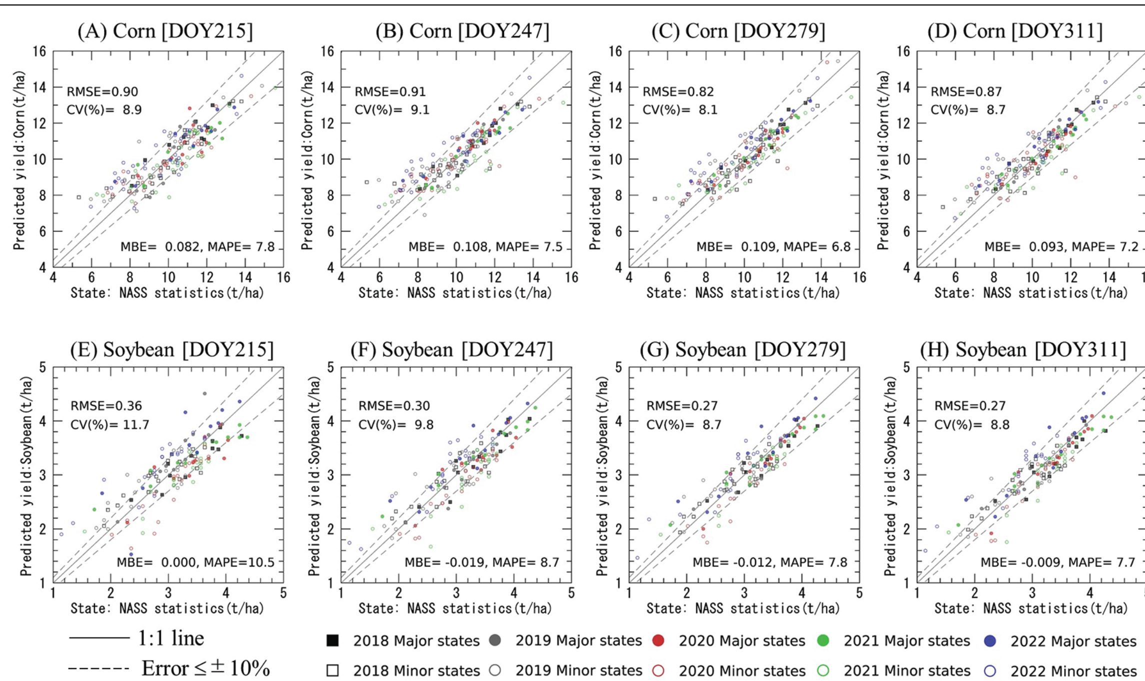

Figure 7. Comparison at state level between the United States Department of Agriculture-National Agricultural Statistics Service (USDA–NASS)-derived fixed statistical data of corn grain (A–D) and soybean (E–H) yields, and the RF05U-IY-derived prediction yields as of day of year (DOY) 215, 247, 279, and 311.

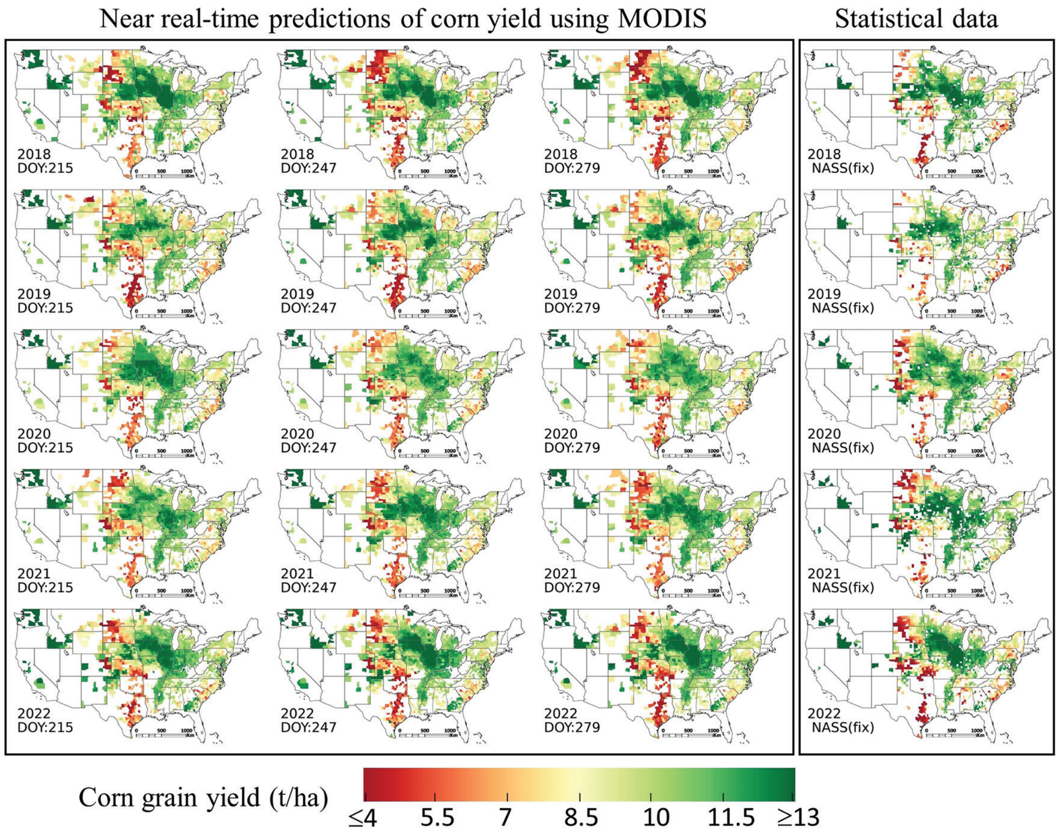

Figure 8. Spatial distribution of county-level corn grain yields predicted by the RF05U-IY model as of day of year (DOY) 215 (first column), DOY 247 (second column), and DOY 279 (third column) as well as the United States Department of Agriculture-National Agricultural Statistics Service (USDA–NASS)-derived fixed statistical data (last column) from 2018 to 2022.

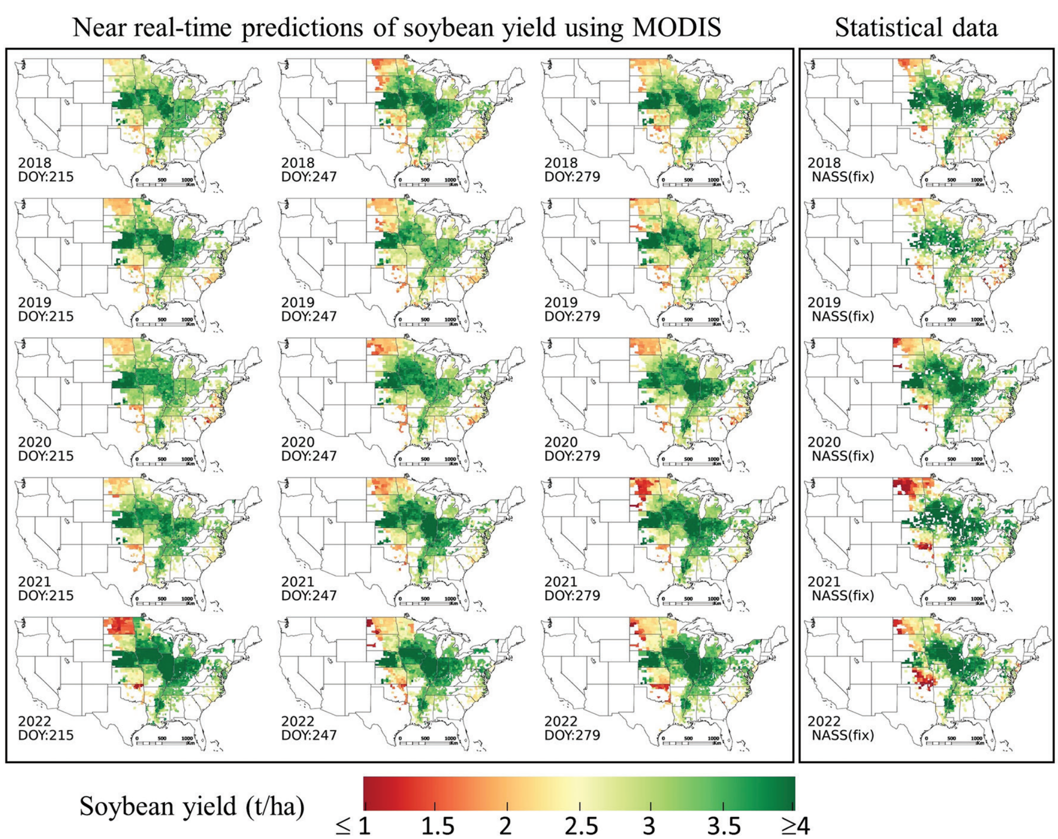

Figure 9. Spatial distribution of county-level soybean yield predicted by the RF05U-IY model as of day of year (DOY) 215 (first column), DOY 247 (second column), and DOY 279 (third column), as well as the United States Department of Agriculture-National Agricultural Statistics Service (USDA–NASS)-derived fixed statistical data (last column) from 2018 to 2022.

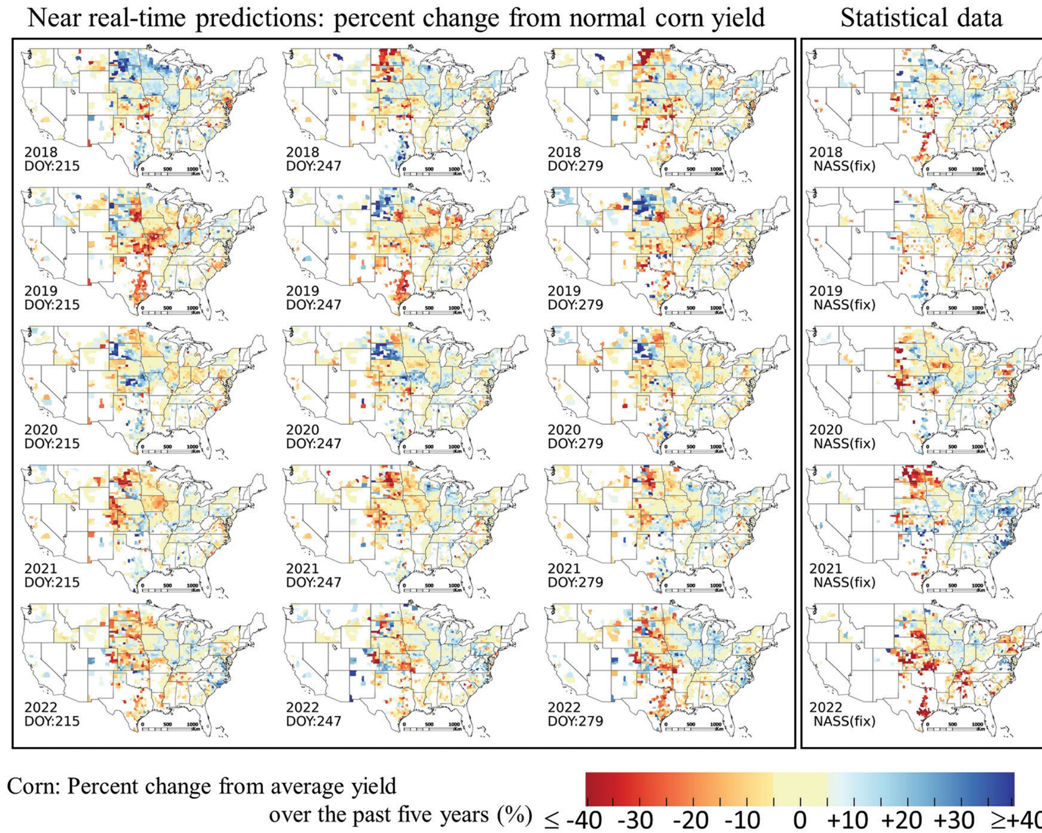

Figure 10. Spatial distribution of percent change from average corn grain yield over the past five years for RF05U-IY-derived predictions as of day of year (DOY) 215 (first column), DOY 247 (second column), DOY 279 (third column), and United States Department of Agriculture-National Agricultural Statistics Service (USDA-NASS) county-level statistical data (last column) from 2018 to 2022.

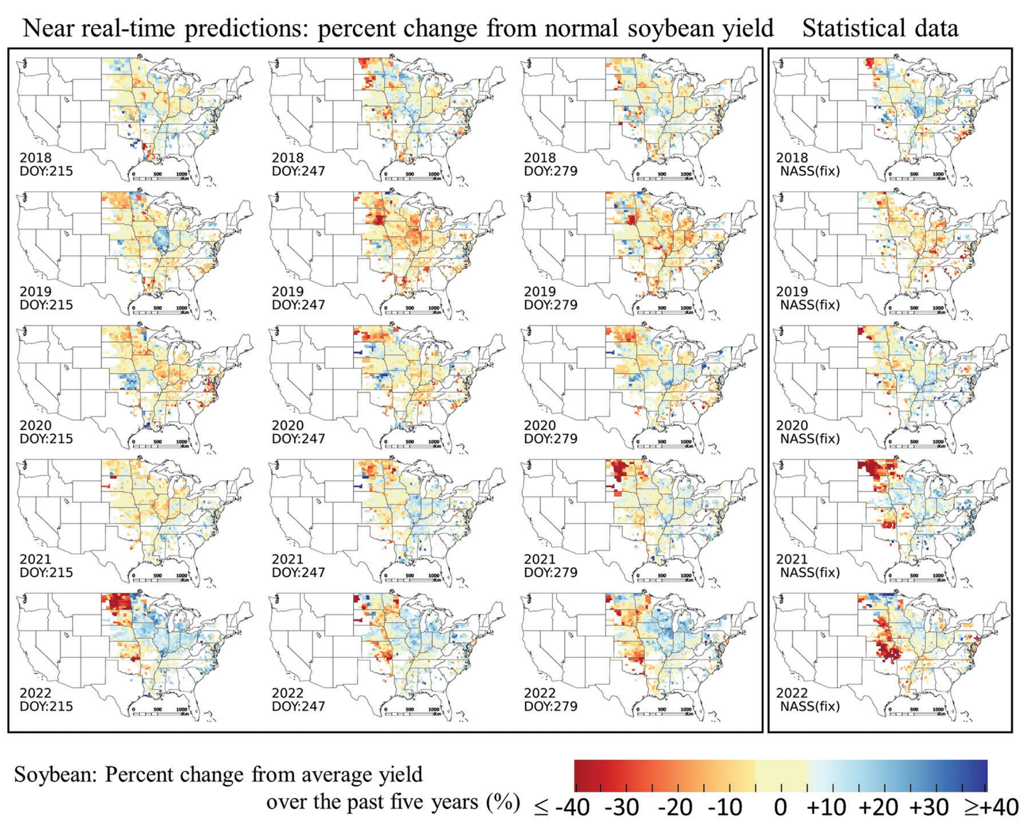

Figure 11. Spatial distribution of percent change from average soybean yield over the past five years for RF05U-IY-derived predictions as of day of year (DOY) 215 (first column), DOY 247 (second column), DOY 279 (third column), and United States Department of Agriculture-National Agricultural Statistics Service (USDA-NASS) county-level statistical data (last column) from 2018 to 2022.

information is useful for businesses that collect corn and soybeans to determine the logistical costs for the year in advance. Such businesses would include country elevators, ethanol plants, and harvest port elevators, which are scattered across the US (Denicoff *et al.* 2014). Then, the proposed method would be a valuable source of information for outlooking the trends in US production of corn and soybeans in years with extreme weather events. In 2022, the continental US suffered from the most severe drought since 2012, with unusually low precipitation (https://www.ncei.noaa.gov/access/monitoring/monthly-report/drought/202209). This caused concern that the 2022 drought may cause a similar poor crop growth as in 2012. According to Figures 10 and 11, the drought regions with crop failure were predominantly limited to the region west of the Nebraska-Iowa boarder in 2022. Moreover, it could be confirmed that most regions of the Corn Belt did not suffer severely from drought damage, and the region had a higher-than-normal crop yield.

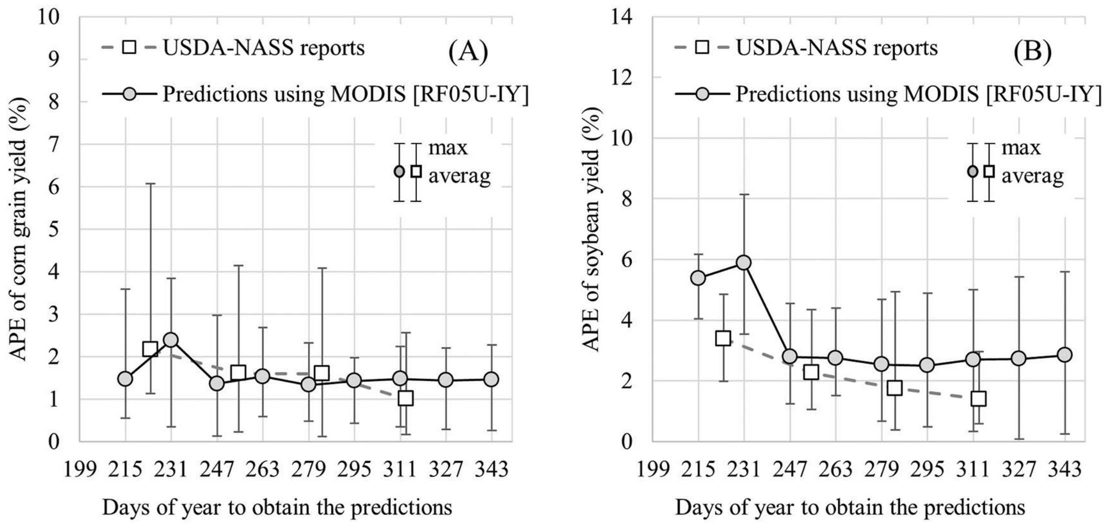

Figure 12. Temporal comparison in absolute percentage error (APE) of early predictions for national-level (A) corn grain, and (B) soybean yields between the United States Department of Agriculture-National Agricultural Statistics Service (USDA-NASS) forecasts and the proposed model (RF05U-IY). The APE values were calculated based on the national-level fixed statistical data for 2018–2022, which were updated on the USDA Quick Stats annually in January of the following year.

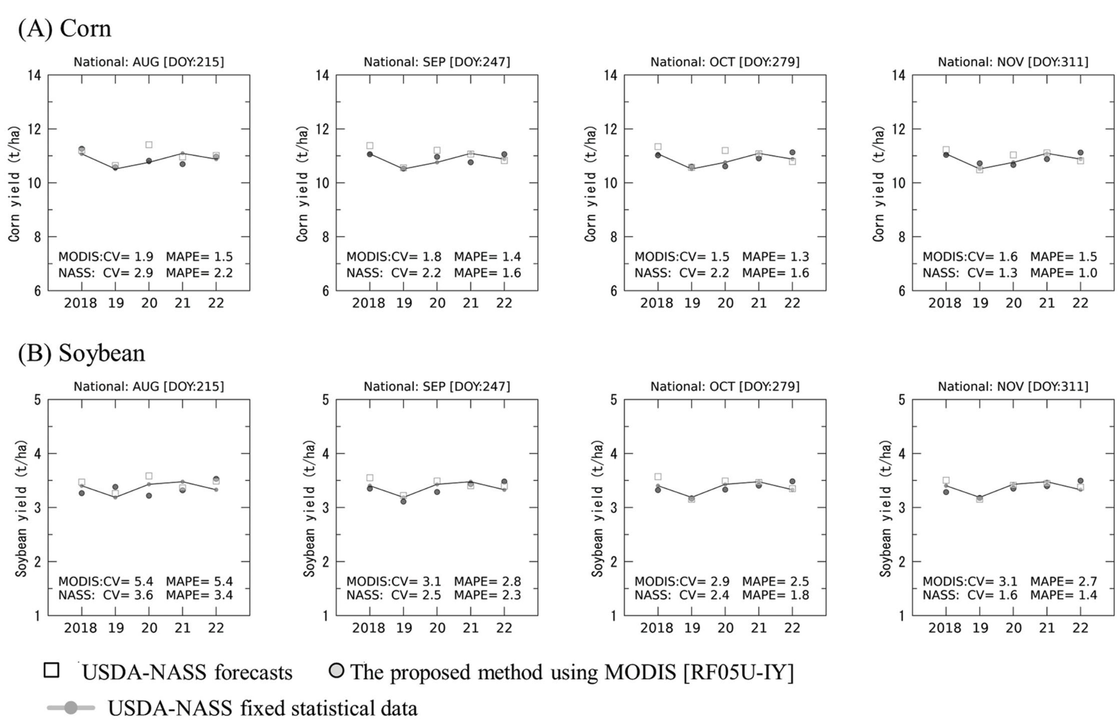

Figure 13. Comparison of national-level corn grain and soybean yields between the United States Department of Agriculture-National Agricultural Statistics Service (USDA-NASS) monthly forecasts and the proposed method (RF05U-IY) against the fixed statistical data. The USDA-NASS monthly forecasts were released at approximately the 8th to the 12th of each month after August. The proposed method could predict the US corn and soybean yield from a few days to a week before the USDA-NASS monthly forecasts were released.

Assessment of Prediction Accuracy for National-Level Yields and Production

Figure 12 shows the APE temporal distribution of national-level yield predictions. The accuracy of RF05U-IY remained almost invariable after DOY 247 for corn and soybeans, consistent with a previous study (Sakamoto *et al.* 2014). The predictions after DOY 311 were slightly less accurate than those of DOY 279. This was probably due to the influence of factors such as post-harvest vegetation growth, including weed growth, which would introduce variability in vegetation indices after harvesting, thereby having a negative effect on the prediction accuracy through the shape-model fitting process over a longer observation period. The prediction performance of RF05U-IY was comparable to the USDA-NASS monthly forecasts for corn as of DOY 215 and for soybeans as of DOY 247 (Figures 12 and 13). The accuracy of the USDA-NASS forecasts has not always been stable. The USDA-NASS October forecasts had overpredicted the national level corn-grain yield by 2.4 and 4.1% in 2018 and 2020, respectively, and 4.9% for soybean yield in 2018. In these years, the comparative advantage of RF05U-IY is emphasized. It accurately predicted these yields (at DOY 279); the corn-grain yield was underpredicted in 2018 and 2020, by only 0.5 and 1.4%, respectively, and the soybean yield was underpredicted by only 2.4% in 2018.

When comparing the national-level crop productions derived from RF05U-IY-predicted yields and the USDA-NASS monthly forecasts on a within-season basis (Figure 14), results showed that one was not always more accurate than the other. In terms of the 2018 and 2020 corn productions and the 2022 soybean production, the APEs of the USDA-NASS October forecasts ranged from 3.05 to 5.90%. Those of RF05U-IY (DOY 279) were smaller and ranged from 0.00 to 0.89%. However, in 2021 and 2022 for corn, the prediction errors of the USDA-NASS October forecasts ranged from 0.37 to 1.21%, while those of RF05U-IY (DOY 279) ranged between 1.94 and 4.39%. The RF05U-IY model is not necessarily superior to the USDA-NASS forecasts, but its comparable prediction accuracy makes it a useful tool to double check the reliability of the USDA-NASS forecasts. In addition, the RF05U-IY APEs were <5% in all cases as of DOY 279. Therefore, the proposed method is expected to have the ability to provide an overview of lower crop production years from a different angle, such as in 2012 for corn, and in 2003 and 2019 for soybeans, when the total production was at least 10% lower than normal. In this study, the simulation of crop-yield prediction was conducted at a 16-day interval. If there are no constraints on computing resources, it would be possible, in principle, to obtain crop-yield prediction results at a near-real time basis by incorporating the MODIS Near Real Time products called "MOD9A1N (https://modaps.modaps.eosdis.nasa.gov/services/about/products/c6-nrt/MOD09A1N.html)", which are daily, updated surface reflectance rolling-eight-day products. Thus, the proposed method would be an additional new intelligence source for supporting global food security to timely monitor the US corn and soybean export supply capacity.

Conclusions

This study developed a within-season crop monitoring system using MODIS time-series data for US corn and soybean yields by integrating three core algorithms designed for crop phenology detection, early crop classification, and yield prediction. The reliability of the proposed method was compared with the USDA-NASS monthly forecasts from 2018 to 2022. This study also attempted to predict national-level corn and soybean production in the US every 16 days after DOY 215 by combining the USDA-NASS monthly forecast data on state-level harvested areas. Then, the advantages and disadvantages of the satellite remote sensing-based crop predictions were clarified on a within-season basis. A minor improvement to the yield prediction algorithm was made using the MODIS-WDRVI with additional experimental variables. As a result, the RF-based yield regression model (RF05U-IY) showed the best performance of state-level yield prediction models, specifically in the major crop producing states. The most unique feature of the RF05U-IY is the inclusion of a new variable; "number of year," which had a significant effect in minimizing bias errors compared to other models. This suggested that the new variable would cancel the bias error such as the long-term increasing trends of potential yield assuming improvements in crop variety and agricultural technology. The county-level prediction errors of the RF05U-IY as of DOY 279 (RMSE values of 1.21 and 0.40 t/ha for corn and soybeans, respectively) was smaller than those of the benchmark algorithm such as CL01NF, which is based on a curvilinear regression model using

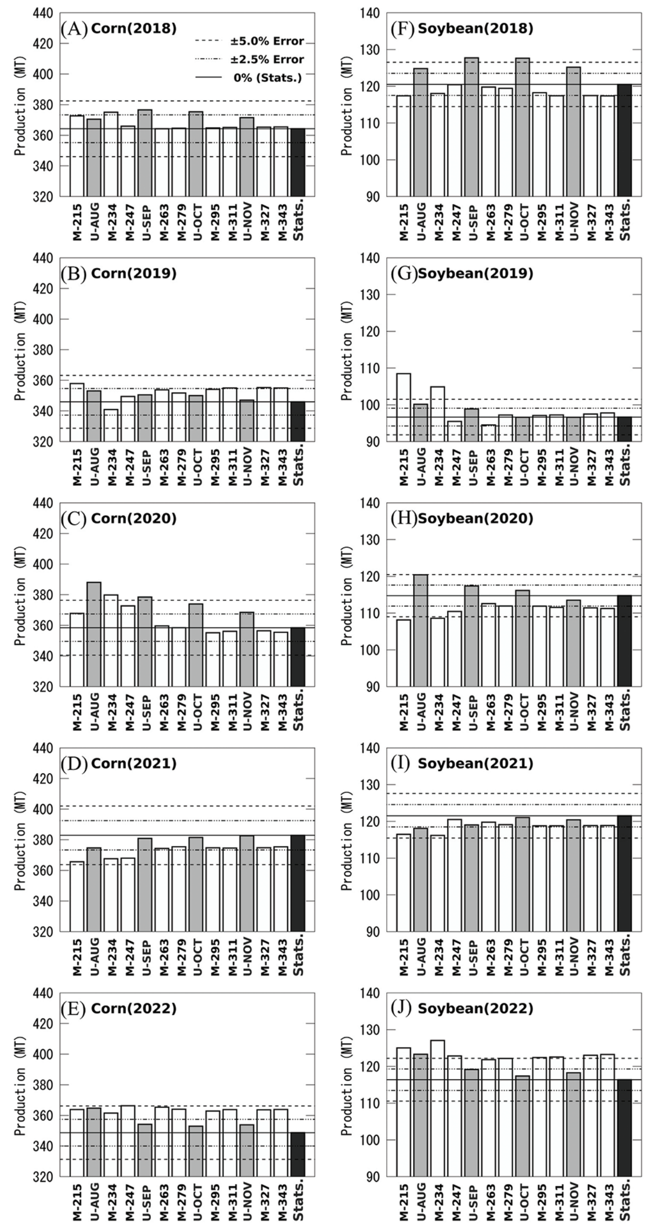

Figure 14. Within-season simulation using the proposed method (RF05U-IY) for predicting the US productions of corn (A–D) and soybeans (E–H) in reference to the United States Department of Agriculture-National Agricultural Statistics Service (USDA-NASS) monthly forecasts. The fixed statistical value is described as "Stats." The designations "U-AUG," "U-SEP," "U-OCT," and "U-NOV" mean the USDA-NASS monthly forecasts in August, September, October, and November, respectively. The designations "M-215," "M-231," "M-247," "M-263," "M-279," "M-295," "M-311," "M-327," and "M-343" mean the early predictions as of day of year (DOY) 215, DOY 231, DOY 247, DOY 263, DOY 279, DOY 295, DOY 311, and DOY 327.

only the MODIS-WDRVI. The state- and national-level yield prediction accuracies gradually improved after DOY 215 and reached the highest accuracy at DOY 279 for both corn and soybeans. The RF05U-IY yield prediction maps can reveal the detailed characteristics of the annual variability in the regional yield. In addition, the yield anomaly maps are expected to aid in visually understanding whether the crop of that year was abnormal. These show that crop-yield variability reaches nearly 40% depending on the annual precipitation variation especially in minor regions with small corn- and soybean-planted areas. This study also confirmed that these overall spatial patterns were consistent with the maps derived from the USDA-NASS fixed statistical data, especially after DOY 247. While the proposed method could not always predict national-level yield and production more accurately than the USDA-NASS monthly forecasts, the prediction accuracies were comparable to those of the USDA forecasts. The APE of predicted total productions (as of DOY 279) were <5% for all simulation years. In conclusion, this study revealed that the proposed system using the RF05U-IY algorithm could provide an alternative intelligence source to build a comprehensive visual understanding of the US corn and soybean export supply capacity. Therefore, remote sensing-based yield prediction maps could make a significant contribution to raising the international community's awareness of global food security because of its appealing visual power. In future, we will expand upon this research into practical applications by combining the use of high-frequency observation satellite data collected by countries around the world, such as VIIRS/*SuomiNPP* and *JPSS-1*, OLCI/*Sentinel-3A* & *3B*, and SGLI/*GCOM-C* in a cloud-based environment using the Google Earth Engine.

Acknowledgments

I appreciate the valuable comments and suggestions of the anonymous reviewers. This study was supported by JSPS KAKENHI (Grant Number JP17K08037). I would like to express my gratitude to Dr. Kentaro Ohigashi, my colleague, for invaluable guidance in the statistical analysis of multiple comparisons. The author declares that they have no known competing financial interests or personal relationships that could have appeared to influence the work reported in this paper.

References

Becker-Reshef, I., E. Vermote, M. Lindeman, and C. Justice. 2010. A generalized regression-based model for forecasting winter wheat yields in Kansas and Ukraine using MODIS data. *Remote Sensing of Environment* 114(6):1312–1323. https://doi.org/10.1016/j.rse.2010.01.010.

Bolton, D. K. and M. A. Friedl. 2013. Forecasting crop yield using remotely sensed vegetation indices and crop phenology metrics. *Agricultural and Forest Meteorology* 173:74–84. https://doi.org/10.1016/j.agrformet.2013.01.007.

Denicoff, M. R., M. E. Prater and P. Bahizi. 2014. Corn Transportation Profile. <https://www.ams.usda.gov/sites/default/files/media/Corn%20Transportation%20Profile.pdf> (last date accessed: 23 June 2023).

Devi, S. 2022. Pakistan floods: Impact on food security and health systems. *The Lancet* 400(10355):799–800. https://doi.org/10.1016/S0140-6736(22)01732-9.

Ferencz, C., P. Bognár, J. Lichtenberger, D. Hamar, G. Tarcsai, G. Timár, G. Molnár, S. Pásztor, P. Steinbach, B. Székely, O. E. Ferencz and I. Ferencz-Árkos. 2004. Crop yield estimation by satellite remote sensing. *International Journal of Remote Sensing* 25(20):4113–4149. https://doi.org/10.1080/01431160410001698870.

Franch, B., E. F. Vermote, S. Skakun, J. C. Roger, I. Becker-Reshef, E. Murphy and C. Justice. 2019. Remote sensing-based yield monitoring: Application to winter wheat in the United States and Ukraine. *International Journal of Applied Earth Observation and Geoinformation* 76:112–127. https://doi.org/10.1016/j.jag.2018.11.012.

Gitelson, A. A. 2004. Wide dynamic range vegetation index for remote quantification of biophysical characteristics of vegetation. *Journal of Plant Physiology* 161(2):165–173. https://doi.org/10.1078/0176-1617-01176.

Gitelson, A. A., B. D. Wardlow, G. P. Keydan and B. Leavitt. 2007. An evaluation of MODIS 250-m data for green LAI estimation in crops. *Geophysical Research Letters* 34(20). https://doi.org/10.1029/2007GL031620.

Green, T. R., H. Kipka, O. David and G. S. McMaster. 2018. Where is the USA Corn Belt, and how is it changing? *Science of the Total Environment* 618:1613–1618. https://doi.org/10.1016/j.scitotenv.2017.09.325.

Guindin-Garcia, N., A. A. Gitelson, T. J. Arkebauer, J. Shanahan and A. Weiss. 2012. An evaluation of MODIS 8- and 16-day composite products for monitoring maize green leaf area index. *Agricultural and Forest Meteorology* 161:15–25. https://doi.org/10.1016/j.agrformet.2012.03.012.

Hilker, T., M. A. Wulder, N. C. Coops, J. Linke, G. McDermid, J. G. Masek, F. Gao and J. C. White. 2009. A new data fusion model for high spatial- and temporal-resolution mapping of forest disturbance based on Landsat and MODIS. *Remote Sensing of Environment* 113:1613–1627. https://doi.org/10.1016/j.rse.2009.03.007.

Ji, Z. L., Y. Z. Pan, X. F. Zhu, J. Y. Wang and Q. N. Li. 2021. Prediction of crop yield using phenological information extracted from remote sensing vegetation index. *Sensors* 21(4). https://doi.org/10.3390/s21041406.

Jia, K., S. L. Liang, X. Q. Wei, Y. J. Yao, Y. R. Su, B. Jiang and X. X. Wang. 2014. Land cover classification of Landsat data with phenological features extracted from time series MODIS NDVI data. *Remote Sensing* 6(11):11518–11532. https://doi.org/10.3390/rs61111518.

Johnson, D. M. and R. Mueller. 2010. The 2009 cropland data layer. *Photogrammetric Engineering & Remote Sensing* 76(11):1201–1205.

Johnson, D. M. 2014. An assessment of pre- and within-season remotely sensed variables for forecasting corn and soybean yields in the United States. *Remote Sensing of Environment* 141:116–128. https://doi.org/10.1016/j.rse.2013.10.027.

Johnson, D. M., A. Rosales, R. Mueller, C. Reynolds, R. Frantz, A. Anyamba, E. Pak and C. Tucker. 2021. USA crop yield estimation with MODIS NDVI: Are remotely sensed models better than simple trend analyses? *Remote Sensing* 13(21):4427. https://doi.org/10.3390/rs13214227.

Khaki, S., H. Pham and L. Z. Wang. 2021. Simultaneous corn and soybean yield prediction from remote sensing data using deep transfer learning. *Scientific Reports* 11(1):11132. https://doi.org/10.1038/s41598-021-89779-z.

Kira, O., A. L. Nguy-Robertson, T. J. Arkebauer, R. Linker and A. A. Gitelson. 2017. Toward generic models for green LAI estimation in maize and soybean: Satellite observations. *Remote Sensing* 9(4):318. https://doi.org/10.3390/rs9040318.

Kogan, F., L. Salazar and L. Roytman. 2012. Forecasting crop production using satellite-based vegetation health indices in Kansas, USA. *International Journal of Remote Sensing* 33(9):2798–2814. https://doi.org/10.1080/01431161.2011.621464.

Kogan, F. N. 1997. Global drought watch from space. *Bulletin of the American Meteorological Society* 78(4):621–636. https://doi.org/10.1175/1520-0477(1997)078<0621:GDWFS>2.0.CO;2.

Kogan, F., B. Yang, G. Wei, P. Zhiyuan and J. Xianfeng. 2005. Modelling corn production in China using AVHRR-based vegetation health indices. *International Journal of Remote Sensing* 26(11):2325–2336. https://doi.org/10.1080/01431160500034235.

Li, Q. T., C. Z. Wang, B. Zhang and L. L. Lu. 2015. Object-based crop classification with Landsat-MODIS enhanced time-series data. *Remote Sensing* 7(12):16091–16107. https://doi.org/10.3390/rs71215820.

Liu, J., J. Shang, B. Qian, T. Huffman, Y. Zhang, T. Dong, Q. Jing and T. Martin. 2019. crop yield estimation using time-series MODIS data and the effects of cropland masks in Ontario, Canada. *Remote Sensing* 11(20):2419. https://doi.org/10.3390/rs11202419.

Meng, W., Fu-Lu, T. and Wen-Jiao,S. 2014. Corn Yield Forecasting in Northeast China Using Remotely Sensed Spectral Indices and Crop Phenology Metrics. Journal of Integrative Agriculture 13(7):1538-1545. https://doi.org/10.1016/S2095-3119(14)60817-0.

Mkhabela, M. S., P. Bullock, S. Raj, S. Wang and Y. Yang. 2011. Crop yield forecasting on the Canadian Prairies using MODIS NDVI data. *Agricultural and Forest Meteorology* 151(3):385–393. https://doi.org/10.1016/j.agrformet.2010.11.012.

National Drought Mitigation Center. 2022. In Summer for the Record Books, the U.S. Hits 106 Weeks Straight with More than 40% of the Lower 48 in Drought. <https://drought.unl.edu/Publications/News.aspx?id=396> (last date accessed: 28 May 2023).

Prasad, A. K., L. Chai, R. P. Singh and M. Kafatos. 2006. Crop yield estimation model for Iowa using remote sensing and surface parameters. *International Journal of Applied Earth Observation and Geoinformation* 8(1):26–33. https://doi.org/10.1016/j.jag.2005.06.002.

Puma, M. J., S. Bose, S. Y. Chon and B. I. Cook. 2015. Assessing the evolving fragility of the global food system. *Environmental Research Letters* 10(2). https://doi.org/10.1088/1748-9326/10/2/024007.

Sakamoto, T. 2018. Refined shape model fitting methods for detecting various types of phenological information on major US crops. *ISPRS Journal of Photogrammetry and Remote Sensing* 138:176–192. https://doi.org/10.1016/j.isprsjprs.2018.02.011.

Sakamoto, T. 2020. Incorporating environmental variables into a MODIS-based crop yield estimation method for United States corn and soybeans through the use of a random forest regression algorithm. *ISPRS Journal of Photogrammetry and Remote Sensing* 160:208–228. https://doi.org/10.1016/j.isprsjprs.2019.12.012.

Sakamoto, T. 2021. Early classification method for US corn and soybean by incorporating MODIS-estimated phenological data and historical classification maps in random-forest regression algorithm. *Photogrammetric Engineering & Remote Sensing* 87:747–758. https://doi.org/10.14358/PERS.21-00003R2.

Sakamoto, T., A. A. Gitelson and T. J. Arkebauer. 2013. MODIS-based corn grain yield estimation model incorporating crop phenology information. *Remote Sensing of Environment* 131:215–231. https://doi.org/10.1016/j.rse.2012.12.017.

Sakamoto, T., A. A. Gitelson and T. J. Arkebauer. 2014. Near real-time prediction of US corn yields based on time-series MODIS data. *Remote Sensing of Environment* 147:219–231. https://doi.org/10.1016/j.rse.2014.03.008.

Sakamoto, T., B. D. Wardlow, A.A. Gitelson, S. B. Verma, A. E. Suyker and T. J. Arkebauer. 2010. A two-step filtering approach for detecting maize and soybean phenology with time-series MODIS data. *Remote Sensing of Environment* 114(10):2146–2159. https://doi.org/10.1016/j.rse.2010.04.019.

Schwalbert, R. A., T. Amado, G. Corassa, L. P. Pott, P.V.V. Prasad and I. A. Ciampitti. 2020. Satellite-based soybean yield forecast: Integrating machine learning and weather data for improving crop yield prediction in southern Brazil. *Agricultural and Forest Meteorology* 284. https://doi.org/10.1016/j.agrformet.2019.107886.

Shen, Y., X. Y. Zhang and Z. W. Yang. 2022. Mapping corn and soybean phenometrics at field scales over the United States Corn Belt by fusing time series of Landsat 8 and Sentinel-2 data with VIIRS data. *ISPRS Journal of Photogrammetry and Remote Sensing* 186:55–69. https://doi.org/10.1016/j.isprsjprs.2022.01.023.

Stepanov, A., K. Dubrovin, A. Sorokin and T. Aseeva. 2020. Predicting soybean yield at the regional scale using remote sensing and climatic data. *Remote Sensing* 12(12). https://doi.org/10.3390/rs12121936.

Sun, J., L. P. Di, Z. H. Sun, Y. L. Shen and Z. L. Lai. 2019. County-level soybean yield prediction using deep CNN-LSTM model. *Sensors* 19(20):4353. https://doi.org/10.3390/s19204363.

The United Nations. 2022. As the World's Population Hits 8 Billion People, UN Calls for Solidarity in Advancing Sustainable Development for All. <https://www.un.org/en/desa/world-population-hits-8-billion-people> (last date accessed 28 May 2023).

USDA-NASS. 2022. Cropland Data Layer—National Download. <https://www.nass.usda.gov/Research_and_Science/Cropland/Release/index.php> (last date accessed 20 November 2022).

USDA-NASS. 2023. Quick STATS. <https://quickstats.nass.usda.gov/> (last date accessed 2 October 2023).

USDA-FAS. 2022a. Grain: World Markets and Trade. <https://apps.fas.usda.gov/psdonline/circulars/grain.pdf> (last date accessed 20 November 2022).

USDA-FAS. 2022b. Oilseeds: World Markets and Trade. <https://apps.fas.usda.gov/psdonline/circulars/oilseeds.pdf> (last date accessed 20 November 2022).

Wang, M., F. Tao and W. Shi. 2014. Corn yield forecasting in Northeast China using remotely sensed spectral indices and crop phenology metrics. *Journal of Integrative Agriculture* 13(7):1538–1545. https://doi.org/10.1016/S2095-3119(14)60817-0.

Zhang, X. Y. and Q. Y. Zhang. 2016. Monitoring interannual variation in global crop yield using long-term AVHRR and MODIS observations. *ISPRS Journal of Photogrammetry and Remote Sensing* 114:191–205. https://doi.org/10.1016/j.isprsjprs.2016.02.010.

Zhou, X. J., P. X. Wang, K. Tansey, S. Y. Zhang, H. M. Li and H. R. Tian. 2020. Reconstruction of time series leaf area index for improving wheat yield estimates at field scales by fusion of Sentinel-2,-3 and MODIS imagery. *Computers and Electronics in Agriculture* 177:105692. https://doi.org/10.1016/j.compag.2020.105692.

Supplemental Tables

S-Table 1. Abbreviations of state and FIPS codes.

Code	State	Abbr.	Code	State	Abbr.	Code	State	Abbr.
01	Alabama	AL	24	Maryland	MD	40	Oklahoma	OK
05	Arkansas	AR	26	Michigan	MI	42	Pennsylvania	PA
06	California	CA	27	Minnesota	MN	45	South Carolina	SC
08	Colorado	CO	28	Mississippi	MS	46	South Dakota	SD
10	Delaware	DE	29	Missouri	MO	47	Tennessee	TN
13	Georgia	GA	30	Montana	MT	48	Texas	TX
16	Idaho	ID	31	Nebraska	NE	51	Virginia	VA
17	Illinois	IL	34	New Jersey	NJ	53	Washington	WA
18	Indiana	IN	35	New Mexico	NM	54	West Virginia	WV
19	Iowa	IA	36	New York	NY	55	Wisconsin	WI
20	Kansas	KS	37	North Carolina	NC	56	Wyoming	WY
21	Kentucky	KY	38	North Dakota	ND			
22	Louisiana	LA	39	Ohio	OH			

S-Table 2. Details of official reports and cropland data layers provided by USDA-NASS.

Data source		Contents	Data release date	spatial resolution
Quick Stats Database	Acerage (forecast)	planted area	JUN 28-30 [DOY: 179-181]	from state to national level
	Crop production (forecast)	yield harvested area production	AUG 10-12 [DOY: 222-224] SEP 10-12 [DOY: 253-255] OCT 9-12 [DOY:282-285] NOV 8-10 [DOY:312-314]	
	Crop production Summary (fixed statistical data)	yield harvested area production	JAN in the following year	from state to national level
	online	yield	FEB in the following year	county
Cropland Data Layers		Digital map	FEB in the following year	30m/pixel

S-Table 3. Correspondence between the input data periods of the MODIS 8-day composite products and the timing at which the early predictions can be published on a non-leap year basis.

Notation in the Figures and Tables	Input data period
(Date of simulation results available)	(MODIS 8-day composite products)
DOY 215 [August 3rd]	DOY 65-201
DOY 231 [August 19th]	DOY 65-217
DOY 247 [September 4th]	DOY 65-233
DOY 263 [September 20th]	DOY 65-249
DOY 279 [October 6th]	DOY 65-265
DOY 295 [October 22nd]	DOY 65-281
DOY 311 [November 7th]	DOY 65-297
DOY 327 [November 23rd]	DOY 65-313
DOY 343 [December 9th]	DOY 65-329

S-Table 4. Summary of crop classification accuracy from DOY215 to DOY311 at the state level for the top five major producing states and at the national level. Each parameter value is averaged over the period from 2018 to 2021.

	Kappa				Overall accuracy			
Area	DOY215	247	279	311	DOY215	247	279	311
Illinois	0.53	0.54	0.64	0.64	0.69	0.70	0.76	0.76
Indiana	0.46	0.47	0.54	0.55	0.66	0.66	0.70	0.71
Iowa	0.56	0.58	0.73	0.73	0.72	0.73	0.82	0.82
Minnesota	0.41	0.42	0.57	0.56	0.60	0.60	0.70	0.70
Nebraska	0.43	0.47	0.59	0.60	0.61	0.64	0.72	0.73
National	0.42	0.42	0.50	0.50	0.59	0.60	0.65	0.65

	Corn				Soybean			
	User's accuracy				User's accuracy			
Area	DOY215	247	279	311	DOY215	247	279	311
Illinois	0.87	0.88	0.89	0.89	0.91	0.91	0.92	0.92
Indiana	0.85	0.86	0.87	0.87	0.90	0.90	0.91	0.91
Iowa	0.91	0.92	0.92	0.92	0.89	0.90	0.93	0.93
Minnesota	0.88	0.89	0.90	0.90	0.85	0.86	0.89	0.89
Nebraska	0.88	0.89	0.90	0.90	0.87	0.89	0.90	0.90
National	0.87	0.88	0.88	0.88	0.86	0.86	0.87	0.88

	Corn				Soybean			
	Producer's accuracy				Producer's accuracy			
Area	DOY215	247	279	311	DOY215	247	279	311
Illinois	0.64	0.65	0.74	0.75	0.50	0.51	0.65	0.66
Indiana	0.51	0.52	0.59	0.60	0.48	0.48	0.57	0.57
Iowa	0.67	0.68	0.80	0.80	0.50	0.53	0.76	0.77
Minnesota	0.51	0.53	0.63	0.63	0.41	0.43	0.66	0.66
Nebraska	0.54	0.57	0.70	0.70	0.38	0.48	0.67	0.68
National	0.48	0.49	0.58	0.59	0.39	0.40	0.54	0.55

S-Table 5. Confusion matrix of the MODIS data classification resulting from the RF-based crop classification algorithm from DOY215 to DOY311 in 2021.

	DOY:215	CDL: Reference data (%)				
	Class	C	S	O	M	Total
MODIS	Corn (C)	47	2	1	3	14
	Soybeans (S)	1	36	1	2	10
	The others (O)	1	1	46	2	8
	Mixture (M)	51	61	52	94	68
	Total	100	100	100	100	100

	DOY:247	CDL: Reference data (%)				
	Class	C	S	O	M	Total
MODIS	Corn (C)	47	2	1	3	14
	Soybeans (S)	1	37	1	2	10
	The others (O)	1	1	42	2	7
	Mixture (M)	51	60	56	94	68
	Total	100	100	100	100	100

	DOY:279	CDL: Reference data (%)				
	Class	C	S	O	M	Total
MODIS	Corn (C)	56	1	1	3	17
	Soybeans (S)	1	51	1	2	14
	The others (O)	1	1	45	2	8
	Mixture (M)	42	47	53	92	61
	Total	100	100	100	100	100

	DOY:311	CDL: Reference data (%)				
	Class	C	S	O	M	Total
MODIS	Corn (C)	57	1	1	4	17
	Soybeans (S)	1	51	2	2	14
	The others (O)	2	1	46	3	8
	Mixture (M)	41	46	51	91	60
	Total	100	100	100	100	100

S-Table 6. Days after emergence date when the determination coefficient between MODIS-derived WDRVI and corn and soybean yield by region were the highest.

Crop	State	DOY215	DOY231	DOY247	DOY263	DOY279	DOY295	DOY311	DOY327	DOY343
Corn	Illinois	65	74	80	76	73	73	73	73	73
	Indiana	70	74	81	78	74	71	71	71	71
	Iowa	62	66	76	75	70	69	69	69	69
	Minnesota	31	73	79	75	72	71	70	70	70
	Nebraska	63	69	78	77	72	71	71	71	71
	National	66	71	77	75	71	70	70	71	71
Soybean	Illinois	35	61	73	78	76	75	75	75	75
	Indiana	38	54	71	77	74	72	72	72	73
	Iowa	46	50	72	78	75	74	74	74	74
	Minnesota	44	59	71	75	74	73	73	73	73
	Nebraska	59	67	74	86	83	82	82	82	82
	National	48	57	74	78	76	75	75	75	75

Supplemental Images

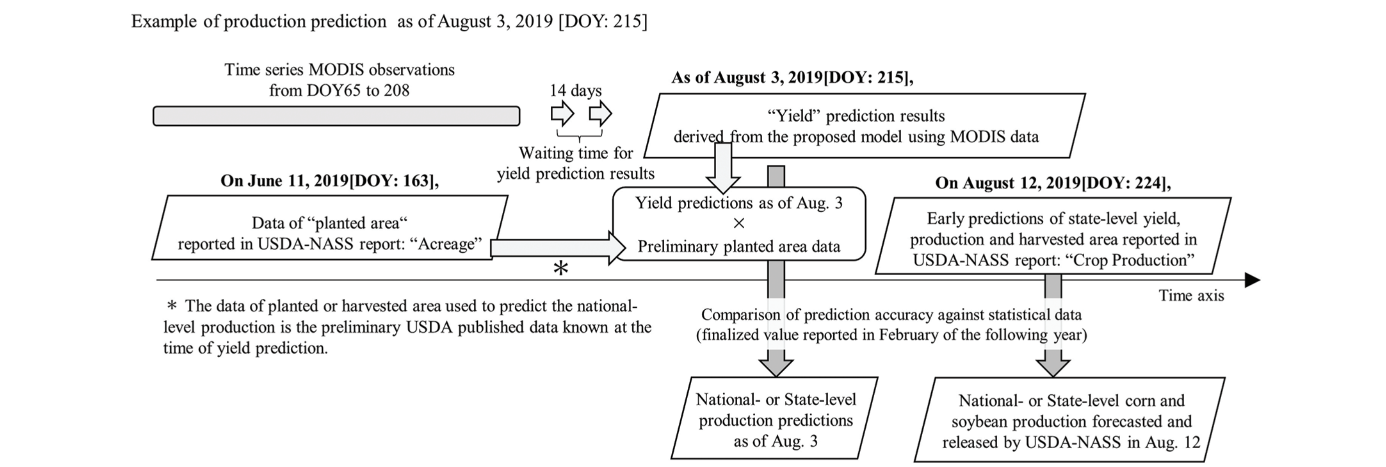

S-Figure 1. Flow of data processing of near real-time prediction of the US corn grain and soybean yield and production as of 3 August 2019.

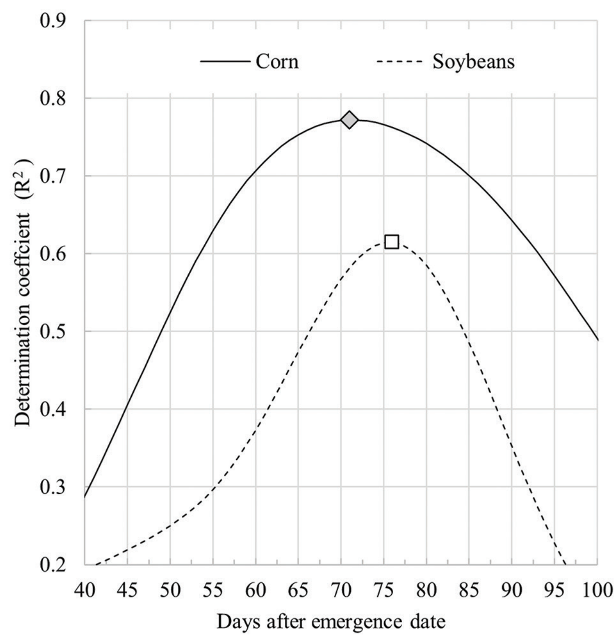

S-Figure 2. Seasonal changes in the determination coefficient between the MODIS-WDRVI and the county-level corn and soybean yields, which were determined using a third-order polynomial regression as of DOY279, at the national level. The time-axis origin is set at the rSMF-estimated emergence date.

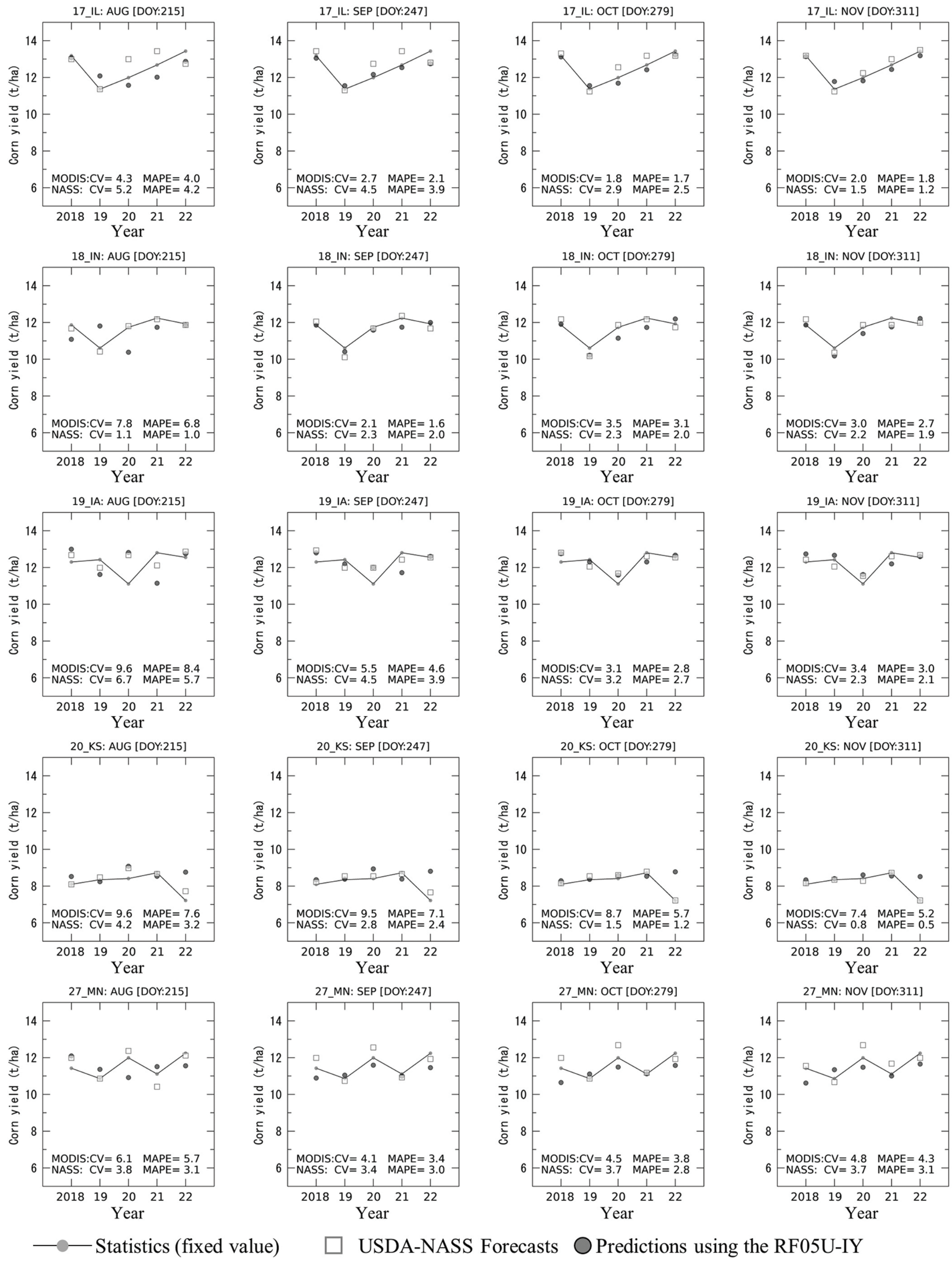

S-Figure 3. Comparison of state-level corn grain yield between the United States Department of Agriculture National Agricultural Statistics Service (USDA-NASS) monthly forecasts and the predictions of the proposed method (RF05U-IY) as of day of year (DOY) 215, DOY 247, DOY 279, and DOY 311 against the fixed statistical data in the major corn producing states.

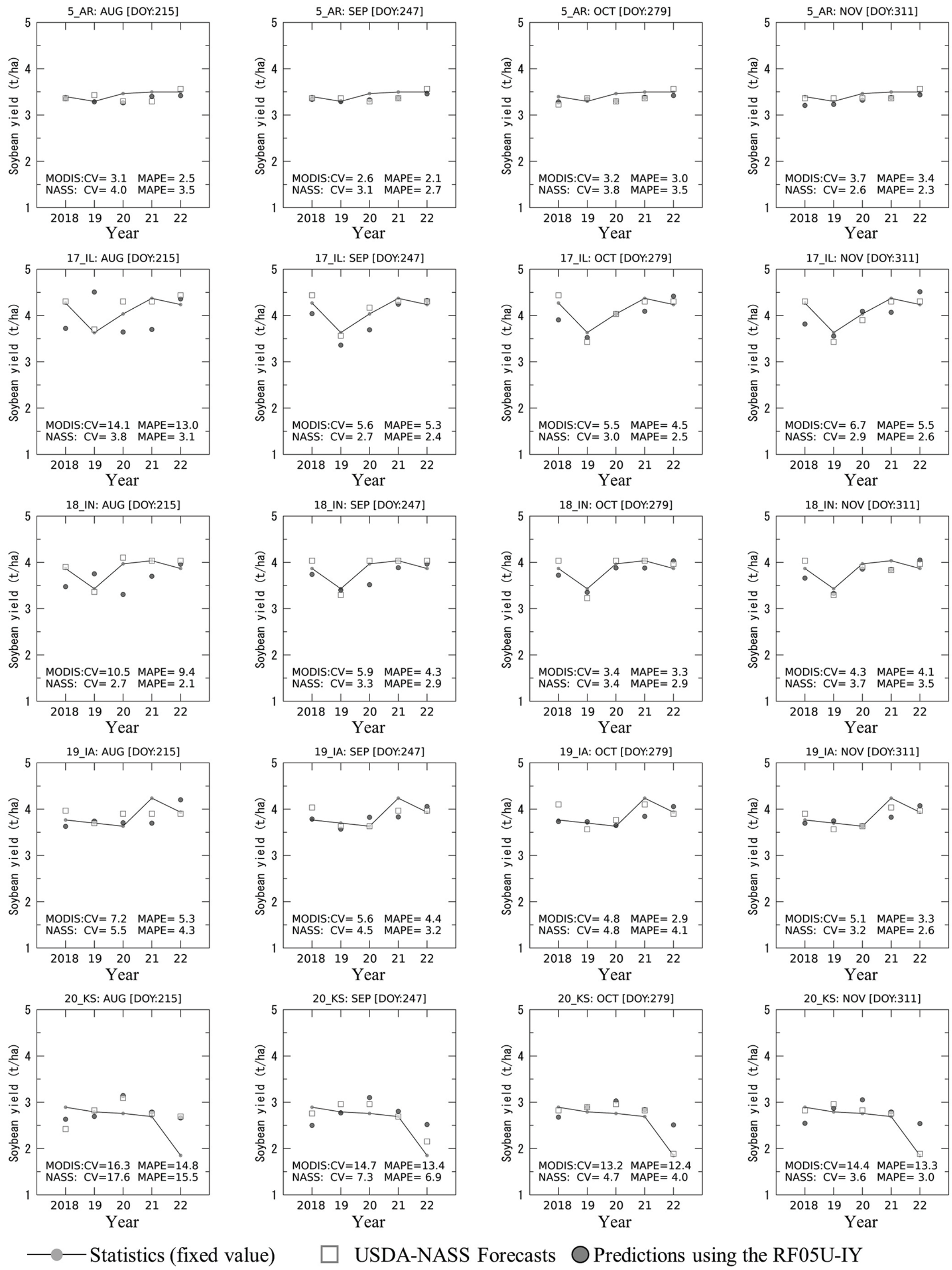

S-Figure 4. Comparison of state-level soybean yield between the United States Department of Agriculture National Agricultural Statistics Service (USDA-NASS) monthly forecasts and the predictions of the proposed method (RF05U-IY) as of day of year (DOY) 215, DOY 47, DOY 279, and DOY 311 against the fixed statistical data in the major soybean producing states.

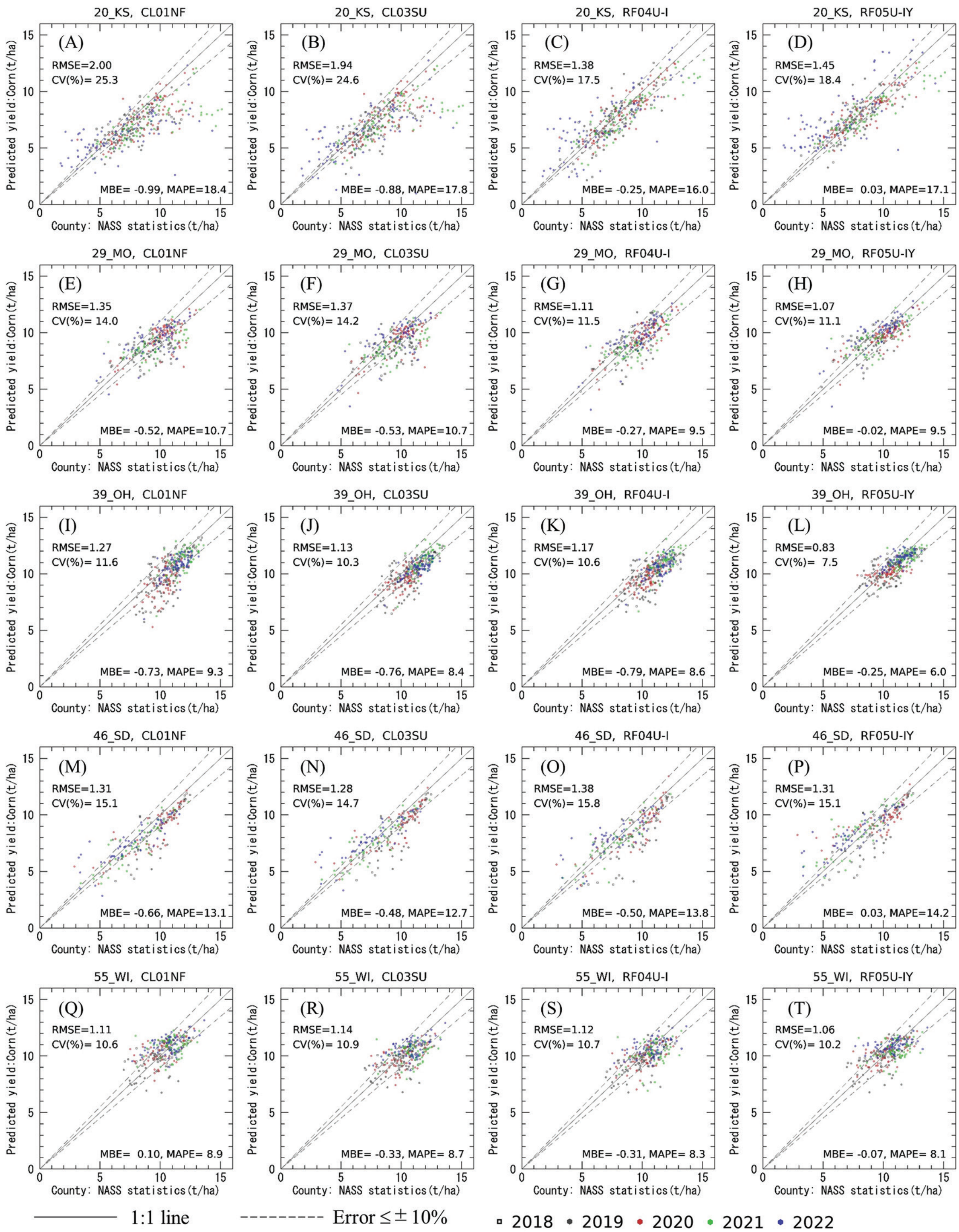

S-Figure 5. Comparison between the United States Department of Agriculture National Agricultural Statistics Service (USDA-NASS)-derived fixed statistical data and the county-level corn grain yields predicted by the tested models (CL01NF, CL03SU, RF04U-I, and RF05U-IY) as of day of year (DOY) 279 in Kansas (A–D), Missouri (E–H), Ohio (I–L), South Dakota (M–P), and Wisconsin (Q–T). RMSE: root mean square error (t/ha), CV: coefficient of variation (%), ME: mean error (t/ha), MAPE: mean absolute percentage error (%).

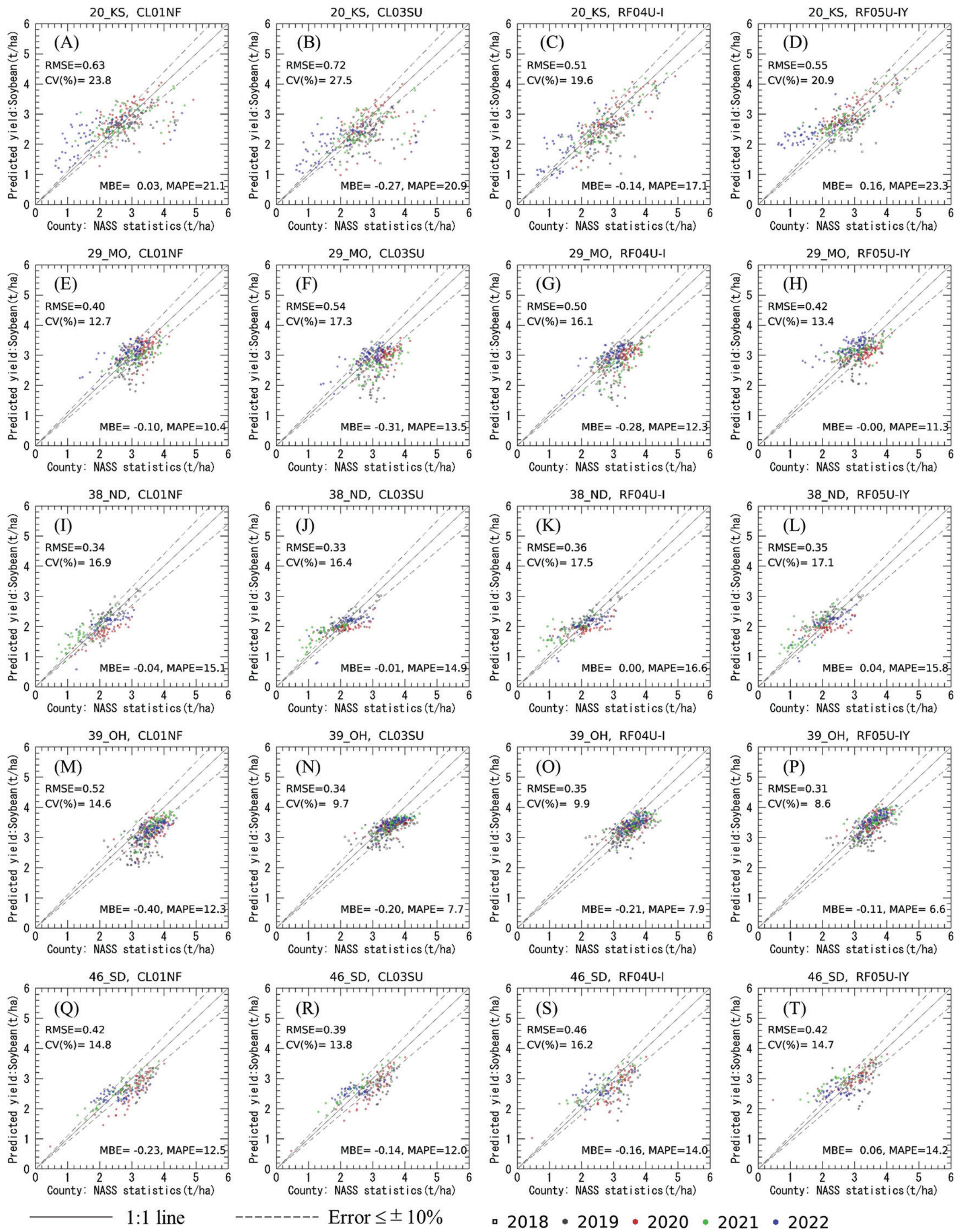

S- Figure 6. Comparison between the United States Department of Agriculture National Agricultural Statistics Service (USDA-NASS)-derived fixed statistical data and the county-level soybean yields predicted by the tested models (CL01NF, CL03SU, RF04U-I, and RF05U-IY) as of day of year (DOY) 279 in Arkansas (A–D), Kansas (E–H), Missouri (I–L), North Dakota (M–P), Ohio (Q–T), and South Dakota (U–Y). RMSE: root mean square error (t/ha), CV: coefficient of variation (%), ME: mean error (t/ha), MAPE: mean absolute percentage error (%).

SUSTAININGMEMBERS

ACI USA Inc.
Weston, Florida
https://acicorporation.com/
Member Since: 2/2018

Aerial Services, Inc.
Cedar Falls, Iowa
www.AerialServicesInc.com
Member Since: 5/2001

Airworks Solutions Inc.
Boston, Massachusetts
Member Since: 5/2022

Applanix
Richmond Hill, Ontario, Canada
http://www.applanix.com
Member Since: 7/1997

Ayres Associates
Madison, Wisconsin
www.AyresAssociates.com
Member Since: 1/1953

Cardinal Systems, LLC
Flagler Beach, Florida
www.cardinalsystems.net
Member Since: 1/2001

Dewberry
Fairfax, Virginia
www.dewberry.com
Member Since: 1/1985

Digital Mapping, Inc.(DMI)
Huntington Beach, California
www.admap.com
Member Since: 4/2002

Environmental Research Incorporated
Linden, Virginia
www.eri.us.com
Member Since: 8/2008

Esri
Redlands, California
www.esri.com
Member Since: 1/1987

GeoCue Group
Madison, Alabama
http://www.geocue.com
Member Since: 10/2003

Geographic Imperatives LLC
Centennial, Colorado
Member Since: 12/2020

GPI Geospatial Inc.
Orlando, Florida
www.aca-net.com
Member Since: 1/1994

Halff Associates, Inc.
Richardson, Texas
www.halff.com
Member Since: 8/2021

Keystone Aerial Surveys, Inc.
Philadelphia, Pennsylvania
www.kasurveys.com
Member Since: 1/1985

Kucera International
Willoughby, Ohio
www.kucerainternational.com
Member Since: 1/1992

L3Harris Technologies
Broomfield, Colorado
www.l3harris.com
Member Since: 6/2008

Merrick & Company
Greenwood Village, Colorado
www.merrick.com
Member Since: 4/1995

Miller Creek Associates
SeaTac Washington
www.mcamaps.com
Member Since: 12/2014

Nearmap
South Jordan, Utah
www.nearmap.com
Member Since: 6/2023

NV5 Geospatial
Sheboygan Falls, Wisconsin
www.quantumspatial.com
Member Since: 1/1974

Pickett and Associates, Inc.
Bartow, Florida
www.pickettusa.com
Member Since: 4/2007

Riegl USA, Inc.
Orlando, Florida
www.rieglusa.com
Member Since: 11/2004

RRC International, LLC
Round Rock, Texas
https://rrccompanies.com/
Member Since: 9/2023

Sanborn Map Company
Colorado Springs, Colorado
www.sanborn.com
Member Since: 10/1984

Surdex Corporation
Chesterfield, Missouri
www.surdex.com
Member Since: 12/2011

Surveying And Mapping, LLC (SAM)
Austin, Texas
www.sam.biz
Member Since: 12/2005

T3 Global Strategies, Inc.
Bridgeville, Pennsylvania
https://t3gs.com/
Member Since: 6/2020

Towill, Inc.
San Francisco, California
www.towill.com
Member Since: 1/1952

Woolpert LLP
Dayton, Ohio
www.woolpert.com
Member Since: 1/1985

SUSTAININGMEMBER**BENEFITS**

Membership

- ✓ Provides a means for dissemination of new information
- ✓ Encourages an exchange of ideas and communication
- ✓ Offers prime exposure for companies

Benefits of an ASPRS Membership

- Complimentary and discounted Employee Membership*
- E-mail blast to full ASPRS membership*
- Professional Certification Application fee discount for any employee
- Member price for ASPRS publications
- Discount on group registration to ASPRS virtual conferences
- Sustaining Member company listing in ASPRS directory/website
- Hot link to company website from Sustaining Member company listing page on ASPRS website
- Press Release Priority Listing in *PE&RS* Industry News
- Priority publishing of Highlight Articles in *PE&RS* plus, 20% discount off cover fee
- Discount on *PE&RS* advertising
- Exhibit discounts at ASPRS sponsored conferences (exception ASPRS/ILMF)
- Free training webinar registrations per year*
- Discount on additional training webinar registrations for employees
- Discount for each new SMC member brought on board (Discount for first year only)

*quantity depends on membership level

A Few-Shot Semi-Supervised Learning Method for Remote Sensing Image Scene Classification

Yuxuan Zhu, Erzhu Li, Zhigang Su, Wei Liu, Alim Samat, and Yu Liu

Abstract

Few-shot scene classification methods aim to obtain classification discriminative ability from few labeled samples and has recently seen substantial advancements. However, the current few-shot learning approaches still suffer from overfitting due to the scarcity of labeled samples. To this end, a few-shot semi-supervised method is proposed to address this issue. Specifically, semi-supervised learning method is used to increase target domain samples; then we train multiple classification models using the augmented samples. Finally, we perform decision fusion of the results obtained from the multiple models to accomplish the image classification task. According to the experiments conducted on two real few-shot remote sensing scene datasets, our proposed method achieves significantly higher accuracy (approximately 1.70% to 4.33%) compared to existing counterparts.

Introduction

Remote sensing has been developing rapidly, as it has a wide range of applications in the real world, such as natural hazard detection (Kamari and Ham 2022; Yang and Cervone 2019), land-use classification (Kafy *et al.* 2022; Wang *et al.* 2022), and urban planning (Ardabili *et al.* 2022; Fu *et al.* 2022; Jiang *et al.* 2022). In these applications, remote sensing scene classification plays an important role as a key technology (Chen *et al.* 2022; Mehmood *et al.* 2022; Roy *et al.* 2022; Shi *et al.* 2022). Due to the large amount of remote sensing scene data, using deep learning to solve remote sensing image processing and application problems is a research hotspot in the remote sensing community. However, scene classification still encounters two challenges in remote sensing image processing. Firstly, although the remote sensing image scene classification methods based on deep learning have achieved high accuracy, the models built based on supervised training cannot deal with the open set problem in which the categories of the training data and the test data are inconsistent. Secondly, traditional deep learning models usually rely on large amounts of labeled data for training, which is a real challenge for new application scenarios. To overcome these shortcomings, few-shot learning is considered to be an effective method (Cheng *et al.* 2021).

Few-shot learning is a new machine learning framework that enables a pre-trained model to generalize over new categories of data using a few labeled samples (Bai *et al.* 2022). Recent studies have proposed various approaches to maintain classification performance while improving generalization ability for new categories. Generally, few-shot learning methods can be divided into three categories: model-based (Zhang *et al.* 2019), metrics-based (Snell, Swersky, and Zemel 2017), and optimization-based (Finn *et al.* 2017; Li *et al.* 2017; Yang *et al.* 2022). Model-based few-shot learning methods focus on quickly updating model parameters based on a few labeled samples, enabling the establishment of discriminative functions to classify input samples, but for new tasks, a lot of parameter updates and adjustments are needed, and more training samples may be required to adapt to the new task. Metrics-based few-shot learning uses the concept of nearest neighbors to classify samples by measuring distances between query and support set samples. In high-dimensional spaces, the calculation of metrics can be difficult and time-consuming. The optimization-based approach acknowledges the limitations of traditional gradient descent methods in adapting to few-shot scenarios and addresses the task by adjusting the optimization method. New tasks can be quickly adapted through the optimization process without requiring a large amount of samples. In addition, the optimization method has good generalization performance and can achieve high accuracy in small sample learning tasks. A commonly used technique for few-shot learning based on optimization (Baik *et al.* 2020; Lai *et al.* 2020; Ravi and Larochelle 2017) to solve the shortage of training samples is the "pre-training finetune"; this method involves pre-training the model on a large data set and fine-tuning the weights on a small data set. However, this approach may not be effective when training samples are extremely limited and can lead to overfitting.

This study proposes a semi-supervised multi-model decision fusion optimization (SMDFO) method for few-shot learning. First, we construct a semi-supervised retraining (SLRT) module to generate pseudo-labels with high confidence coefficient. Then, the pseudo-labels are used to fine-tune the weight parameters of model to solve the overfitting of the model. Finally, a multi-model decision fusion (MMDF) module is designed to classify images in the target domain. The decision fusion method is used to maximize the classification results across multiple models and reduce the impact of misjudgments on the final classification results. The main contributions of this work are summarized as follows:

(1) A SLRT strategy is proposed to increase training targets to reduce the overfitting problem of the model.
(2) For the classification results, a decision fusion method is proposed in the MMDF module to enhance classification accuracy by combining the results of multiple models and minimizing the influence of misjudgments.
(3) Experimental results on two remote sensing image data sets show the compelling performance of our model in the scene classification task.

Methodology

Figure 1 shows the main process of the proposed few-shot learning method, which can be divided into pre-training and testing phases. In the pre-training phase, the feature extractor is trained on the source domain; we randomly extract a large number of n-way k-shot tasks from the source domain, put them into the model for training, calculate the cross-entropy loss, and finally update the gradient. The test

Yuxuan Zhu, Erzhu Li, Wei Liu, and Yu Liu are with the School of Geography, Geomatics and Planning, Jiangsu Normal University, Xuzhou, China.

Zhigang Su is with ShanDong ZhengYuan Aerial Remote Sensing Technology Co., Ltd., Jinan, China.

Alim Samat is with State Key Laboratory of Desert and Oasis Ecology, Xinjiang Institute of Ecology and Geography, Chinese Academy of Sciences, Urumqi, China.

Corresponding author: Erzhu Li (liezrs2018@jsnu.edu.cn)

Contributed by Ravi Dwivedi, September 13, 2023 (sent for review October 18, 2023; reviewed by Devesh Kumar, Chandrakanth Ravikanti, Rajeshreddy Datla).

Photogrammetric Engineering & Remote Sensing
Vol. 90, No. 2, February 2024, pp. 121–125.
0099-1112/22/121–125
© 2024 American Society for Photogrammetry and Remote Sensing
doi: 10.14358/PERS.23-00067R2

PEER-REVIEWED CONTENT IS ONLY AVAILABLE TO ASPRS MEMBERS AND SUBSCRIBERS

FOR MORE INFORMATION VISIT MY.ASPRS.ORG

PEER-REVIEWED CONTENT
IS ONLY AVAILABLE TO
ASPRS MEMBERS AND SUBSCRIBERS

FOR MORE INFORMATION VISIT
MY.ASPRS.ORG

PEER-REVIEWED CONTENT
IS ONLY AVAILABLE TO
ASPRS MEMBERS AND SUBSCRIBERS

FOR MORE INFORMATION VISIT
MY.ASPRS.ORG

PEER-REVIEWED CONTENT IS ONLY AVAILABLE TO ASPRS MEMBERS AND SUBSCRIBERS

FOR MORE INFORMATION VISIT MY.ASPRS.ORG

Call for *PE&RS* Special Issue Submissions

Ushering a New Era of Hyperspectral Remote Sensing to Advance Remote Sensing Science in the Twenty-first Century

Great advances are taking place in remote sensing with the advent of new generation of hyperspectral sensors. These include data from, already in orbit sensors such as: 1. Germany's Deutsches Zentrum fur Luftund Raumfahrt (DLR's) Earth Sensing Imaging Spectrometer (DESIS) sensor onboard the International Space Station (ISS), 2. Italian Space Agency's (ASI's) PRISMA (Hyperspectral Precursor of the Application Mission), and 3. Germany's DLR's Environmental Mapping and Analysis Program (EnMAP). Further, Planet Labs PBC recently announced the launch of two hyperspectral sensors called Tanager in 2023. NASA is planning for the hyperspectral sensor Surface Biology and Geology (SBG) to be launched in the coming years. Further, we already have over 70,000 hyperspectral images of the world acquired from NASA's Earth Observing-1 (EO-1) Hyperion that are freely available to anyone from the U.S. Geological Survey's data archives. These suites of sensors acquire data in 200 plus hyperspectral narrowbands (HNBs) in 2.55 to 12 nm bandwidth, either in 400-1000 or 400-2500 nm spectral range with SBG also acquiring data in the thermal range. In addition, Landsat-NEXT is planning a constellation of 3 satellites each carrying 26 bands in the 400-12,000 nm wavelength range. HNBs provide data as "spectral signatures" in stark contrast to "a few data points along the spectrum" provided by multispectral broadbands (MBBs) such as the Landsat satellite series.

The goal of this special issue is to seek scientific papers that perform research utilizing data from these new generation hyperspectral narrowband (HNB) sensors for a wide array of science applications and compare them with the performance of the multispectral broadband (MBB) sensors such as Landsat, Sentinels, MODIS, IRS, SPOT, and a host of others.

Papers on the following topics are of particular interest:

1. Methods and techniques of understanding, processing, and computing hyperspectral data with specific emphasis on machine learning, deep learning, artificial intelligence (ML/DL/AI), and cloud computing.
2. Issues of hyperspectral data volumes, data redundancy, and overcoming Hughes' phenomenon.
3. Building hyperspectral libraries for purposes of creating reference training, testing, and validation data.
4. Utilizing time-series multispectral data and hyperspectral data over many years to build data cubes and apply advanced computational methods of ML/DL/AI methods and approaches on the cloud.
5. Discussions of hyperspectral data analysis techniques like full spectral analysis versus optimal band analysis.
6. Developing hyperspectral vegetation indices (HVIs) for targeted applications to model and map plant biophysical (e.g., Yield, biomass, leaf area index), biochemical (e.g., Nitrogen, anthocyanins, carotenoids), plant health/stress, and plant structural quantities.
7. Classification of complex vegetation and crop types/species using HNBs and HVIs and comparing them with the performance of multispectral broadband data.

All submissions will be peer-reviewed in line with *PE&RS* policy. Because of page limits, not all submissions recommended for acceptance by the review panel may be included in the special issue. Under this circumstance, the guest editors will select the most relevant papers for inclusion in the special issue. Authors must prepare manuscripts according to the *PE&RS* Instructions to Authors, published in each issue of *PE&RS* and also available on the ASPRS website, https://www.asprs.org/asprs-publications/pers/manuscript-submission.

Special Issue Editors

Dr. Prasad S. Thenkabail, pthenkabail@usgs.gov, thenkabail@gmail.com
Senior Scientist (ST), USGS, Flagstaff, Arizona

Dr. Itiya Aneece, ianeece@usgs.gov
USGS, Flagstaff, Arizona

Dr. Pardhasaradhi Teluguntla, pteluguntla@usgs.gov
USGS, Flagstaff, Arizona

Important Dates

Manuscripts Due — March 31, 2024

Final Papers Due — May 1, 2024

Tentative Publication Date — August 2024

Please submit your manuscript —
www.editorialmanager.com/asprs-pers/
select "Hyperspectral Remote Sensing"

ASPRS
CODE OF ETHICS

Honesty, justice, and courtesy form a moral philosophy which associated with mutual interest among people should be the principles on which ethics are founded.

Each person who is engaged in the use development and improvement of the mapping sciences (Photogrammetry Remote Sensing Geographic Information Systems and related disciplines) should accept those principles as a set of dynamic guides for conduct and a way of life rather than merely for passive observance. It is an inherent obligation to apply oneself to one's profession with all diligence and in so doing to be guided by this Code of Ethics.

Accordingly, each person in the mapping sciences profession shall have full regard for achieving excellence in the practice of the profession and the essentiality of maintaining the highest standards of ethical conduct in responsibilities and work for an employer all clients colleagues and associates and society at large and shall…

asprs THE IMAGING & GEOSPATIAL INFORMATION SOCIETY

www.asprs.org

1. Be guided in all professional activities by the highest standards and be a faithful trustee or agent in all matters for each client or employer.
2. At all times, function in such a manner as will bring credit and dignity to the mapping sciences profession.
3. Not compete unfairly with anyone who is engaged in the mapping sciences profession by:
   a. Advertising in a self-laudatory manner;
   b. Monetarily exploiting one's own or another's employment position;
   c. Publicly criticizing other persons working in or having an interest in the mapping sciences;
   d. Exercising undue influence or pressure or soliciting favors through offering monetary inducements.
4. Work to strengthen the profession of mapping sciences by:
   a. Personal effort directed toward improving personal skills and knowledge;
   b. Interchange of information and experience with other persons interested in and using a mapping science with other professions and with students and the public;
   c. Seeking to provide opportunities for professional development and advancement of persons working under his or her supervision;
   d. Promoting the principle of appropriate compensation for work done by person in their employ..
5. Undertake only such assignments in the use of mapping sciences for which one is qualified by education training and experience and employ or advise the employment of experts and specialists when and whenever clients' or employers' interests will be best served thereby.
6. Give appropriate credit to other persons and/or firms for their professional contributions.
7. Recognize the proprietary privacy legal and ethical interests and rights of others. This not only refers to the adoption of these principles in the general conduct of business and professional activities but also as they relate specifically to the appropriate and honest application of photogrammetry remote sensing geographic information systems and related spatial technologies. Subscribers to this code shall not condone promote advocate or tolerate any organization's or individual's use of these technologies in a manner that knowingly contributes to:
   a. deception through data alteration;
   b. circumvention of the law;
   c. transgression of reasonable and legitimate expectation of privacy.
8. Promote equity, inclusion and intellectual diversity in the mapping sciences. Encourage participation without regard to race, religion, gender, disability, age, national origin, political affiliation, sexual orientation, gender identity, or gender expression.

PUBLISHING OPEN-ACCESS IN *PE&RS* IS NOW EASIER!

ASPRS is changing the subscription model of our monthly journal, *PE&RS*. ASPRS is waiving open-access fees for primary authors from subscribing institutions. Additionally, primary authors who are Individual Members of ASPRS will be able to publish one open-access article per year at no cost and will receive a 50% discount on open-access fees for additional articles.

- **Open Access matters!** By providing unrestricted access to research we can advance the geospatial industry and provide research that is available to everyone.
- **Institutions and authors receive more recognition!** Giving permission to everyone to read, share, reuse the research without asking for permission, as long as the author is credited.
- **Reputation matters!** Known for its high standards, *PE&RS* is the industry leading peer-review journal. Adding open access increases authors' visibility and reputation for quality research.
- **Fostering the geospatial industry!** Open access allows for sharing without restriction. Research is freely available to everyone without an embargo period.

Under the previous subscription model, authors and institutions paid $1500 or more in open-access fees per article. This will represent a significant cost savings. Open-access publications benefit authors through greater visibility of their work and conformance with open science mandates of funding agencies.

Subscriptions asprs.org/subscribe
Membership asprs.org/membership

asprs THE IMAGING & GEOSPATIAL INFORMATION SOCIETY

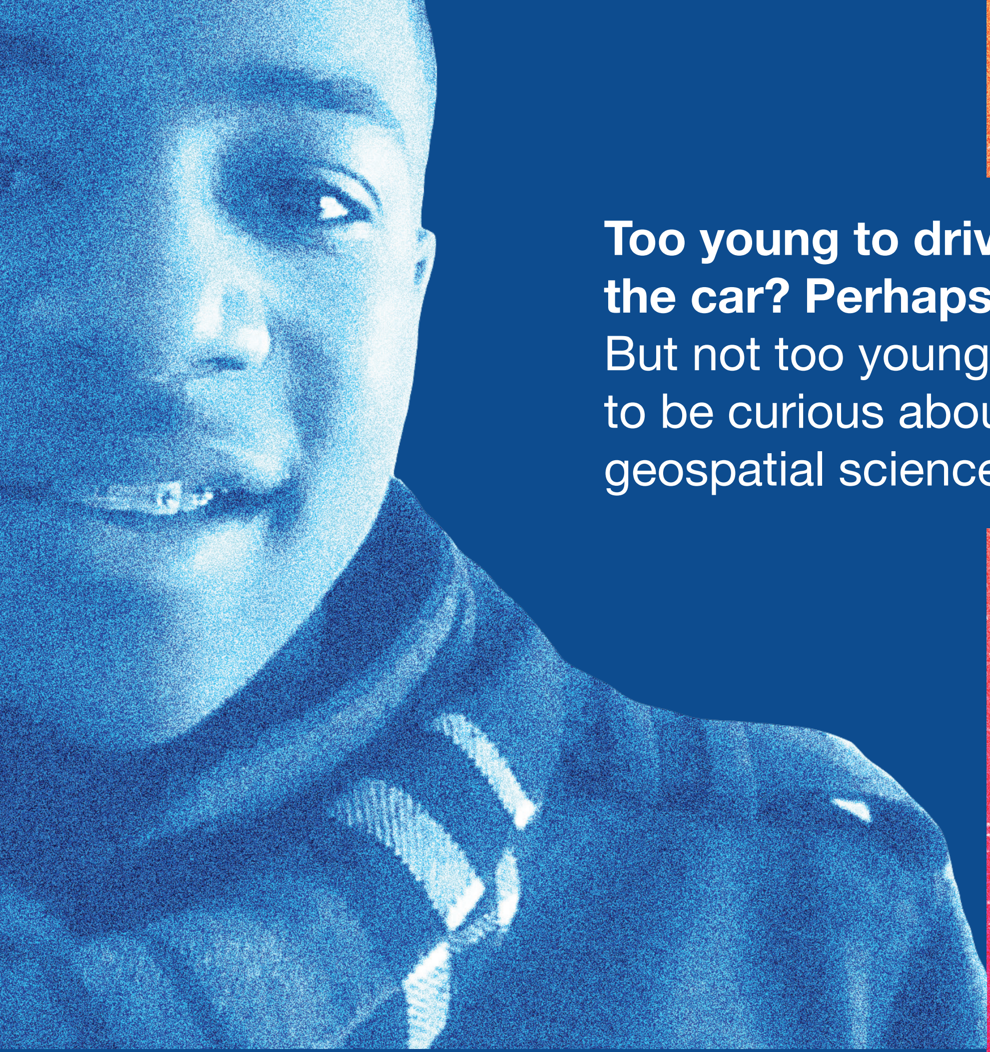

Too young to drive the car? Perhaps!
But not too young to be curious about geospatial sciences.

The ASPRS Foundation was established to advance the understanding and use of spatial data for the betterment of humankind.

The Foundation provides grants, scholarships, loans and other forms of aid to individuals or organizations pursuing knowledge of imaging and geospatial information science and technology, and their applications across the scientific, governmental, and commercial sectors.

Support the foundation, so when they are ready, we are too.

asprsfoundation.org/donate

JOIN ASPRS TODAY!

asprs THE IMAGING & GEOSPATIAL INFORMATION SOCIETY

ACCELERATE YOUR CAREER!

PHOTOGRAMMETRY · REMOTE SENSING · GIS · LIDAR · UAS …and more!

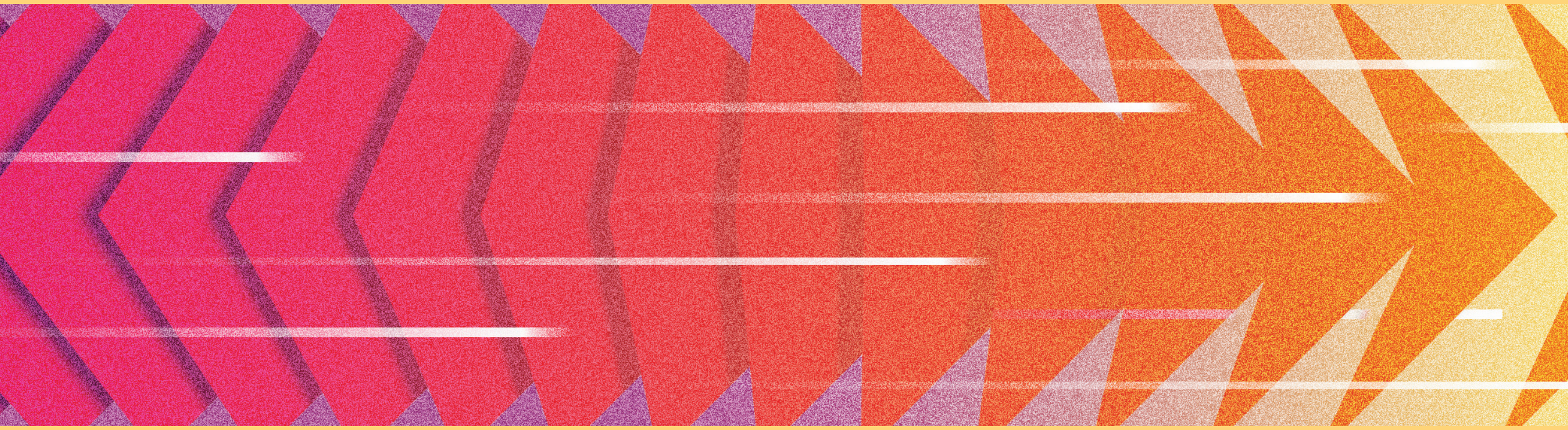

LEARN

- Read our journal, *PE&RS*
- Attend professional development workshops, GeoBytes, and online courses through the ASPRS ProLearn platform
- Earn professional development hours (PDH)
- Attend our national & regional meetings and conferences

DO

- Write for *PE&RS*
- Innovate to create new geospatial technologies
- Present at our national & regional meetings and conferences
- Engage & network

GIVE

- Participate in the development of standards & best practices
- Influence state licensure through our NCEES affiliation
- Mentor colleagues & support students
- Educate others about geospatial science & technology

BELONG

- Establish yourself as a geospatial expert
- Grow business relationships
- Brand yourself and your company as geospatial leaders
- Connect to the world via our affiliation with ISPRS

Don't delay, join today at **asprs.org**